

Undersized ball pigging

An experimental study in a horizontal
pipe

E. Verlaan

November 2021



Undersized ball pigging

An experimental study in a horizontal pipe

by

E. Verlaan

As part of the fulfillment of the requirements for the degree of master of

”Mechanical Engineering”

Track: Energy, Flow & Process Technology

at the Delft University of Technology,
to be defended publicly on 17 November 2021

Student number: 4561554
Project duration: November 2020 – November 2021
Thesis committee: Prof. dr. ir. R.A.W.M. Henkes, TU Delft, supervisor
Dr. ir. A. Greidanus, TU Delft, supervisor
Dr. ir. M.J. Tummers, TU Delft

Cover image from ¹. An electronic version of this thesis is available at
<http://repository.tudelft.nl/>.

¹<https://www.offshore-technology.com/news/southwest-gas-questar-pipeline-1-9bn/>

Abstract

Onshore and offshore multiphase pipelines provide a safe and effective solution for the transport of fluids from wells to production plants in the oil and gas industry. For the control of the accumulated amount of liquid present in the pipeline (the so-called liquid hold-up) and for the regular maintenance of the pipeline, pigs (Pipeline Inspection Gauges) are conventionally used. To reduce the pig-generated volume (which is the amount of extra liquid that is removed from the pipeline due to the pig traverse), research in the past decades showed that a by-pass pig can be used as a more attractive alternative. With the by-pass pig, the size of the slugcatcher (which temporarily stores the pig-generated volume at the end of the pipeline) can be reduced. To reduce the risk of stalling of the by-pass pig in the pipeline and the risk of exceeding the available liquid storage volume of the slugcatcher, undersized ball pigs can be deployed prior to launching the by-pass pig. The undersized ball pig will be smaller than the pipe internal diameter (e.g., $0.9 \cdot D$) and will not experience significant friction with the pipe wall. Furthermore, the pig-generated volume will be smaller than what is found with the by-pass pig as the ball pig will leak some liquid volume; this means that not all liquid is driven out of the pipe by the pig, but some liquid is moved to and left behind the pig. Although ball pigging is already used in some field operations, its use can be extended if the fluid physics are better understood and reliable models for preparing such operations are available.

In this Master Thesis Project, small scale experiments were carried out to investigate the undersized ball pig behaviour in a 52 mm diameter, 60 m long multiphase flow loop located in the Process & Energy Laboratory at the campus of Delft University of Technology. Air and water are used as the working fluids. The performed experiments were used to get a better understanding of the parameters that determine the flow around an undersized ball pig. The pig velocity and the liquid leakage were of particular interest. Two pressure sensors, a liquid hold-up sensor, three cameras, and a weighing scale were used as the measurement system. Three buoyant pigs were created using a 3D-printer. The three ball pigs varied in size: 42 mm, 45 mm, and 48 mm. In addition, a flexible ball pig of 50 mm was used. The pigs were released in a stratified flow through a pig launcher. The presence of (wavy) stratified flow in this flow loop maintained up to a certain upper limit for the flowrates ($u_{SG} = 4$ m/s, $u_{SL} = 0.0628$ m/s). Higher liquid flow velocities would rapidly create intermittent slugs.

The pigging observations showed that it is recommended for industrial applications to create buoyant pigs (e.g., 3D-printed balls) when using a diameter ratio (the ratio between the pig diameter and the inner pipe diameter) of approximately 0.9. This reduces the risk of stalling of the undersized ball pig. From the local video recordings, it can be observed that undersized ball pigs accumulate liquid while creating one or multiple liquid slugs. The created liquid slug will propagate and separate from the pig, whereafter a new liquid accumulation at the front of the pig is created. The local pig velocity is found to be oscillatory in time, due to liquid slug accumulation and liquid slug propagation.

It is found that the normalized pig velocity (being the pig velocity divided by the mixture velocity) increases with increasing superficial gas velocity according to three different regions. In the first region, almost no increase in the normalized pig velocity can be observed. In the second region, the normalized pig velocity increases significantly. In the third region, the normalized pig velocity reaches a stable level. The transition from the first to the second region was found to have a local Reynolds number of about 2000 - 3000 for the gas. The normalized pig velocity in the second region and in the third region can be approximated with a power law correlation for the various pigs.

It is found that the liquid leakage increases with increasing superficial gas velocity and decreases with increasing superficial liquid velocity. The liquid leakage versus the superficial gas velocity increases linearly from approximately $u_{SG} = 2$ m/s onward. A larger diameter ratio results in a lower liquid leakage. The difference in liquid leakage between the various pigs decreases for large superficial gas velocities ($u_{SG} \approx 4$ m/s). For low superficial gas velocities ($u_{SG} \approx 0.5$ m/s), a liquid leakage below zero was found. Undersized ball pigging becomes ineffective for these low velocities because the liquid flow will overtake the pig instead of leaking past the pig. The experimental leakage results

have been approximated with a power law fit. At last, an analytical leakage model, provided by the OLGA commercial package for dynamic multiphase pipeline simulations, is used to compare the experimental liquid leakage. It is found that the OLGA model significantly underpredicts the values of the experimentally found liquid leakage. Improving this model is desirable so that it can be used in multiphase pipe simulations in the industry.

The results in this study show that undersized ball pigging is associated with some distinct observed phenomena. These observations contribute to the understanding of the fundamental fluid flow structures around an undersized ball pig. The influence of the diameter ratio and the fluid flow velocities on the pig velocity and on the liquid leakage were determined. The measured influence of these parameters will help in the estimation of the pig velocity and the estimation of the leaked volume when industrial pipeline conditions are known.

It is recommended for future research to focus on improved models to determine the pig velocity and the liquid leakage such that the use of undersized ball pigs can be reliably extended. Additional pigging experiments with local video recordings can be helpful.

Preface

The last part of my studies, my graduation project at the Delft University of Technology has come to the final stage. Last year, amidst Covid-19, I have been able to perform an experimental project on pigging. I am thankful for this opportunity. The combination of using practical and theoretical skills really helped me to keep focus.

I would have never been able to reach this point without help from others. Therefore, I would like to take the chance to thank the ones who contributed to this. First of all, I would like to thank my supervisor Ruud Henkes for providing me with this research project. He helped from the start with the project, kept me on the right track, and gave useful feedback on the writing. Next, I would like to thank my other supervisor Arnoud Greidanus for helping me with feedback on the adjustments of the flow loop for multiphase pigging and on the analysis of the results. It was very pleasant to work with both supervisors, receiving advice and prompt responses to questions. Moreover, I would like to thank Dr. M.J. Tummers for agreeing to be a member in my graduation committee and for taking the time to read my thesis.

For the construction of the experimental set-up, I would like to thank the technical staff of the Process & Energy Department and in particular Bart Hoek. He helped and gave me advice on gathering the right parts for the experimental loop.

Next, I would like to give a big thanks to Gersom Willems, who accompanied me during this 5 year journey of study together and for the help on the experimental loop.

At last, I would like to give a special thanks to my parents. Their help during my studies was not always of technical nature, but their moral support was evenly important.

*E. Verlaan
Delft, November 2021*

Contents

List of figures	xi
List of tables	xiii
1 Introduction	1
1.1 What is ball pigging?	1
1.2 Literature overview	4
1.2.1 Fluid flow models	4
1.2.2 Experimental measurement techniques	5
1.2.3 Ball pigging in engineering pipeline operations	6
1.3 Research question	7
1.4 Master project structure	7
2 Flow equations	9
2.1 Problem analysis	9
2.2 Governing equations of pipe flow	9
2.3 Governing equations of the undersized ball pig	13
2.4 Non-dimensional analysis	16
3 Experimental setup	19
3.1 Characteristics of the flow loop	20
3.2 Measurement devices	22
3.2.1 Gas flow meter	22
3.2.2 Liquid flow meter	22
3.2.3 Pressure sensors	23
3.2.4 Weighing scale	23
3.2.5 Hold-up sensor	24
3.2.6 Camera recordings	25
3.2.7 Data acquisition	28
3.3 Undersized ball pig characteristics	28
3.3.1 Dimensions	28
3.3.2 Weight and material	28
3.3.3 Final undersized ball pigs	31
3.4 Operation	32
3.4.1 Operational explanation	32
3.5 Signal processing and data analysis	32
3.5.1 Signal processing	32
3.5.2 Data analysis	35
4 Results	41
4.1 General observations	41
4.1.1 Undersized ball pig behaviour	41
4.1.2 Slug shooting	42
4.1.3 Repeatability	43
4.1.4 Recovery time	45
4.2 Experimental observations and results	46
4.2.1 Pig velocity	46
4.2.2 Leakage	48
4.2.3 Number of slugs	52

4.3	Local observations	53
4.3.1	Global and local velocities	53
4.3.2	Local velocity	54
5	Analysis and Comparison	55
5.1	Pig velocity	55
5.1.1	Scaling	55
5.1.2	Correlations	55
5.1.3	Interpretation	57
5.2	Leakage	60
5.2.1	Correlations	60
5.2.2	Comparison with a model	61
5.3	Discussion	63
6	Conclusions	65
7	Recommendations	69
A	Experimental setup	71
A.1	Flowloop characteristics	71
A.2	Calibration certificate liquid flow meter	74
B	Pigging results	77
B.1	Performed combinations for the experimental conditions	77

List of Figures

1.1	Zhuhai Gaolan Terminal slug catcher designed for a maximum of 44000 barrels ($\approx 5246 \text{ m}^3$). Reproduced from Thronson [33].	2
1.2	Pipeline multiphase flow with a Conventional pig (a) and By-pass pig (b). Reproduced from Hendrix et al. [16].	2
1.3	Pipeline multiphase flow with undersized ball pigging prior to by-pass pigging. Reproduced from Jiang [19].	3
1.4	A typical sphere launcher with a number of spheres stored for remote controllable use. Reproduced from Cordell and Vazant [8]	6
2.1	Velocity profiles for developing pipe flow and pipe flow in the fully developed region. Reproduced from Starks et al. [32].	11
2.2	Velocity profile for multiphase flow with gas on the top of the pipe and liquid on the bottom of the pipe. y-axis: Non-dimensional position in the pipe with radius r . x-axis: Velocity of the flow in the pipe. Reproduced from Henkes [18].	11
2.3	Different flow regimes for two-phase gas and liquid flow in horizontal pipes. Reproduced and adapted from Diaz [10].	13
2.4	Flow-map indicating the different regimes for two-phase gas and liquid flow in a horizontal pipe. The superficial liquid velocity is shown on the horizontal axis and the superficial gas velocity on the vertical axis. Reproduced from Weisman et al. [35].	14
2.5	Sketch of the multiphase flow around an undersized ball pig in the pig's frame of reference. In (a) the velocities and pressure around the pig are defined. In (b) the net forces on the pig from the gas and liquid are visualized for steady state conditions.	15
2.6	Chosen key parameters for the non-dimensional analysis of the pigging experiments.	16
3.1	Sketch of the flow loop.	20
3.2	Pig launcher and inlet section 3D visualized with SolidWorks. Reproduced from Hendrix et al. [16].	20
3.3	Vertical deviation over the length of the horizontal flowloop.	21
3.4	Calibration curves, pressure as function of the voltage. For pressure sensor 1 (left) and pressure sensor 2 (right)	24
3.5	Calibration of the capacitance hold-up sensor. Fitted with a 5th order polynomial curve and combined with 95% prediction bounds.	24
3.6	Video image processing flowchart	27
3.7	A meshed 3D print for a 45 mm ball. The shell is shown in yellow and the 30% infill in red. The mesh is shown for the lower half of the ball (left) and upper half of the ball (right).	29
3.8	A meshed 3D print for a 45 mm ball. The shell is shown in yellow and the 4% infill in red. The mesh is shown for the lower half of the ball (left) and upper half of the ball (right).	29
3.9	Which fraction of the ball should float in the water? This can be determined with the law of Archimedes. Shown in 2D representation.	30
3.10	Representation of a spherical cap with the needed parameters shown. Reproduced from [15].	30
3.11	Left: Top printed surface of the balls with detailed accuracy. Right: Bottom printed surface of the balls with roughness from support material. The marked part is rough due to support material.	31
3.12	Raw output of the pressure sensors combined with a pre-pigging run. The pressure is plotted against time. A random run is chosen with an air flow of 180 L/min, 6 L/min water flow and 45 mm ball.	33
3.13	Raw pressure data of Figure 3.12 filtered with a low-pass filter and passband frequency of 10 Hz.	33

3.14	Output of the liquid hold-up sensor versus time. The unfiltered and low-pass filtered signal are shown. A restriction in hold-up fraction with a maximum of 1 is added for the filtered signal.	34
3.15	Output of the weighing scale during a pigging run.	35
3.16	Full output of one registered pigging run. Measurement signals are filtered and plotted with a shared time axis. The weight, hold-up fraction, and pressures are shown. Liquid velocity: 6 L/min, Air velocity: 180 L/min, Ball diameter: 45 mm.	36
3.17	Same pigging run as 3.16. The two manually black and red marked lines represent a time difference. It is the difference in time of the pig passing the first pressure sensor and the pig passing the end of the hold-up sensor. The time difference is used to compute the average pig velocity (V_{pig}).	37
3.18	Same pigging run as 3.16. The computed surge weight for every pigging run is found by subtracting the steady state weight (black marked linear line) from the measured slug weight (red line). The end time of weighing is found with a remote camera in the vessel.	38
3.19	Registered hold-up fraction for a random pigging run. The defined limit for a new slug is set at a fraction of 0.5. For this particular run it results in 4 slugs being created during the whole run.	39
4.1	Snapshots of a video recording during a pigging run. The specific conditions were: 45 mm ball, 270 L/min air, 6 L/min water. It can be observed that the accumulation behind the ball grows in time and eventually creates a slug. The slug and pig both accelerate. The pig accelerates with a time delay after the acceleration of the slug. A new accumulation directly starts to grow. The liquid accumulation and slug are marked in black.	42
4.2	Measured weight and hold-up for two runs under almost the same experimental conditions. The two runs correspond well as is clear from the total weight and the number of slugs.	43
4.3	Measured pressure by pressure sensor 1 for two runs with approximately the same experimental conditions. The pressure for the two runs corresponds quantitatively well. On the right half, a shift in pressure logging is seen due to a time shift in slug passing.	44
4.4	Measured pressure by pressure sensor 2 for two runs with approximately the same experimental conditions. The pressure for the two runs corresponds quantitatively well. On the right half, a shift in pressure is seen due to a shift in slug passing time.	44
4.5	A full pigging run with logged hold-up fraction. Specific experimental conditions: $Q_{liq} = 6$ L/min, $Q_{air} = 270$ L/min and $D_{pig} = 45$ mm. Here t_1 , t_2 and t_3 represent the start of pigging, end of pigging, and the time to reach initial hold-up again, respectively. The blue line represents the initial hold-up fraction before pigging.	45
4.6	Pig velocity versus superficial air velocities for all the pigging runs. The difference in water flow rate with the same air flow rate can be observed as the cluster points at each superficial gas velocity. Yellow, red, blue and green represent the 42 mm, 45 mm, 48 mm and 50 mm ball pig diameter, respectively.	47
4.7	Pig velocity versus superficial liquid velocity for the 48 mm pig at four different air flow rates. The scattered points show no relation for when the superficial liquid velocity is changed, while keeping the air flow rate fixed. The dashed line shows the averaged pig velocity for each air flow rate.	47
4.8	Leakage versus superficial gas velocity for 42 mm pig with varying liquid flow rate.	49
4.9	Leakage versus superficial gas velocity for 45 mm pig with varying liquid flow rate.	49
4.10	Leakage versus superficial gas velocity for 48 mm pig with varying liquid flow rate.	50
4.11	Leakage versus superficial gas velocity for 50 mm pig with varying liquid flow rate.	50
4.12	Leakage versus superficial gas velocity for 42 mm, 45 mm, 48 mm, and 50 mm ball pigs zoomed in between $u_{SG} = 3.74$ m/s and $u_{SG} = 3.82$ m/s with varying liquid flow rate.	51
4.13	Number of created slugs during pigging runs versus superficial gas velocity for the 42 mm, 45 mm, 48 mm, and 50 mm pig.	52
4.14	The global and local pig velocity versus air velocity. The global pig velocity is determined as discussed in Chapter 3.5.2. The maximum error for this specific data set is 12%.	53
4.15	Local pig velocity found with the use of the video recordings. The tracked pig velocity is shown during the time that the pig is approximately present in the FOV of the cameras.	54

5.1	Left: Averaged pig velocity divided by the mixture velocity versus u_{SG} for the experimental data. Right: Averaged pig velocity divided by mixture velocity and divided by area ratio of the pig. Data points with difference in u_{SL} are averaged to $\overline{u_{SL}} = 0.0471$ m/s.	56
5.2	Averaged pig velocity divided by the mixture velocity and area ratio versus u_{SG} . There are three distinguished regions, called Region A, Region B and Region C for small to large u_{SG} , respectively.	56
5.3	Fitted power law correlation for the normalized pig velocity versus u_{SG} . The power law formulas are made for the three various pig diameters and can be used for Region B and Region C. The coefficients for the power law formulas are presented in Table 5.1.	57
5.4	Cross-sectional view of an undersized ball pig in a pipe. Here, the cross-sectional view is divided in different cross-sectional areas. Reproduced and adapted from Richa [28].	58
5.5	Left: Leakage of the pig versus u_{SG} . Right: Leakage of the pig versus u_{SG} with fitted power laws for the various pig diameters. The difference in u_{SL} , for the experimental conditions, is averaged to $\overline{u_{SL}} = 0.0471$ m/s for the left and right graphs.	60
5.6	The leakage results from experiments, for $u_{SL} = 0.0314$ m/s, is plotted versus u_{SG} . The results are shown for the 42 mm, 45 mm, and 48 mm pig in red, blue and orange, respectively.	62
A.1	Inlet section of air and water	71
A.2	Pig launcher	71
A.3	Air flowmeter and controller	71
A.4	Liquid flowmeter	71
A.5	Picture taken at the end of the flowloop showing the upstream loop	72
A.6	End of the flowloop	72
A.7	Hold-up sensor	72
A.8	Pressure sensor (left) and the new pipe coupling (right)	72
A.9	GoPro camera	73
A.10	Lighted flowloop for the video recordings	73
A.11	Calibration certificate of the liquid flowmeter	74

List of Tables

2.1	Chosen key parameters for the non-dimensional analysis of pigging experiments. . . .	16
3.1	Specifications of the undersized ball pigs	31
5.1	Correlation coefficients for Figure 5.3.	57
5.2	Computation results of the local Reynolds number for air at the transition from Region A to Region B.	58
5.3	Correlation coefficients for Figure 5.5.	60
B.1	Experimental conditions for 42 mm pig. Here the performed combinations of water and air flow are shown. Total of 26 pigging runs.	77
B.2	Experimental conditions for 45 mm pig. Here the performed combinations of water and air flow are shown. Total of 24 pigging runs.	77
B.3	Experimental conditions for 48 mm pig. Here the performed combinations of water and air flow are shown. Total of 24 pigging runs.	78
B.4	Experimental conditions for 50 mm pig. Here the performed combinations of water and air flow are shown. Total of 16 pigging runs.	78

Nomenclature

α_G	Gas hold-up fraction	[–]
α_L	Liquid hold-up fraction	[–]
λ	Pipe friction coefficient	[–]
μ	Dynamic viscosity of the fluid	[kg m ⁻¹ s ⁻¹]
ν	Kinematic viscosity of the fluid	[m ² s ⁻¹]
ρ	Density of the fluid	[kg m ⁻³]
τ_w	Wall shear stress	[kg m ⁻¹ s ⁻²]
A	Inner surface area of the pipe	[m ²]
A_G	Used surface area by the gas	[m ²]
A_L	Used surface area by the liquid	[m ²]
A_{ratio}	Surface area ratio of frontal pig surface divided by pipe surface	[–]
D	Inner pipe diameter	[m]
d	Diameter of the pig	[m]
f	Body forces	[kg m ⁻¹ s ⁻²]
$F_{buoyancy}$	Buoyancy force of the pig	[kg m s ⁻²]
$F_{friction}$	Friction force between the pig and the pipe wall	[kg m s ⁻²]
F_{GL}	Froude number	[kg m ¹ s ⁻²]
F_{net}	Net force on the pig	[kg m s ⁻²]
g	Gravitational acceleration	[m s ⁻²]
L	Length of the pipe	[m]
l	Reference length	[m]
L_{local}	Local Reynolds length scale between pig and pipe	[m s ⁻¹]
m_G	Mass flow rate for gas	[kg s ⁻¹]
m_L	Mass flow rate for liquid	[kg s ⁻¹]
p	Pressure	[kg m ⁻¹ s ⁻²]
Q_{air}	Air volumetric flow rate	[L min ⁻¹]
Q_{fl}	Liquid volumetric leakage flow rate	[m ³ s ⁻¹]
Q_{liq}	Water volumetric flow rate	[L min ⁻¹]
R	Radius of the pipe	[m]
S_{pig}	Surface area of the pig	[m ²]

T	Temperature	[K]
t	Time	[s]
T_{sur}	Surface force exerted on the pig	$[\text{kg m}^{-1} \text{s}^{-2}]$
U	Reference velocity	$[\text{m s}^{-1}]$
u_i	Velocity in the i-th direction	$[\text{m s}^{-1}]$
u_j	Velocity in the j-th direction	$[\text{m s}^{-1}]$
u_G	Bulk velocity of gas flow	$[\text{m s}^{-1}]$
u_{local}	Local fluid velocity past the pig	$[\text{m s}^{-1}]$
u_L	Bulk velocity of liquid flow	$[\text{m s}^{-1}]$
u_{SG}	Superficial gas velocity	$[\text{m s}^{-1}]$
u_{SL}	Superficial liquid velocity	$[\text{m s}^{-1}]$
V'_{pig}	Pig velocity	$[\text{m s}^{-1}]$
V_f	Average liquid film velocity	$[\text{m s}^{-1}]$
V_G	Gas volumetric flow rate	$[\text{m}^3 \text{s}^{-1}]$
V_L	Liquid volumetric flow rate	$[\text{m}^3 \text{s}^{-1}]$
V_m	Mixture velocity	$[\text{m s}^{-1}]$
V_{pig}	Averaged pig velocity	$[\text{m s}^{-1}]$
V_{sphere}	Volume of the sphere	$[\text{m}^3]$
W	Weight	[kg]
x_i	Distance in the i-th direction	[m]
x_j	Distance in the j-th direction	[m]

Introduction

1.1. What is ball pigging?

Onshore and offshore pipelines provide a safe and effective solution for the transport of fluids from wells to the production plants in the oil & gas industry. As the reservoirs can be at remote locations, these pipelines could span a large distance, especially gas-condensate pipelines, with existing examples between 100 and 200 kilometers [8].

Some of these pipelines are used to transport single-phase fluids (gas or oil) and others operate under multiphase flow conditions (gas with condensate or water). The gas phase moves with a relatively high velocity and is driven by a pressure drop. The liquid phase is transported by the drag of the gas phase with a velocity lower than the gas phase. When the gas phase velocity becomes too low, it is no longer able to drive the liquid phase forward. An accumulation (a.k.a. hold-up) of liquid in the pipe system will occur. As a result, a slug flow can develop. These characteristics can be present at low production rates or at the end of the field life of a reservoir.

An extension of the life span of reservoirs can be obtained with the control of the liquid holdup, guaranteeing steady flow and production. For the control of this liquid hold-up and regular maintenance of the pipeline, so-called pigs are conventionally used. A pig (Pipeline Inspection Gauge) is a device that is launched from a 'pig launcher', into the pipeline, and is received at the 'pig receiver'. Propelled by the production fluids transported in the pipe, the pig can be used to collect the liquid in front of it, controlling the liquid hold-up and generating a liquid slug. The liquid slug will grow during the time that the pig resides in the pipeline, creating a so-called pig-generated volume. As the downstream production plant requires an uninterrupted supply, the pig-generated volume needs to be temporarily stored downstream of the pipeline and upstream of the plant in a slugcatcher. These slugcatchers need to be able to capture the pig-generated slug and guarantee uninterrupted gas supply to the plant. Therefore, the size of these slugcatchers are reported to be as large as 5000 m³. These slugcatchers require a significant amount of space and are expensive. Figure 1.1 shows an enormous slugcatcher designed for a maximum of 44000 barrels (≈ 5246 m³).

To reduce this pig-generated volume, research has been done in the past decades to improve the conventional pig. The conventional pig is fully sealed and travels with a velocity equal to the mixture velocity of the fluid. A by-pass pig can be used as a more attractive alternative. This pig has an opening in the centre of the pig, in which gas is able to propagate through the pig. In Figure 1.2 the difference between a by-pass pig and a conventional pig can be observed. The holes in the body of a by-pass pig will result in a lower travel velocity of the by-pass pig, compared to the conventional pig. A lower travel velocity of the by-pass pig will achieve a longer residence time in the pipeline. As more time will be available for the pig-generated slug to be drained from the slugcatcher, the size of the slugcatcher for storing the liquid can be smaller.



Figure 1.1: Zhuhai Gaolan Terminal slug catcher designed for a maximum of 44000 barrels ($\approx 5246 \text{ m}^3$). Reproduced from Thronson [33].

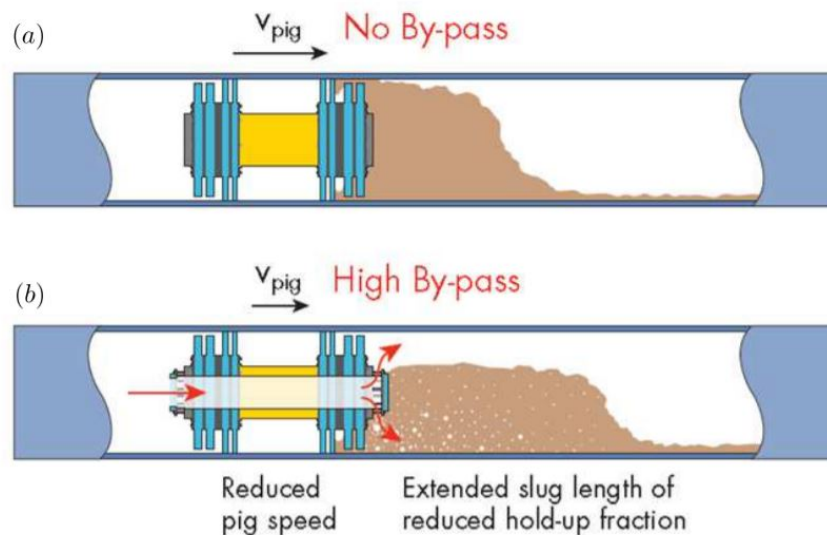


Figure 1.2: Pipeline multiphase flow with a Conventional pig (a) and By-pass pig (b). Reproduced from Hendrix et al. [16].

With a by-pass pig, less pig-generated liquid needs to be temporarily stored in the slugcatcher and therefore the size can be reduced; the size of the slugcatchers can be reduced by a factor of 4-5 if a by-pass pig is used, according to Singh and Henkes [31].

The use of by-pass pigs has been a success and companies such as Shell deployed this technology globally [11]. Even though the by-pass pig will generate a lower slug volume than the conventional pig, it can still pose volumes exceeding the slugcatcher. Furthermore, the combination of pigging in long pipelines at low flow rates can impose a large liquid volume, which increases the risk of pig stalling in the pipeline. To reduce the risk of stalling and exceeding the volume of the slugcatcher, undersized ball pigs can be deployed prior to launching the by-pass pig. The sketch of an undersized ball pig deployment is given in Figure 1.3. The undersized ball pig will be smaller than the pipe internal diameter (e.g., $0.9 \cdot D$) and will not experience significant friction with the pipe wall. Depending on the amount of liquid in the pipe and the density of the ball pig, the pig may flow to the top or bottom of the pipe and experience some wall friction. The combination of the continuous leaking volume of liquid across the ball pig and

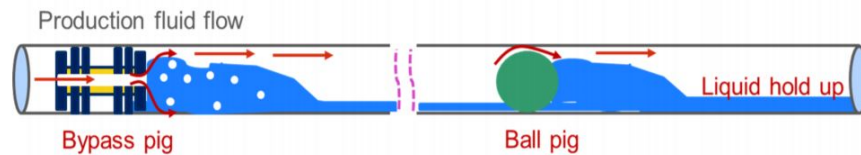


Figure 1.3: Pipeline multiphase flow with undersized ball pigging prior to by-pass pigging. Reproduced from Jiang [19].

the small wall friction will practically eliminate the risk of stalling. Furthermore, the pig-generated volume for the ball pig will be smaller than for the by-pass pig as the ball pig will leak more liquid volume. As a result, the required capacity size of the slugcatchers can be reduced. The use of undersized ball pigging has been applied in the F-14 pipeline in Sarawak [4]. A successful operation in a 20" diameter and 30 kilometer long pipeline has shown positive results of this application. The ball pig used in the F-14 pipeline did not show significant wear after use. This means that undersized ball pigging is both technically and operationally feasible.

1.2. Literature overview

This section will give an overview of the available literature related to undersized ball pigging. First of all, a brief overview of the history of pigging. After the first oil pipelines were taken into service in the 1870s, it was noted that appropriate internal maintenance is needed when transporting large amounts of fluids. The appearance of higher pumping pressures did lead to the build-up of wax, other debris, and internal flow restriction [9]. It became clear that cleaning of these pipes over time was essential. The first pigs used were straightforward bundles of rags tied together. Over time, these bundles of rags were replaced by bundles of leather. Leather resulted in a stronger pig, absorbing more fluid and giving a better seal between the pig and the pipe. Later on, steel body pigs with urethane cups or discs were purposefully built [16]. The 1960s gave birth to polyurethane foam pigs. Moreover, instrumented pigs not only to clean but also inspect the condition of the pipe were built [9]. From the 1960s till now, numerous sorts of cleaning and inspection pigs have been designed. From the removal of solids and liquids to the spraying of corrosion inhibitors into the pipe and measuring the remaining wall thickness with Magnetic Flux Leakage technology [13]. These are only a few examples for which pigs can be used.

The 1960s also gave birth to the research on the characteristics of ball pigging. Numerical and experimental models have been established to understand the dynamics of ball pigging. An overview of the relevant literature related to undersized ball pigging will be discussed below as divided into three sections:

- 1. Fluid flow models for ball pigging
- 2. Experimental measurement techniques for undersized ball pigging
- 3. Ball pigging in engineering pipeline operations

1.2.1. Fluid flow models

Ball pigging is directly related to the classical flow around a sphere and the flow around a sphere in a pipe. Extensive research on the five distinct fluid flow ranges of single phase flow around a sphere can be found in Jones and Clarke [20]. In the present study, not single phase, but multiphase flow is researched. Adding a second phase to the fluid flow around a sphere in a pipe creates an enormous complexity. Two-phase flow in a horizontal pipe can be observed in different flow regions depending on the superficial gas and liquid velocities. Several authors have researched the flow patterns and made flow regime maps from experimental work for different conditions [24, 35]. The flow patterns are not only depending on the velocities of both phases, but also on more parameters such as the geometry, fluid types and pressure. Vallee et al. [34] did multiphase experiments in a horizontal rectangular channel instead of a pipe and made a flow pattern map. Belgacem et al. [3] did multiphase experiments for a horizontal pipeline subjected to a sudden contraction and reviewed it with correlations from literature. Zoetewij [39] derived relations for the slug length and slug frequency valid for the short and long slug derived regime in multiphase pipe flow.

It is clear that two-phase flow in a horizontal pipe without a sphere is quite complex. Ball pigging - a sphere in a two-phase pipe flow - will even give a more complex flow behaviour. The first relevant publication on ball pigging is probably the one by McDonald et al. [25] with a mathematical pigging model for gas-liquid pipelines. Barua [2] improved this mathematical model. Kohda et al. [21] presented a pigging model for full two-phase transient pipe flow with spheres. A study of Minami et al. [26] presented a model for estimating the liquid slug size and outlet flow rate during the production of a slug.

The models and literature referred to are valid for oversized ball pigs, meaning that the ball pig is completely sealed within the pipe. No leakage of liquid and gas can occur across the ball pig and friction of the pig with the pipe wall exists. As a consequence, these models and correlations cannot be used for undersized ball pigging. Undersized ball pigging gives leakage and experiences a rather small friction.

Models and literature of undersized ball pigging is scarce. Bhattacharjee et al. [4] developed and validated a dynamic model to simulate undersized ball pigging in a multiphase pipeline. The dynamic

model developed employed the OLGA transient pig model. This model incorporates an empirical correlation of the pressure loss across an undersized ball pig by specifying the static force between the flow and the pig. Benchmarking model with field data from the F-14 pipeline in Sarawak showed good results for capturing the liquid outflow recovery and gas outflow rate. Richa [28] developed an analytical steady-state 1-D model for undersized ball pigging. The analytical model can be used to estimate the residence time of the pig and the pig generated slug. This analytical model is also compared with the field data from the F-14 pipeline in Sarawak. The comparison showed an overprediction of 14% for the residence time and a significant inaccuracy in predicting the pig generated slug size.

1.2.2. Experimental measurement techniques

To validate the fluid flow models for ball pigging, experiments need to be done as well. Here, an overview of the used techniques in previous pigging experiments will be given. Earlier studies [16, 17] have done experiments on by-pass pigging with an experimental loop available at TU Delft. This loop will also be used for the undersized ball pigging experiments in the present study. In [16] an experimental study was done for single phase by-pass pigging. At the beginning of the loop, a pig 'launcher', operated by a set of valves, is used. Furthermore, pressure sensors and cameras were used. Two pressure sensors can be used to measure the pressure difference over the pipe length between the sensors. As for the cameras, multiple GoPros were used and can be stitched together to form a wide video. This wide video can analyze the behaviour of the pig over a longer distance. In multiphase flow, it can even observe the liquid hold-up behind the pig. Flow meters for gas and liquid were also implemented. A similar experimental setup for the research of by-pass pigging was used by Chen et al. [7].

Another Master Thesis on the design of an experimental loop for pigging activity [23] suggested the operation of the pig 'launcher' and pig 'receiver' by a set of valves. Tracking of the pig was suggested to be done by GPS.

Zhou et al. [38] used a high speed camera to determine the pig speed at ten different observation marks. Five pressure sensors were used to determine the driving pressure of the pig and flow meters were used to accurately choose the flow velocities. A water pump and air compressor were used to create multiphase flow. Furthermore, a pig 'launcher' and pig 'receiver' were built in. The experimental setup was designed to track and analyze the pigging event in a pipe system with a negative slope.

The use of wheels which measure the velocity of the pig, called an odometer, can also be applied in pigging experiments [29]. The odometer is connected to the pig and the wheels touch the pipe wall. The pig velocity is derived from the time needed for every revolution. The position and velocity of the pig can then be analyzed. For experimental ball pigging, the use of an odometer is not possible due to the large influence on the flow around a ball pig.

Field tests with modern smart balls for pipeline inspection are described by Selvaraj [22]. The balls, including Lagrangian Autonomous Sensors, are equipped with a tri-axial accelerometer, gyroscope and magnetometer. This combination is commonly referred to as 'the inertial motion unit (IMU)' or 'the inertial navigation system (INS)' with additional sensors. IMU systems are used to obtain the position and angular orientation of the pig, but have an inherent bias and high magnitude noise. The position and angular orientation of the pig will very quickly drift away from the true position. An additional velocity sensor as an external reference is needed to correct this error [1]. Without the additional sensor, an accuracy of 1-5% of the travelled distance can be obtained. Zhang et al. [37] also used an IMU system and in particular an acceleration sensor to measure the vibration phenomenon of pigging in natural gas pipelines.

Fethke et al. [12] used two photo-diodes on the pig pointing to the inner wall of the pipe to measure the velocity. The light intensity picked up by the photo-diodes along the pipe is used to determine the time lag between the photo-diodes with the help of cross-correlation. The fixed distance between the photo-diodes in combination with the time lag will give the velocity of the pig. The performance of their processor was not good enough to accurately determine the velocity of the pig. A better processor can provide a reasonably accurate velocity measurement. Next to the two photo-diodes, another kind of

measurement is needed to notify when the pig has a low velocity or stalls because the diodes are not able to measure this. Using photo-diodes attached to the pig will not be possible for ball pigging. It will obstruct the measurements and it is difficult to mount on the pig.

Concerning the available experimental loop at TU Delft, a choice was made on the techniques that were already available and other techniques that could be implemented. Pressure sensors and cameras were already available in the experimental loop. Comparing the techniques and the possibilities of implementing them into the existing experimental loop, a choice was made to improve the current measurement techniques and install a couple of new measurement devices.

1.2.3. Ball pigging in engineering pipeline operations

How does ball pigging work in actual field operations? Here, the literature about pigging operations will be reviewed. Cordell et al. [8] reviewed the general pig 'launching' and pig 'receiving' stations for different types of pigs. Furthermore, the pig launching and receiving stations for spheres are shown. Figure 1.4 shows a typical sphere launcher with a number of spheres stored for remote-controlled use. Some valves are required to fill the pig launcher with spheres and release them in the pipeline. More information can be found in [8]. The pig receiver works in the same manner to catch the pigs. There also is a downstream slugcatcher for the temporary storage of the pig-generated liquid slug.

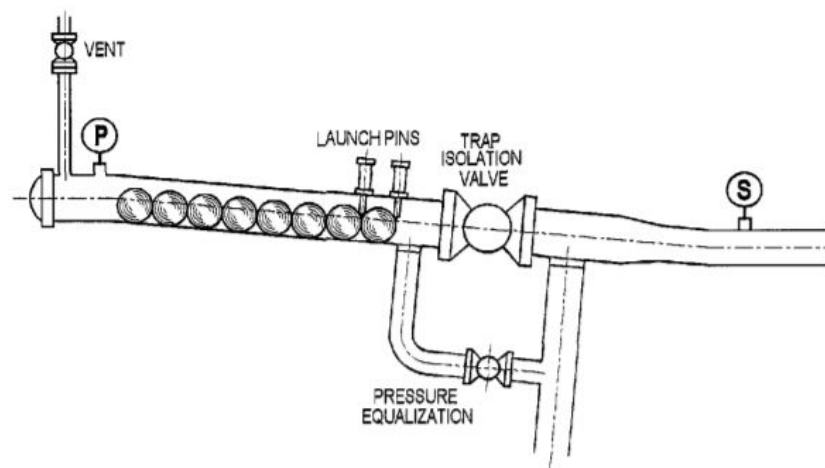


Figure 1.4: A typical sphere launcher with a number of spheres stored for remote controllable use. Reproduced from Cordell and Vazant [8]

The pipeline can also have all sorts of valves, bends, and tees. In [5] it is stated that every new pipeline section should be able to accommodate internal inspection devices according to governmental rules. Since ball pigs have a spherical shape, they are able to flow in pipeline tees or get stuck in sections of pipeline with a smaller diameter than the ball pig. This could result in damage to the equipment. Therefore, precautions and research on the pipeline to be pigged need to be accomplished for. In this study, safe operation in experimental pigging was also needed. Safety precautions and procedures are developed and rerated from previous TU Delft documents with equivalent experimental setups.

1.3. Research question

Section 1.1 has shown the advantages and motivation of the use of undersized ball pigging prior to by-pass pigging in industrial applications of pipeline transport of single-phase and multiphase fluids. Furthermore, the available literature on undersized ball pigging has been reviewed, which was found to be scarce. Reliable correlations are lacking.

This study builds on the recent Master Thesis study by M. Jiang [19], who carried out undersized ball pigging simulations under single phase flow conditions, using the Fluent Ansys CFD package. In the present Master Thesis project, multiphase undersized ball pigging experiments are carried out in the available water-air flow loop in the Process & Energy Laboratory of TU Delft.

The research question of the present study is: "Which observations and what factors are associated with the flow around an undersized ball moving in a pipe driven by multiphase flow, and how can that knowledge be used to derive a better understanding and an engineering correlation for the use of pigs in industrial pipeline operations?" The particular interest is in the pig velocity and in the amount of leakage past the pig.

With the help of a non-dimensional analysis, an engineering correlation is developed for undersized ball pigging. The observations, results, and correlations are expected to help obtaining a more precise and extended operation of undersized ball pigging in the industry. The correlations can be used in one-dimensional pipeline models which are extensively used for the simulation of multiphase flows in the industry.

1.4. Master project structure

The first part of this study, as described in Chapter 2, will focus on the theoretical background and governing equations for multiphase flow and the undersized ball pig. A non-dimensional analysis is performed using Buckingham's π theorem. This result will be used later in this study.

Thereafter, the preparation of the experimental loop will be discussed in Chapter 3. Improvement of the experimental loop was needed for safe and 'easy to use' multiphase experiments. In the past years, mainly single phase experiments were done. Equipment for multiphase experiments was available; however, improvements such as leakage prevention were required. Parallel to this, the measurement techniques in the experimental loop are reviewed, prepared, and improved. Before the start of the experiments, test runs have been done. Camera tracking, pressure measurements, liquid hold-up measurements, and a weighing scale are used. These measurement apparatus will be explained. Furthermore, the use of signal processing and data analysis is presented.

In Chapter 4, the results of the pigging experiments will be discussed. First of all, the general observations found during pigging will be discussed. The behaviour, repeatability, and recovery time of a pigging run will be presented. Next, global observations and results from the experiments are shown. Different experimental conditions were used for various size undersized ball pigs. The average pig velocity, leakage, and number of slugs will be presented with the help of multiple graphs. At last, local observations from the camera recordings and visual notes during pigging experiments are reviewed.

In Chapter 5, the results from Chapter 4 and the non-dimensional analysis from Chapter 2 are used to find a correlation and scaling for the undersized ball pig diameter ratio versus the average pig velocity. The derived leakage will also be looked at. Here, also a discussion will be made on the found results and correlation. A comparison with a numerical leakage model will also be presented. This model originates from the OLGA commercial package.

In Chapter 6, the conclusions of the current study are given. Conclusions will be made from the obtained observations, correlations, and scaling.

In Chapter 7, recommendations will be given for future research. Furthermore, advice is given for the possible continuation of this study.

2

Flow equations

In this chapter, the theoretical background of the pig in a pipe will be evaluated. First, a general analysis of the problem is sketched. Based on the analysis, some simplifications and assumptions are made. Second, the governing equations for the undersized ball pig and fluid are described. At last, a non-dimensional analysis is performed to find the dimensionless groups related to the pig.

2.1. Problem analysis

The pig under investigation in this study comprises an undersized sphere in a pipe. The diameter of the sphere is smaller than the internal diameter of the pipe and can vary between zero and the pipe inner diameter. The sphere can be located vertically anywhere in the pipe depending on the flow. In this study, it is apparent that the sphere will touch the top or bottom of the pipe. Due to complexity, it is decided that the friction will not be considered.

Depending on the forces on the sphere and material of the sphere, a deformation can occur. In this study, it is assumed that the pipe and ball pig are rigid and impermeable so that no deformations occur. Next to the sphere, a multiphase (air and water) flow is present in the pipe. The flow in the pipe before pigging is a wavy stratified flow with the liquid (water) at the bottom and gas (air) at the top of the pipe. The ball pig is inserted when a wavy stratified flow exists. During wavy stratified flow, the liquid phase velocity will be a lot smaller than the gas phase velocity. After release, detailed exerted forces are present on the pig. Assuming steady state, the pig will have a velocity between the gas phase and liquid phase velocity. In reality, the pig will have a constantly varying velocity between the gas phase and liquid phase velocity due to liquid accumulation.

2.2. Governing equations of pipe flow

In fluid mechanics, the general governing equations for fluid flow are the Navier-Stokes equations. The equations express the conservation of mass and conservation of momentum for Newtonian fluids. The flow field variables of velocity and pressure can be described by the coupled nonlinear partial differential equations. The Navier-Stokes equations are really useful, because they are able to describe many physical phenomena with fundamental and engineering relevance. The general mass and momentum conservation equations for a Newtonian fluid, making use of the Einstein summation convention, are:

$$\frac{\partial u_i}{\partial x_i} = 0 \quad (2.1)$$

$$\rho \left[\frac{\partial u_i}{\partial t} + \frac{\partial}{\partial x_j} (u_j u_i) \right] = - \frac{\partial p}{\partial x_i} + \mu \frac{\partial}{\partial x_j} \left(\frac{\partial u_i}{\partial x_j} + \frac{\partial u_j}{\partial x_i} \right) + f \quad (2.2)$$

Where:

- ρ is the density of the fluid
- μ is the viscosity of the fluid

- f is the body force acting on the fluid
- u_i and p are the velocity and pressure variables used to describe the motion of the flow.
- x_i defines each direction in a coordinate system.

Both equations (2.1) and (2.2) are the Navier-Stokes equations for an incompressible flow. An extended version of the Navier-Stokes equations, taking compressibility into account, should be used for air and can be found in [30]. Water is assumed incompressible.

In fluid mechanics, dimensionless numbers are often used to describe and analyze the behaviour of fluids. When considering the dimensionless form of the Navier-Stokes equations, the Reynolds (Re) number comes into play. The Reynolds number, widely used, represents the ratio of the inertia force and the viscous force in a flow. The general definition of the Reynolds number, originating from the ratio of the forces, is:

$$Re = \frac{\rho U^2 / l}{\mu U / l^2} = \frac{\rho U l}{\mu} \quad (2.3)$$

Where:

- U is the reference velocity of the fluid
- l is a characteristic reference length

The choice for the reference velocity of the fluid and the characteristic reference length depends on the considered configuration. In pipe flow, the reference velocity of the fluid is the bulk velocity over the cross-sectional area of the pipe and the characteristic reference length is the diameter of the pipe. For single-phase fully developed flow, it has been found in experiments that a transitional flow from laminar to turbulent occurs between Reynolds numbers 2000 to 3000. The Reynolds number is often used for single phase flow and calculated to determine the behaviour of the flow.

The general equations given above are the most commonly used equations for any flow. Here, pipe flow will be discussed in more detail. An important quantity in pipe flow is the pressure drop. When the fluid flows through a pipe, there will be a pressure drop as a result of resistance to flow. Furthermore, elevation between the start and end of the pipe can result in a pressure loss or pressure gain. The overall pressure difference in a pipe is related to:

- *Friction between fluid and the wall of the pipe*
- *Friction loss as fluid passes through pipe components*
- *Friction alongside layers of fluid*
- *Pressure loss due to change in elevation if the pipe is not horizontal*
- *Pressure gain due to fluid head added by a pump*

Here, a single-phase horizontal circular pipe without a pump is considered which reduces the Navier-Stokes equations to a formula for the pressure loss in a pipe equation (2.4):

$$\Delta p = \lambda \cdot \frac{L}{D} \cdot \frac{\rho}{2} \cdot U_x^2 \quad (2.4)$$

With:

- λ the pipe friction coefficient (for turbulent flow to be determined via correlations)
- L, D, ρ, U_x the length, diameter, density and bulk velocity of the pipe and fluid respectively.

For the calculation of this pressure loss, a bulk velocity of the fluid is needed. This bulk velocity can be calculated with Equation (2.5) while using polar coordinates:

$$U_x = \int_0^R 2\pi r \bar{u}_x dr / (\pi R^2) \quad (2.5)$$

R is the radius of the pipe and \bar{u}_x is the averaged velocity of the fluid along the radius of the pipe. Here, an incompressible, fully developed turbulent flow is assumed. Fully developed turbulent flow means that the velocity profile along the length of the pipe will not change. This means that $\frac{\partial}{\partial x}(\bar{u}_x) = 0$. The following velocity profiles for single phase pipe flow can be observed in Figure 2.1.

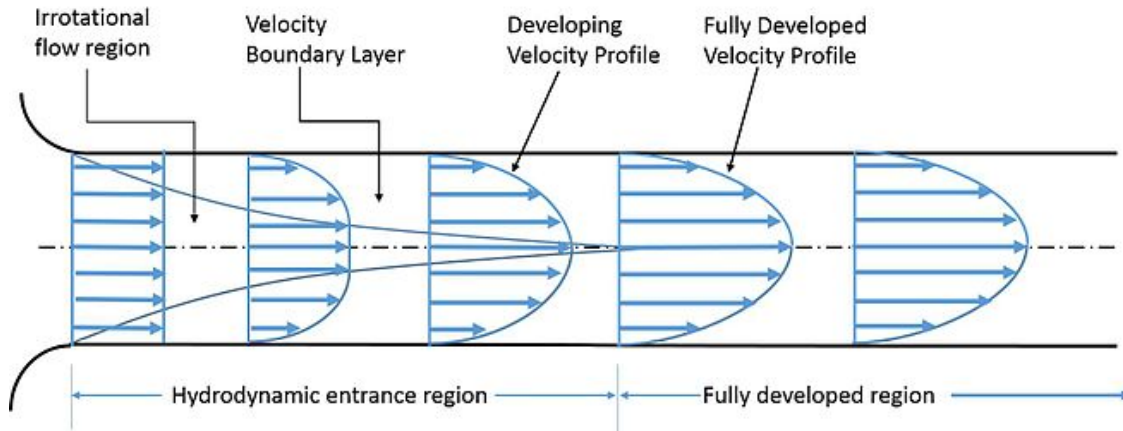


Figure 2.1: Velocity profiles for developing pipe flow and pipe flow in the fully developed region. Reproduced from Starks et al. [32].

These velocity profiles are for single phase flow. The velocity profiles become different when observing stratified multiphase flow. Both phases will have a no-slip condition at the pipe wall, but will also interfere with each other at the interface. At the wall, large velocity gradients are present for both phases just as in single-phase flow. Now, at the interface of the two phases, a so-called slip velocity will arise. Here, at the interface, also large velocity gradients are present. A stratified velocity profile for a gas (lighter) on the top of the pipe and a liquid (heavier) on the bottom of the pipe can be seen in Figure 2.2.

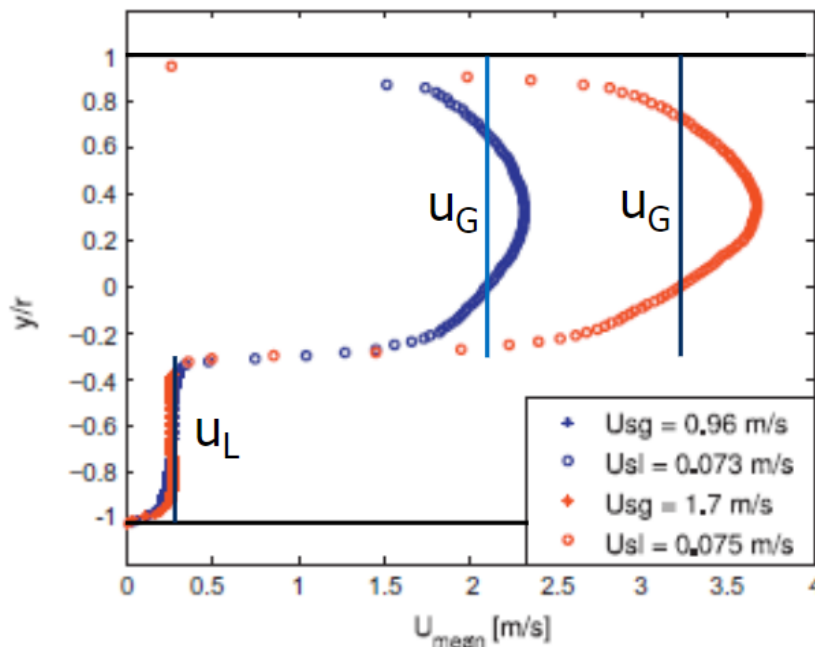


Figure 2.2: Velocity profile for multiphase flow with gas on the top of the pipe and liquid on the bottom of the pipe. y-axis: Non-dimensional position in the pipe with radius r . x-axis: Velocity of the flow in the pipe. Reproduced from Henkes [18].

Often used quantities for multiphase pipe flow and in this study are superficial velocities (2.6)(2.7), hold-up (2.8)(2.9), bulk velocities (2.10)(2.11), and mixture velocity (2.12). These definitions are, respectively, as follows:

$$u_{SG} = \frac{\dot{V}_G}{A} = \frac{\dot{m}_G}{\rho_G A} \quad (2.6)$$

$$u_{SL} = \frac{\dot{V}_L}{A} = \frac{\dot{m}_L}{\rho_L A} \quad (2.7)$$

$$\alpha_G = \frac{A_G}{A} \quad (2.8)$$

$$\alpha_L = \frac{A_L}{A} \quad (2.9)$$

$$u_G = \frac{\dot{V}_G}{A_G} = \frac{u_{SG}}{\alpha_G} \quad (2.10)$$

$$u_L = \frac{\dot{V}_L}{A_L} = \frac{u_{SL}}{\alpha_L} \quad (2.11)$$

$$V_m = \frac{\dot{V}_G + \dot{V}_L}{A} \quad (2.12)$$

Where:

- \dot{V}_G and \dot{V}_L are the volumetric flow rates of the gas and liquid, respectively.
- \dot{m}_G and \dot{m}_L are the mass flow rates of the gas and liquid, respectively.
- ρ_G and ρ_L are the densities of the gas and liquid, respectively
- A is the surface area of the pipes flow direction
- A_G and A_L are the surface area used by the gas and liquid, respectively.

These equations can be used for stratified and non-stratified flow. Stratified multiphase flow shown in Figure 2.1 is able to transition from a stratified to a non-stratified flow. The result of a stability analysis (ignoring friction) in a pipe [18] gives that a stratified flow becomes unstable if:

$$\frac{F_{GL}}{\sqrt{\cos(\theta)}} > \sqrt{\alpha_G \left(1 + \frac{\rho_G \alpha_L}{\rho_L \alpha_G}\right) \frac{\pi D}{4p_i}} \quad (2.13)$$

$$F_{GL} = \sqrt{\frac{\rho_G}{\Delta\rho} \frac{(u_G - u_L)^2}{gD}} \quad (2.14)$$

Where:

- g is the gravity constant
- θ is the pipe angle with respect to the horizontal
- F_{GL} is the Froude number

Equation (2.13) and (2.14) are called the inviscid Kelvin-Helmholtz instability criterion for twophase pipe flow. The Kelvin-Helmholtz instability is used to determine the stability between two liquid interfaces. Whenever a stratified flow is not stable enough to exist, then either slug or bubble flow will appear. Depending on α_G the result is:

- α_G high - Slug flow
- α_G low - Bubble flow

- α_G medium - Bubble blow only if turbulence is strong

In this study, a wavy stratified multiphase flow will be created. Because of the presence of the undersized ball pig with disturbances at the interface of the ball, the multiphase flow will produce a condition for the flow to become unstable. The created instability will be discussed below. Figure 2.3 displays the discussed stratified and stratified wavy flow. Furthermore, it shows the appearance of slug flow and bubble flow whenever stratified flow can not exist. Figure 2.3 shows all the different flow regimes for two-phase gas and liquid flow in horizontal pipes.

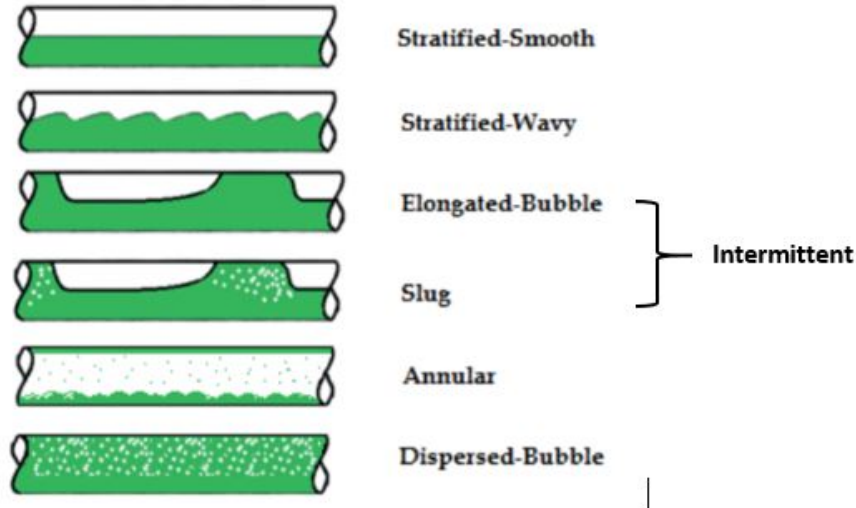


Figure 2.3: Different flow regimes for two-phase gas and liquid flow in horizontal pipes. Reproduced and adapted from Diaz [10].

To create stratified and or stratified wavy flow, certain conditions in a horizontal pipe need to be satisfied. These conditions in particular are the superficial gas u_{SG} and superficial liquid velocity u_{SL} . The indicated flow regimes for two-phase gas and liquid flow are indicated with a flow-map in Figure 2.4. The superficial gas velocity and superficial liquid velocity can be chosen such that a specific flow regime is created.

2.3. Governing equations of the undersized ball pig

The fluid mechanics of the present multiphase flow in the pipe will propel the undersized ball pig through the pipe. The liquid and gas will push the pig forward. Multiple forces have interaction with this undersized ball pig. Using the second law of Newton, a general equation for the motion of the pig can be derived:

$$m \frac{dV_{pig}}{dt} = T_{sur} \cdot S_{pig} - F_{friction} - (mg_i - F_{buoyancy}) \cdot \cos(\theta) - (mg_i - F_{buoyancy}) \cdot \sin(\theta) \quad (2.15)$$

In this equation, m and V'_{pig} are the mass and velocity of the pig, respectively. The left hand side is the acceleration of the pig and the right hand side are the forces exerted on the pig in the axial and perpendicular direction of the pipe. When the summed forces on the right are zero, no acceleration of the pig will be present. The T_{sur} represents the surface force that can be decomposed into a viscous and pressure force. The decomposition is found by applying the constitutive equation. S_{pig} stands for the surface area of the pig. A surface force times a surface will give a force. The second term, $F_{friction}$, is the friction of the pig with the pipe wall. The dynamics of the flow in combination with the pig can push the pig to the wall of the pipe. Obtaining quantitative data for this friction value will be merely difficult due to the rapidly changing dynamics and behaviour in the pipe. The third and fourth term represent the gravity and buoyancy terms decomposed in the perpendicular and axial direction of the pipe, respectively. The inclination angle (θ) is used to perform this decomposition. Depending on

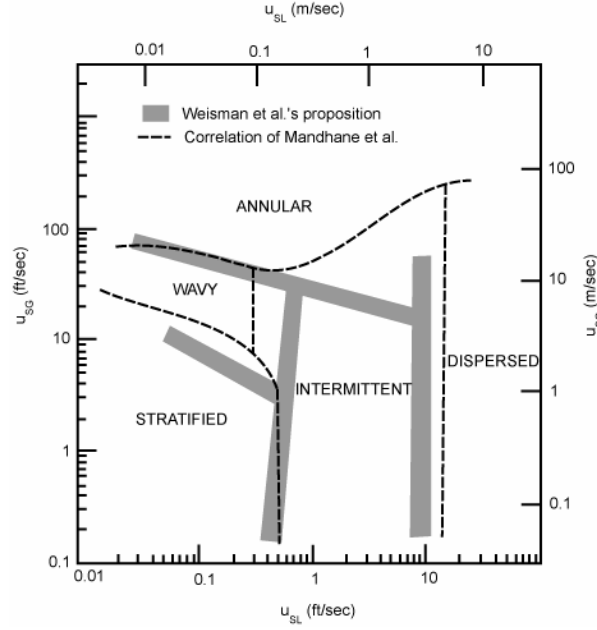


Figure 2.4: Flow-map indicating the different regimes for two-phase gas and liquid flow in a horizontal pipe. The superficial liquid velocity is shown on the horizontal axis and the superficial gas velocity on the vertical axis. Reproduced from Weisman et al. [35].

the amount of liquid in the pipe and the weight and volume of the ball, a buoyant pig can occur. Pigs will be created with a certain buoyancy.

When neglecting the acceleration, assuming the friction to be equal to zero, and having a horizontal pipe (i.e., $\theta = 0$), only the surface force will remain in the axial force direction. In this case, a momentum conservation law can be applied over the flow domain and the following expression for the net axial force on the pig can be obtained with Equation (2.16):

$$F = \int_{inlet} (p + \rho uu) \cdot ds + \int_{outlet} (p + \rho uu) \cdot ds + \int_{wall} \tau_w \cdot ds \quad (2.16)$$

The first two terms on the right hand side represent the integration of the pressure and momentum over the surface of the pig at the inlet and outlet of the pig for both the gas and liquid phase, respectively. The third term is the wall shear stress integrated over the surface of the pig for the gas and liquid phase.

The net axial momentum equation can be further divided for the two fluids. This is visualized in Figure 2.5 in the pig's frame of reference. This shows the balance between the positive drag force from the gas phase and the negative drag force from the liquid phase. This means, as mentioned before, that the undersized ball pig will have a velocity that is smaller than the velocity of the gas phase and larger than the velocity of the liquid phase. In the pig's frame of reference, the pig will be stationary, the gas phase velocity will be positive, and the liquid phase velocity will be negative. The pipe wall will be moving upstream with the pig velocity. Furthermore, the gas phase outlet will be downstream and the liquid phase outlet will be upstream. When assuming the defined velocities and pressure to be far away from the pig and fully developed, some conditions will be known. The exact change in pressure from (p_{G1}) to (p_{G2}) from the inlet to the outlet at every position of the pig will not be known without extensive numerical simulation. Besides, the change from ($u_G - V_{pig}$) to ($u_{G,outlet} - V_{pig}$) at every position of the pig will not be exactly known, eliminating the possibility to analytically compute the momentum and wall shear stress. This is the same for the computation of the liquid phase at every position of the pig, flowing in the upstream direction in the pig's frame of reference.

To solve this complex multiphase fluid flow, numerical simulation is needed. A start for defining the boundary conditions for the multiphase flow around an undersized ball pig has been made by M. Jiang [19].

Figure 2.5 (b) shows the net axial forces around an undersized ball pig in steady state in the pig's frame of reference. A positive force by the gas and a negative force by the liquid. The difference in the central point of contact results in a torque around the pig, which causes rotation of the pig. The influence of rotation of the pig on the flow is not captured in this study and will not be discussed further on.

Assuming negligible acceleration, assuming the friction to be equal to zero, and assuming the influence of the rotation of the pig to be negligible, will be used in the analysis of the results, even though this is not fully satisfied. The experimental measurements in this study will observe some acceleration because the velocity of the pig will start at zero. Furthermore, friction and rotation can also be present. The focus of this experimental setup are the averaged steady state parameters. This is of importance to determine correlations for the averaged pig velocity and leakage.

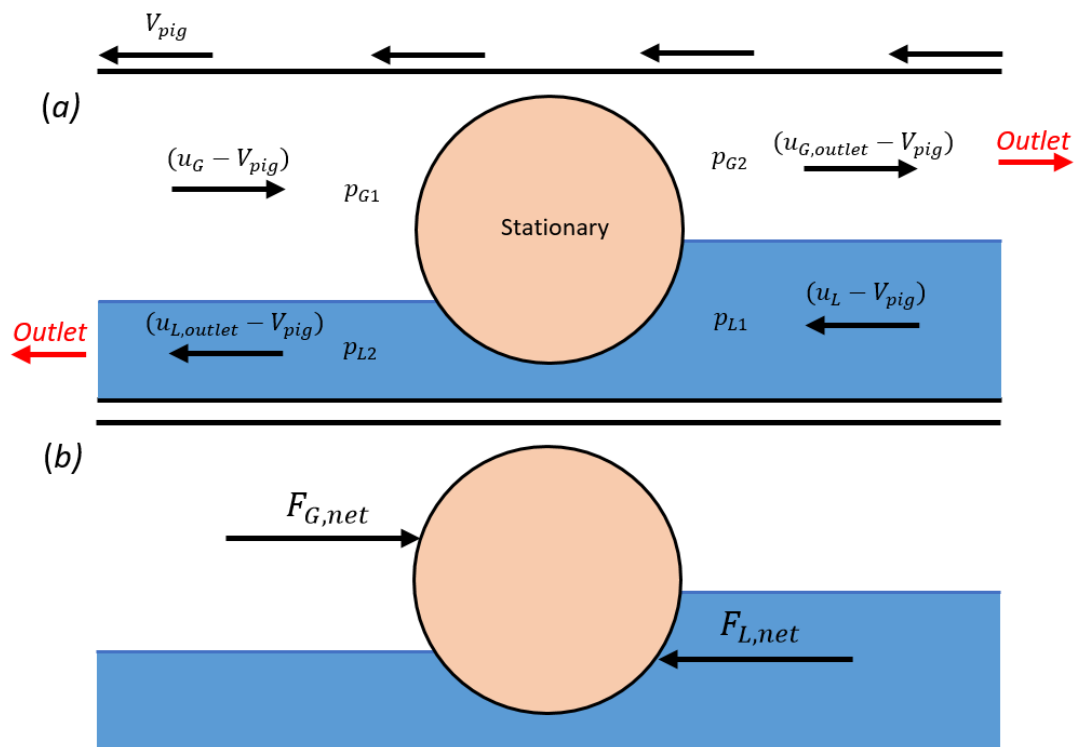


Figure 2.5: Sketch of the multiphase flow around an undersized ball pig in the pig's frame of reference. In (a) the velocities and pressure around the pig are defined. In (b) the net forces on the pig from the gas and liquid are visualized for steady state conditions.

2.4. Non-dimensional analysis

Non-dimensional analysis is the keystone for the analysis of relationships between different physical quantities. Using the rules of algebra and SI units of measure, the 'Buckingham π theorem' can be applied. This is one of the various methods used to perform a non-dimensional analysis. The goal is to simplify the physical problem and find fundamental dependencies between different quantities. The non-dimensional analysis will also be used when trying to find correlations (see Chapter 5). A simplified sketch is shown in Figure 2.6 with the assumed dependent parameters in multiphase pigging. A selection of dependent parameters for pigging experiments is chosen to be analyzed. In reality, more parameters will come into play, such as roughness of the pipe, roughness of the pig, inclination angle at every position of the pipe, pressure, and actual weight of the pig. The chosen key parameters are shown in Table 2.1 with the SI units of measure: mass (kilogram), length (m), and time (s). According to Buckingham's theory, 7 (10 - 3) dimensionless parameters can be defined.

Parameter	Units
d	[m]
D	[m]
V_{pig}	[m][s ⁻¹]
u_{SG}	[m][s ⁻¹]
u_{SL}	[m][s ⁻¹]
ρ_G, ρ_L	[kg][m ⁻³]
μ_G, μ_L	[kg][m ⁻¹][s ⁻¹]
α_L	[-]

Table 2.1: Chosen key parameters for the non-dimensional analysis of pigging experiments.

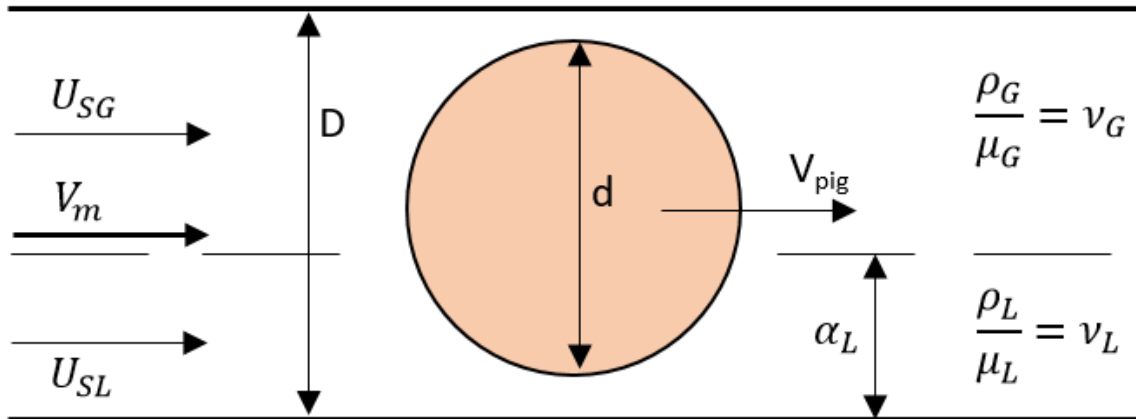


Figure 2.6: Chosen key parameters for the non-dimensional analysis of the pigging experiments.

The dimensionless parameters are as follows:

- The undersized area ratio $\frac{d^2}{D^2}$ presents the 3D area fraction of the presence of the pig in the pipe. Another approach, $1 - \frac{d^2}{D^2}$, indicates the area ratio for the flow to pass the pig.
- $\frac{V_{pig}}{u_{SG}}$ and $\frac{V_{pig}}{u_{SL}}$ are the normalized pig velocities for the gas and liquid flow. It is the ratio of the pig velocity versus the velocities of gas and liquid when one of the two would be present. Generally, these two dimensionless parameters can also be translated into $\frac{V_{pig}}{V_m}$ which represents the ratio of the pig velocity and the multiphase flow velocity. It shows the velocity of the pig in comparison with the multiphase flow velocity.

- $Re_G = \frac{\rho_G u_{SG} D}{\mu_G}$ is the Reynolds number of the gas when it would be the only flow present in the pipe. It indicates, to a certain extent, the ratio of the inertial forces versus the viscous force of the gas.
- $Re_L = \frac{\rho_L u_{SL} D}{\mu_L}$ is the Reynolds number of the liquid when it would be the only flow present in the pipe. It indicates, to a certain extent, the ratio of the inertial forces versus the viscous force of the liquid.
- $\frac{\mu_G \rho_L}{\rho_G \mu_L} = \frac{\nu_G}{\nu_L}$ is the ratio of the kinematic viscosity of the gas and liquid. It indicates the difference in fluid properties.
- The liquid hold-up α_L is already a dimensionless parameter. It indicates the fraction of liquid area compared to the total area present in the pipe. $1-\alpha_L$ represents the fraction of gas present in the pipe.

3

Experimental setup

This chapter describes the experimental flow loop, in which different kinds of experiments can be conducted, located in the Process & Energy Laboratory on the campus of Delft University of Technology. The 40 -year-old history of the flow loop started in the Shell Technology Centre in Amsterdam (STCA), where mainly slug flow experiments were done. The loop moved to the university about 20 years ago. Since then, several modifications have been made. The multiphase flow loop consisted of two straight segments with a U-turn connecting them, such that the inlet of air and water returned to the same location. The water was pumped from and captured in the same tank.

In 2016 [16] one straight segment was decoupled and a pig launcher and pig receiver were added. Single phase pigging experiments with air were conducted. This study will use the same single straight segment including the pig launcher, but improvements to the individual sections will be made. This is done such that two-phase pigging experiments can be performed. The water flow will continuously be weighed at the end of the loop and afterwards pumped back to the tank. Furthermore, some improvements in the measurement apparatus will be made. In the first section, the main characteristics of the flow loop for this study are listed. The second section presents the measurement devices. In the third section, the undersized ball pig characteristics and sizes will be shown. The fourth section discusses the operation of the experiments. The last section will present the signal processing and data analysis of each pigging run. In Appendix A.1 photos of the experimental loop and measurement equipment can be found.

3.1. Characteristics of the flow loop

A sketch of the loop is given in Figure 3.1. The 40-year-old flow loop was originally built from optically transparent PMMA pipe segments, with an individual length of 2m. Originally, two straight segments were used in the loop which were coupled with a U-bend at the end of the loop. In this study, one straight segment is decoupled and used for the experiments. The straight segment, excluding the pig launcher, has a total length of 51.92 m. The distance between the two pressure sensors is 41.40 m. The pig launcher is marked as the blue section in Figure 3.1 and is made of PVC.

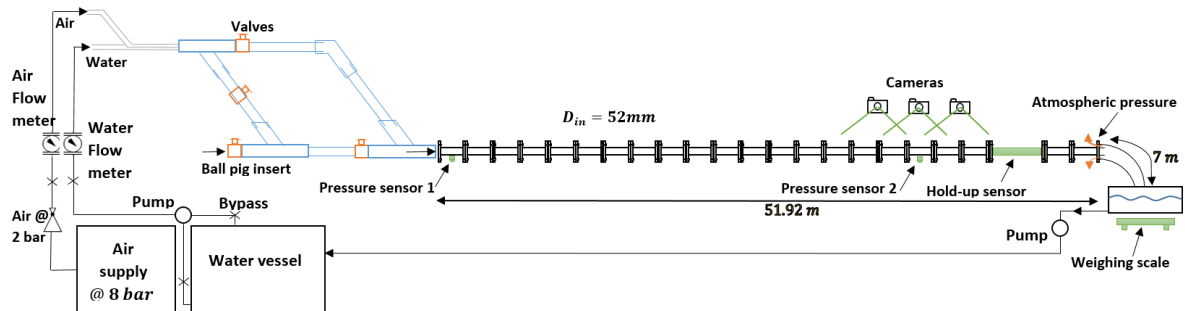


Figure 3.1: Sketch of the flow loop.

Water is pumped from a water tank passing an electro-magnetic logging liquid flow meter (explained later in detail) and pumped into the inlet section via a hose. Pressurized air is tapped from a central system and reduced from 8 bar to 2 bar with a pressure reducing valve. The air passes a gas flow meter (explained later in detail) and is transported to the inlet section with a hose. The air and water flow into the pig launcher and by using valves a pipe segment can be decoupled from the flow loop. In this case, a ball pig can be inserted into the loop while the air and water keep flowing. Switching valves redirects the flow from the upper pipes to the bottom pipes as shown in Figure 3.1. The pig launcher and inlet section used in the experimental setup are visualized in Figure 3.2. The ball pig will flow through the pig launcher and flow into the straight segment of pipes leading to a water vessel at the outlet using a flexible tube. The amount of water produced by the ball pig (a.k.a slug size) will be measured with a weighing scale before returning to the main water vessel. To reduce the suction effect of the water slug leaving the last tube segment, a short near-horizontal hose is connected to the last segment. This hose enters a larger diameter tube such that atmospheric conditions at the outlet are maintained and air can escape.

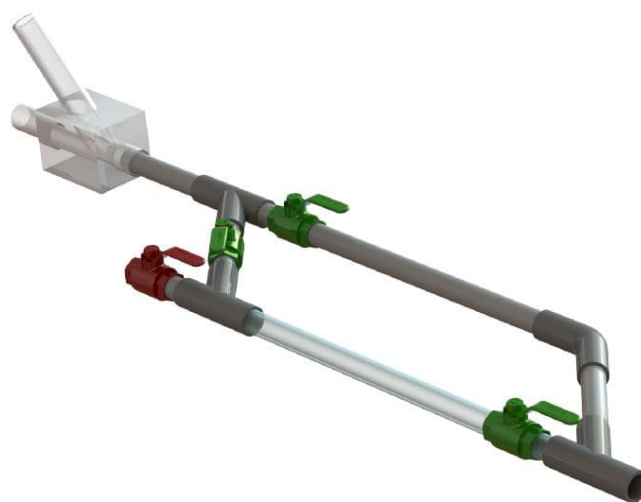


Figure 3.2: Pig launcher and inlet section 3D visualized with SolidWorks. Reproduced from Hendrix et al. [16].

The individual pipe segments are made from PMMA (PolyMethylMethAcrylaat), also known with two commercial brand names: perspex or plexiglas. The pipes are produced in two different ways. They can either be extruded or moulded. In the flow loop, both kinds of pipes are present. The inner and outer diameters of the pipes are 52 mm and 60 mm, respectively. The tolerances of the inner and outer diameters of the pipes are ± 0.7 mm and ± 0.8 mm consecutively. A previous Master Thesis Project that used this experimental setup [16] found that the manufacturer tolerances were in accordance with the measurement observations made. To connect the individual segments in the setup, PMMA couplings were used in the past. These couplings consisted of cylindrical PMMA tubes with an inner diameter larger than the outer diameter of the pipes. The couplings contained four grooves with a rubber ring to seal the flow from the outside environment. Leakage still occurred in the past and therefore new couplings are used in this study. So-called STRAUB pipe couplings are used, which are radially rated up to a pressure of 16 bar. The couplings are axially not constrained. Therefore, the loop is axially fixed at the end keeping a clearance for thermal expansion. STRAUB pipe couplings are flexible couplings with a stainless steel housing and an EPDM cuff.

The tolerances of the pipe segments as discussed above give continuous variation within a pipe segment. At the connection of the pipes, using the STRAUB pipe coupling, a sudden variation is present. With the variations present, the flow loop is aligned as horizontally as possible. According to the instruction manual of the STRAUB pipe coupling, a distance of 5 mm between the mounted pipes is needed. The couplings are mounted with ≤ 5 mm distance between the pipes to reduce flow interference and still give room for the pipes to expand. The interference of the flow with the transitions of the pipes are accepted as inevitable. The pipes are supported by small brackets and can be adjusted to get the right alignment. The alignment is done with the use of a hose reel, measuring certain points of the loop. The hose, filled with water, is fixed onto the bottom of the loop at two different points. Measuring the difference in water level in millimeters will show the difference in horizontal alignment. Figure 3.3 shows the results of the measurement of the vertical deviation in millimeters on the y-axis versus the horizontal distance from the start of the flow loop on the x-axis. The vertical difference of a couple millimeters over a 60 meter horizontal distance is relatively small and could thus be accepted.

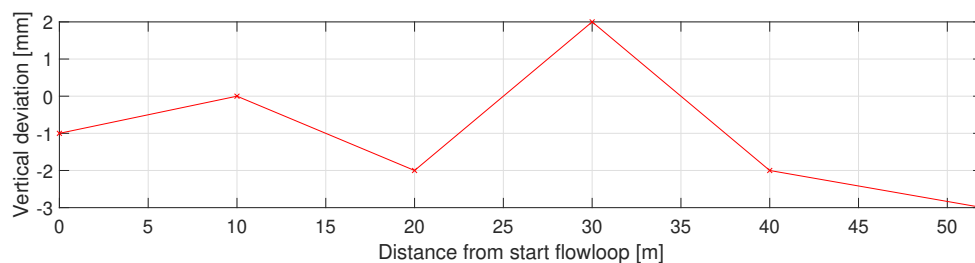


Figure 3.3: Vertical deviation over the length of the horizontal flowloop.

The measurement devices used in the experimental setup are also indicated. Two pressure sensors, three cameras, a hold-up sensor, and a weighing scale are used. The first pressure sensor is 74 cm behind the pig launcher. The second pressure is mounted 41.4 m further downstream. At the location of the second pressure sensor, three GoPro cameras are mounted. The location and field of view of the three cameras will be called the measurement section. 2.86 m before the end of the loop an 50 mm inner diameter inline hold-up sensor is placed to measure the water fraction in the pipe. At the end of the loop, a weighing scale is placed. Photos of the hold-up sensor and the flow loop can be found in Appendix A.1.

3.2. Measurement devices

Several measurement devices are used to control, monitor, and measure the pigging operations. The devices used in the experimental setup will be individually discussed. Furthermore, the data acquisition used for pigging experiments will be described.

3.2.1. Gas flow meter

In this project, an existing gas flow meter in the setup will be used. The gas flow meter (Bronkhorst - Mass-stream Series D-6300) is a mass flow meter and regulator with a fluid flux ranging from 18 L/min to 900 L/min. The output here is given in normal liters per minute. According to the manufacturer, an accuracy of 2% of the maximum flux is found under calibration conditions. The meter is calibrated at 3 bar and 20 °C. With every bar of pressure increase or decrease, the accuracy will deviate by 2%. The reducing valves in the setup reduce the air from 8 bar to 2 bar. Thus, an accuracy of 4% for the air flow measurement will be found. When taking into account the accuracy of the flow meter and the tolerance of the pipe segments, a minimum and maximum superficial gas velocity can be computed when setting a prescribed superficial gas velocity. The derivation of this minimum and maximum can be found in a previous study on by-pass pigging [16] and is shown in Equations (3.1) and (3.2):

$$u_{SG,min} = \overline{u_{SG}}(1 - a) - 0.2825(1 - a) \quad (3.1)$$

$$u_{SG,max} = \overline{u_{SG}}(1 + b) + 0.2825(1 + b) \quad (3.2)$$

Where:

- $\overline{u_{SG}}$ = the prescribed superficial gas velocity
- $a = 0.0264$
- $b = 0.0275$

Next to the accuracy of the flow meter and the tolerance of the pipe segments, a difference in actual air flow and logged air flow is present due to the output of air flow in normal liters per minute (L_n). Normal liters per minute for Bronkhorst mass flow controllers are given at $T = 273.15$ K and $p = 1013.25$ hPa(a) reference conditions. Actual conditions are different and can be computed with the following equation (3.3)

$$L/min = L_n/min \cdot \frac{T_{gas}}{273.15} \cdot \frac{1.013}{p_{gas}} \quad (3.3)$$

Where T_{gas} is approximated at 293.15 K during pigging and could in reality have differed from time to time with ± 5 K. The pressure after the gas flow meter is constantly changing during a pigging run. Therefore, the maximum mean overpressure during a whole pigging run is calculated and found to be 0.2 bar. This is the maximum found when checking all the pigging runs. This results in a maximum difference of 7% for the temperature and 2% for the pressure. The temperature difference is implemented and accounted for in the pigging runs. The pressure difference is not implemented due to constantly changing pressure and the small difference. Nevertheless, it is of importance to mention the difference.

3.2.2. Liquid flow meter

In this project, a new liquid flow meter is installed in the setup. In the past, four rotameters with different ranges were used. The new magnetic liquid flow meter (Bronkhorst MAG-VIEW MVM 200-QA) is a logging device with a measuring fluid flux ranging from 4 L/min to 200 L/min. According to the manufacturer, an accuracy of $\pm 1\%$ reading difference is found under calibration conditions. The reading difference is defined as: "Closeness to the actual value expressed as percentage of the actual value"¹. The output of the liquid flow meter is a current output between 4 mA and 20 mA. A precision resistor (Alpha PDY250R00A | accuracy: $\pm 0.05\%$) of 250 Ohm for the acquisition device is used. This will change the current output to a voltage measurement over the resistor. Using Ohm's law, this translates into a voltage measurement between 1 V and 5 V. 1 Volt will be 4 L/min and 5 Volt will be 200 L/min. Calibration runs have been done by the manufacturer and can be found in Appendix A.2. The test condition is water at 23°Celsius. The measurement is, according to Bronkhorst, independent of

¹<https://www.bronkhorst.com/int/blog-1/flow-meter-accuracy-repeatability/>

temperature, viscosity, pressure, and density. Using the same procedure as for the gas flow meter, a minimum and maximum superficial liquid velocity can be defined. The derivation of this range for the superficial liquid velocity can be found in Appendix A.2. The result is presented in Equation (3.4) and Equation (3.5).

$$u_{SLmin} = \overline{u_{SL}}(1 - a) - 6.59 \cdot 10^{-4}(1 - a) \quad (3.4)$$

$$u_{SLmax} = \overline{u_{SL}}(1 + b) + 6.59 \cdot 10^{-4}(1 + b) \quad (3.5)$$

Where:

- $\overline{u_{SL}}$ = the prescribed superficial gas velocity
- $a = 0.0264$
- $b = 0.0275$

3.2.3. Pressure sensors

Pressures at two different locations in the loop are measured with Validyne DP15 pressure transducers. Validyne DP15 pressure transducers are differential pressure sensors and therefore one end of the pressure sensor is exposed to atmospheric conditions. The other side is connected via a tube to the loop. Inside this device, a diaphragm is used which deforms due to a differential pressure. The deformation of the diaphragm results in different electronic resistances which can be measured and logged with a carrier demodulator. The output of the carrier demodulator is logged on the acquisition device. Different ranges of the Validyne pressure transducers are available. For safety reasons, a transducer with a range of 0.86 barg is chosen. The maximum measured pressure in the loop during the experiments was approximately 0.4 barg.

The pressure sensors use a carrier demodulator to create a voltage output. Therefore, a calibration between the pressure sensor and a carrier demodulator needs to be done. A fixed tube with a maximum height of 238 cm is used as a water column and connected to one side of the pressure sensor. At the other connection point, a short tube was attached with very little water. The pressure difference over the diaphragm can then be computed from the hydrostatic pressure difference. Using the gravity constant (9.81 m/s^2) and the density of water (998 kg/m^3) a pressure difference is found when changing the height. The tolerance in height for the calibration is approximately a centimeter. The carrier demodulator is set at a certain span and offset and the output is measured with a multimeter. The measured pressure versus voltage can be found in Figure 3.4 for both sensors. As suggested by the manufacturer (Validyne), a linear relation between pressure and voltage can be used. Therefore, a linear curve fit is computed using the least square method in MATLAB. The method minimizes the sum of the squared errors. The errors are defined as the difference between the curve fit and measurement points [16]. The curve fit for both pressure sensors can be found in Figure 3.4. The linear relationships match well with the measurements. The pressure transducers provide, according to Validyne, an accuracy of $\pm 0.25\%$ of the full scale. This corresponds to an accuracy of 215 Pa.

3.2.4. Weighing scale

The slug size created by the undersized ball pig will be measured with a weighing scale. The weighing scales (MyWeigh HDCS-150) are used as a high precision shipping scale with a capacity of 150 kg and a resolution of 50 grams. The accuracy of the weighing scale is ± 25 grams. It consists of a stainless steel platform with one load cell used in combination with a load-cell amplifier. The signal is changed and transferred to a couple of chips and the weight is eventually shown on the display. USB communication between the weighing scale (at the end of the loop) and the acquisition device (at the beginning of the loop) is made through a 60 meter long Cat6 Ethernet cable. A USB extender (Aten UCE260) amplifies the USB signal with an AC-adaptor and converts the signal for Cat6 communication. The Cat6 signal is converted back to a USB signal at the acquisition device.

Continuous reading from the weighing scale is not possible and communication is only made when pressing a button on the display. With the use of a relay, an electronic switch is made which can be controlled via Labview. The high voltage side of the relay is extended with 60 meters of cable and soldered to the button on the display of the weighing scale. Using Labview, a weight measurement is logged with a sampling rate of 1.67 Hz.

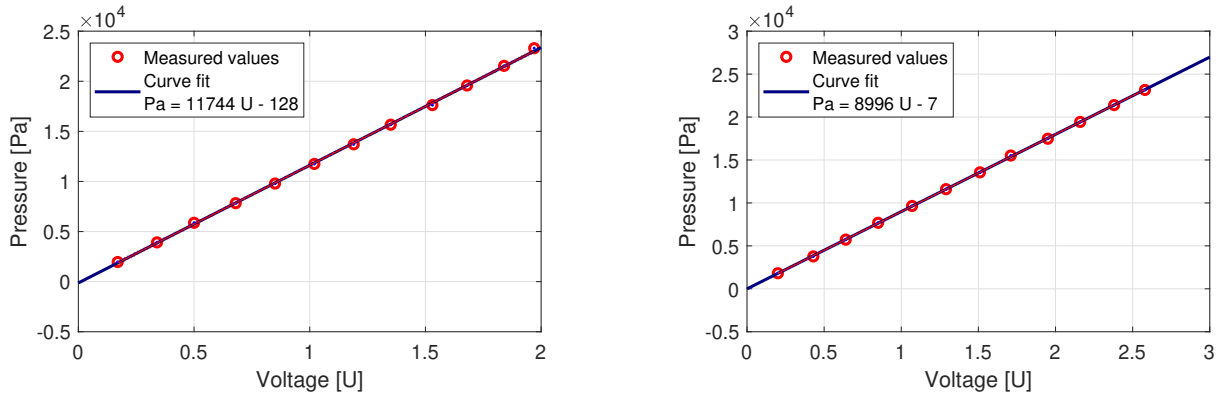


Figure 3.4: Calibration curves, pressure as function of the voltage. For pressure sensor 1 (left) and pressure sensor 2 (right)

3.2.5. Hold-up sensor

To measure the liquid hold-up in the pipe at stratified flow, a hold-up sensor is used. This liquid hold-up sensor with an inner diameter of 50 millimeters uses four-helix twisted capacitance plates and was built in 1985 by a TU Delft graduate at the time. Whenever the capacitance differs due to water flowing, a difference in electrical capacitance will be measured. The four-helix twisted capacitance plates lead to a sensor which is independent of rotation. The measuring signal is independent of the distribution of gas-liquid. The sensor with an inner diameter of 50 mm is smaller than the flow loop segments (52 mm). A sudden small contraction will change the flow structure in the pipe. This effect is assumed to be negligible because of the really small contraction and placement of the sensor at the end of the loop. Due to the age and initialization of the sensor, a measurement calibration is done. The sensor is horizontally aligned and filled with water from empty to full in ten steps. A 5th order polynomial is used to fit a curve through the measured points. Combining the curve with 95% prediction bounds gives the calibration as shown in Figure 3.5. The local measurement of the hold-up sensor at the end of the loop is assumed to be equal to the value at the beginning of the loop. It is assumed that the local measurement of the hold-up sensor can be used as a global measurement for the whole loop, which is in reality not true. This assumption will be used during the rest of the study and during the presentation of the results.

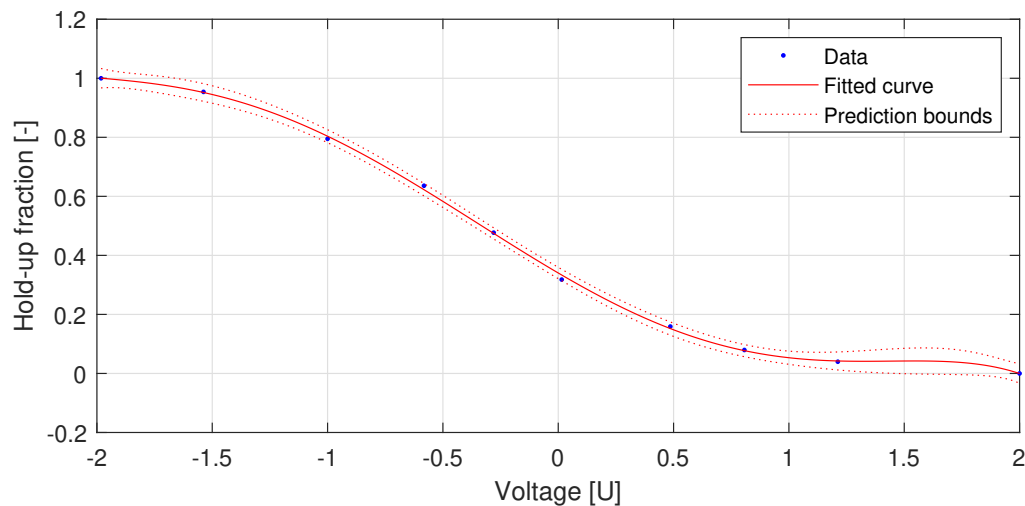


Figure 3.5: Calibration of the capacitance hold-up sensor. Fitted with a 5th order polynomial curve and combined with 95% prediction bounds.

3.2.6. Camera recordings

Visualization of the pigging operations is done with three GoPro Hero 7 cameras. The cameras are positioned roughly 40 meters downstream of the inlet and placed approximately 3 meters from the loop on a detachable arm. The detachable arms are mounted on big beams on which the loop is mounted as well. The individual distance between the cameras is chosen such that the individual field of view of the cameras overlap. A MATLAB code created in another pigging thesis project [16] is used to stitch and synchronize the individual video recordings together into one wide video. The video is then analyzed with a pig detection routine to calculate the speed of the pig. Figure 3.6 shows a flowchart of the whole MATLAB process and the steps taken to find the velocity of the pig. The images in the figure are stretched vertically and shrunk horizontally to give a more readable view. The process will be discussed step by step below.

1. General information

The GoPro cameras are known for their good quality and wide functionality in recording adventurous sports. The field of view (FOV) and the amount of stabilization in the recording can be changed. In this project, a linear FOV is chosen so that the fish-eye effect is removed from the recordings. Furthermore, stabilization is turned off in the recordings. For the recording, the frame rate was set to 120 frames per second with a resolution of 920p. A trade-off is made between the two since a higher frame rate goes along with a lower resolution. The output file of the GoPro is an MPEG4 file compressed with h.264. The three cameras are simultaneously turned on with the use of a remote controller. The compared start of the videos can deviate ± 0.1 s. Therefore, synchronization is needed which will be explained below. In this study, four construction lamps have been mounted to increase visibility in the loop. They work on the national power grid and have a generic frequency of 50 Hz.

2. Rotating

First of all, the first frame of each GoPro recording is rotated such that horizontally aligned recordings can be used in the remainder of the process. Clicking on two points left and right in the image, which should be horizontal, will give a calculated rotation angle for the image. The rotation angles are applied to each GoPro so that three horizontally aligned recordings can be used.

3. Synchronizing

Next, the videos are synchronized in time. Every GoPro is able to observe a LED light mounted just above the flow loop. The LED lights are switched on simultaneously with the use of the data acquisition device. The time of waiting and shining for the LED lamps can be controlled. By delineating the LED regions and looking at a part of the individual images, detection of the light intensity can be found by summing the pixel intensities of that region. Every recording will show a shift and a certain increase in light intensity in a specific frame. The shift as found in every recording is the synchronization frame.

4. Stitching

Rotating and synchronizing the video recordings are the steps before stitching of the recordings is done. The field of view of every GoPro is wide and will overlap with the recordings of the other GoPro's. The middle camera overlaps the view of the neighbouring left and right cameras. The image in the overlapping region is for the two neighbouring cameras roughly the same. Objects placed in the overlapping region can be used to correlate individual images and perform stitching. Doing this requires taking some aspects into account. When two neighbouring cameras are looking at the overlapping region, they both have a different angle at which they are looking at the region. This results in a discrepancy. Minimizing this discrepancy can be done by using a very thin object oriented parallel to the lens of the camera. Stitching of the images can be done when the flow loop and object are in the same plane. Therefore, two figures are cut from cardboard (thin object) and placed on top of the flow loop at the overlapping regions. The same code used for rotating and synchronizing is also used for stitching. The code asks to select the region used for stitching. After selecting the object placed on top of the flow loop for two neighbouring cameras, a cross-correlation is computed to find where the images overlap. This cross-correlation is done for both overlapping regions. The overlap position is then used to stitch the three video recordings into one video recording. Next, the field of view is narrowed down to the flow loop only. This gives a wide but small window covering approximately 8 m of the flow loop.

5. Creating binary images

On the stitched image, a ball pig detection is followed. This detection starts with an average of a couple of hundred frames in which the ball pig is not present. Next, the frame interval in which the pig is present is chosen. The averaged background frame is subtracted from every frame in this frame interval. The results are images with a highlighted region with higher light intensity where the pig and slugs are seen. These differences are gathered in a matrix and converted to a binary matrix. Choosing a threshold for this conversion, a matrix with only zeros and ones will become apparent. The presence of multiphase flow and noise from activities around the cameras create a difference in light intensity during recording. This makes it difficult to create a binary matrix with only the ball pig present. The flowchart in Figure 3.6 shows a binary image with not only the pig, but also parts of the interface between water and air. Iterating this step and changing the threshold values for the conversion to the binary image gives a sufficient result. A recommendation for future research is to improve this method.

6. Algorithm to find circles in the image

The binary image is then analyzed by a function in MATLAB searching for a circle in the image. The function is called 'ImFindCircles'. The function uses a Circular Hough Transform (CHT) algorithm for finding circles. More information about this algorithm can be found in [36]. In this function, a minimum and maximum number of pixels for the diameter of the ball pig must be given. Besides, the brightness and sensitivity of the ball pig need to be given. The number of pixels for the ball pig is computed with the knowledge of real distances such as the distance between two couplings. With some tolerance taken into account, a minimum of 15 pixels and a maximum of 35 pixels are taken. The settings of this function are sensitive to changes and therefore set such that the pig is not found in every image. The advantage is that the algorithm will not compute the gas and liquid interface as a found circle. The disadvantage is a less accurate pig detection. Whenever the pig is not detected, the matrix will be filled with a NaN for that specific image. The computed data for every image are put together into an array and smoothed. It is, for example, known that the pig can not be detected whenever present in the coupling. Moreover, the general movement of the pig is known. The jumps of unreal pig movement are removed. Taking the time and distance between two pig detected images and making use of linearization, the average velocity between these two images can be computed. Doing this for the whole frame interval will give the local velocity of the pig moving through the measurement section. In this study, local and global pig velocities are analyzed and compared. For future research, it is possible to extract more detailed information from the recordings.

Accuracy of the recordings

The accuracy of this pig detection method is subject to a lot of settings. Furthermore, the higher the velocity of the pig, the more blurry the boundary of the pig becomes. The shutter speed and scattering of light increase the blurriness. The construction lamps also shine with a frequency of 50Hz giving a small change in light intensity in every frame. The threshold value for the conversion to a binary image also reacts differently to each individual image. This is because of the slugs being accumulated in front of the pig or being pushed away from the pig. The range of the number of pixels for the pig will also result in changes when using the algorithm. From a lot of samples from different recordings, it is observed that the pig detected centre of the circle is never more than 4 cm away from the real pig centre. This observation is taken on the safe side. Therefore, an accuracy of ± 8 cm is plausible.

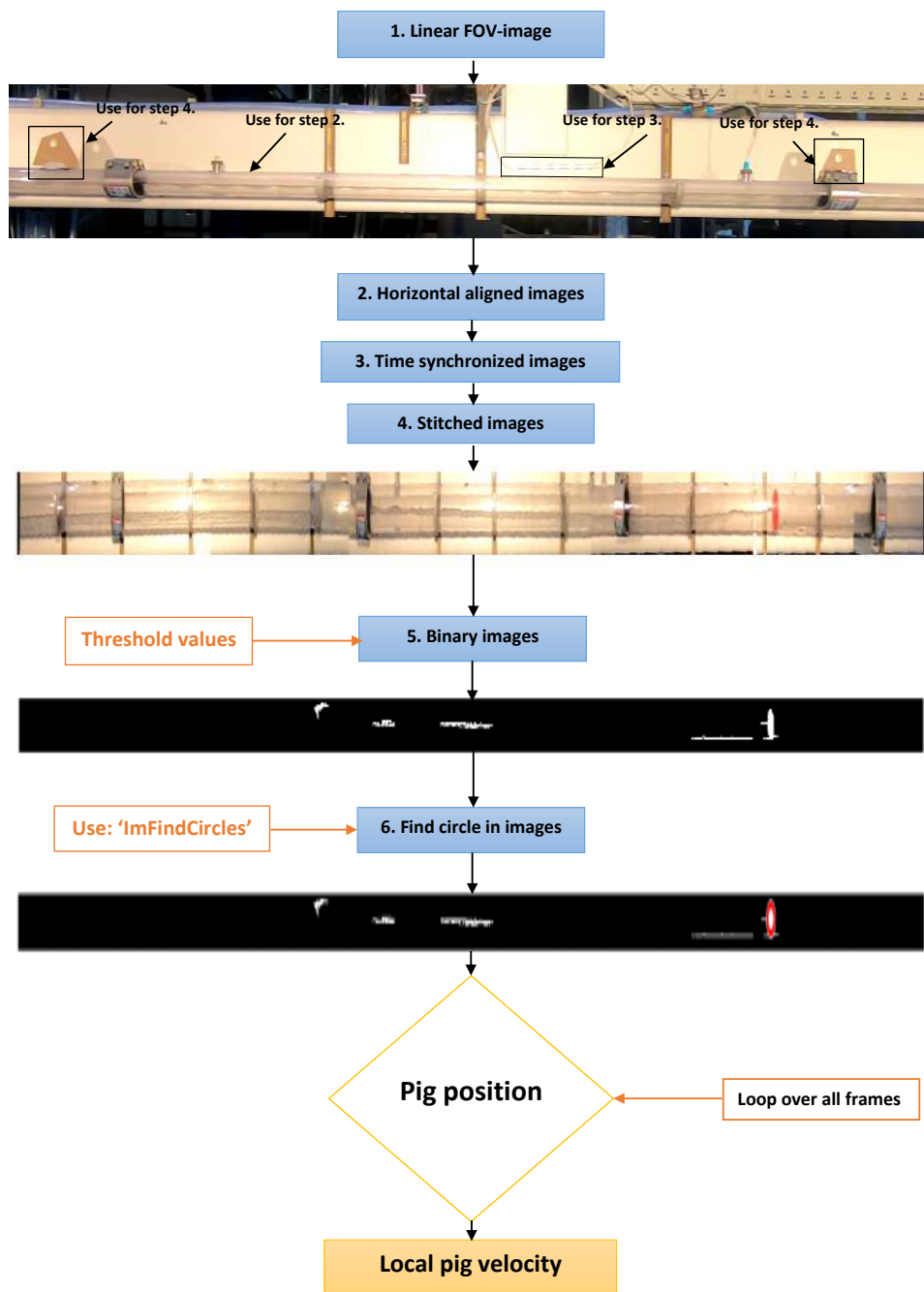


Figure 3.6: Video image processing flowchart

3.2.7. Data acquisition

The devices discussed above are used to control and monitor the pigging operations. The monitoring of the flow meters, weighing scale, hold-up sensor, led lamps, and pressure sensors is done with a National Instruments USB 6008 DAQ device which is connected to the computer. The control of the devices is incorporated in an easy-to-use script written in Labview (National Instruments). A dashboard in the script shows the inputs and outputs of the measurement devices and visualizes these in different graphs. The device simultaneously logs the input and outputs of the measurement devices. The flow meters have a different sample rate than the other measurement devices. Therefore, two different datasets are created. At the end of the measurement, these sets are synchronized and coupled creating a data set which can be analyzed. A dataset containing the following information is collected:

- 1. Number of sample [-]
- 2. Voltage pressure sensor 1 [V]
- 3. Voltage pressure sensor 2 [V]
- 4. Voltage liquid flow meter [V]
- 5. Voltage hold-up sensor [V]
- 6. Time [ms]
- 7. Setpoint gas flow [%]
- 8. Measured gas flow [%]
- 9. Valve output [%]
- 10. Weight [kg]

The three GoPro cameras are used simultaneously with the above-mentioned devices. A remote control is used to turn on the cameras. This remote controller can be turned on at the beginning of the loop. The recordings can be removed from the GoPro cameras after pigging by an easy to use extracting cable. Analysis of the recordings can be done afterwards in MATLAB.

3.3. Undersized ball pig characteristics

3.3.1. Dimensions

The variation in diameter, weight, material, and roughness of undersized ball pigs is large. The ball pigs used in this study are restricted to mainly three different diameters, each with their own weight. In a previous undersized ball pig study by M. Jiang [19], a recommendation was made on the ball to pipe diameter ratio ($\frac{d}{D}$). A ball to pipe ratio of approximately 0.9 was recommended. The inner diameter of the flow loop was found to be 52 ± 0.7 mm and the inner diameter of the hold-up sensor was found to be 50 mm. Therefore a ball diameter smaller than 50 mm is needed even though a large part of the flow loop is 52 mm; a ball diameter of 42 mm, 45 mm, and 48 mm, respectively, is chosen. This results in a ball/pipe diameter ratio of $\frac{42mm}{52mm} = 0.808$, $\frac{45mm}{52mm} = 0.865$ and $\frac{48mm}{52mm} = 0.923$. After extensive use of the solid balls with a diameter of 42 mm, 45 mm, and 48 mm a flexible 50 mm ball is used. The 50 mm ball has the flexibility to easily deform at the hold-up sensor, not increasing the pressure to much and being able to safely pig the flow loop. The diameter ratio for this flexible ball is 1 at the hold-up sensor and $\frac{50mm}{52mm} = 0.961$ for the rest of the loop.

3.3.2. Weight and material

The weight of the balls is an essential parameter, especially when using undersized ball pigs. Therefore, a couple of different materials with different densities (PU, silicone, natural rubber) have been tested in multiphase flow. Using an undersized ball pig with a density higher than water will generally result in the ball rolling over the bottom of the pipe. Whenever the liquid accumulation in front of the ball was too high, a slug was created at the interface of the ball. The disturbance of the slug would sometimes push the ball up and down in the pipe. Overall, a ball with a higher density than water would mostly cause the ball to roll. It is most desirable if the ball pig will be neutrally buoyant in the flow. The air flow has a higher cross-sectional area for passing when a heavy rolling ball is present. The pressure and viscous forces in the air will be lower when the passing area is increased. This will not propel the ball as much when neutrally buoyant. At low velocities, the ball would approximately flow with the water velocity and sometimes even stop moving. The inertia of the ball and the air flow not being able to build pressure, resulted in a hardly moving pig. This behaviour was more strongly present for smaller pig diameter ratios.

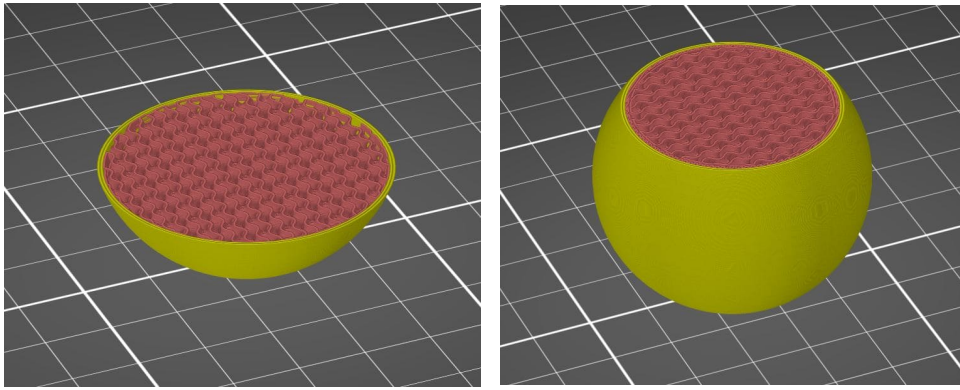


Figure 3.7: A meshed 3D print for a 45 mm ball. The shell is shown in yellow and the 30% infill in red. The mesh is shown for the lower half of the ball (left) and upper half of the ball (right).

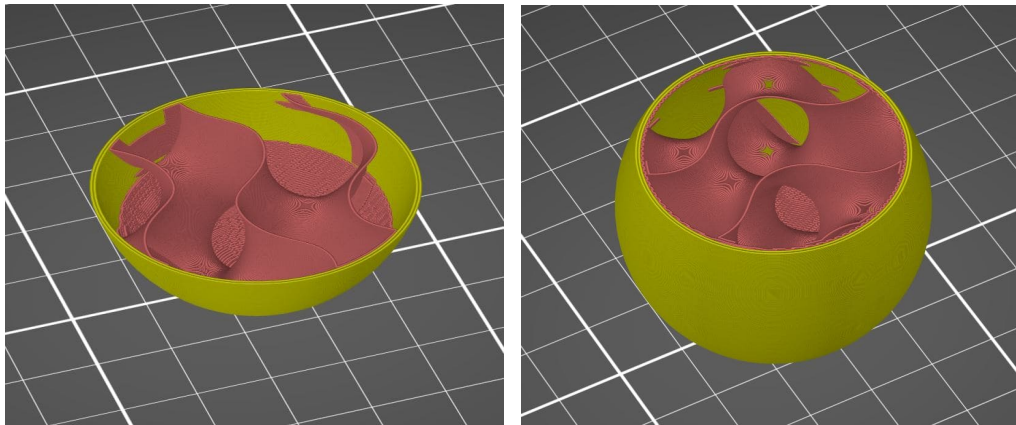


Figure 3.8: A meshed 3D print for a 45 mm ball. The shell is shown in yellow and the 4% infill in red. The mesh is shown for the lower half of the ball (left) and upper half of the ball (right).

A 3D printer can be used to create a more neutrally buoyant pig. By decreasing the cross-sectional area for the air flow to pass, the pressure behind the pig will be increased, which in turn increases the pig velocity. A 3D-printer is able to print structures with a certain infill of air giving a lower density. In Figure 3.7 and 3.8 such a structure for a 45mm ball can be found. The outside of the ball is, in this particular case, 3 layers thick and filled with a so-called gyroïde structure. A gyroïde structure is a naturally occurring structure that can be found in butterfly wings and even within membranes inside cells [14]. It has exceptionally good strength properties at low densities (so less filament is needed) and has better properties against failure compared to the normal types of infill. Furthermore, it is found that the gyroïde infill is close to isotropic, creating homogeneous ball pigs. The periodic wavy structure can be trigonometrically approximated by the following equation (3.6) [27]:

$$\sin(x) \cdot \cos(y) + \sin(y) \cdot \cos(z) + \sin(z) \cdot \cos(x) = 0 \quad (3.6)$$

In Figure 3.7 a 30% infill is used in the print. When lowering to a 4% infill it will mesh the print as shown in Figure 3.8. Lowering the infill percentage will make the printed structure weaker. Furthermore, it is not possible to create a 3D-print with 0% infill because the filament can physically not be printed in the air. Due to this reason, weight restrictions are apparent in this design. At a certain point, it is not possible to print the structure even lighter. To determine the weight of the balls needed for the experiments, a schematic drawing will give good insight. The schematic drawing is shown in Figure 3.9. Using the law of Archimedes for the height h which should float in the water it is possible to determine the infill percentage of the 3D-print for radius r . Some formulas are used to determine the infill percentage. The volume of a sphere is a trivial equation and shown in Equation (3.7):

$$V_{sphere} = \frac{4}{3} \cdot \pi \cdot R^3 \quad (3.7)$$

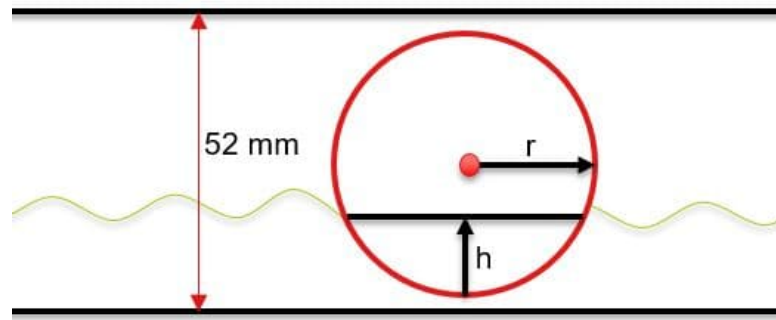


Figure 3.9: Which fraction of the ball should float in the water? This can be determined with the law of Archimedes. Shown in 2D representation.

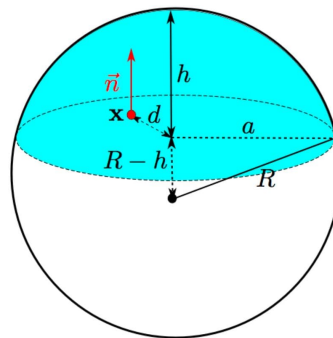


Figure 3.10: Representation of a spherical cap with the needed parameters shown. Reproduced from [15].

Where "R" is in meters and can be found in Figure 3.10. The volume of a spherical cap is less known and as following (3.8):

$$V_{sphere,cap} = \frac{\pi \cdot h}{6} (3a^2 + h^2) \quad (3.8)$$

Where "R", "h", and "a" are in meters and can be found in Figure 3.10. When "h" and "R" are known, "a" can be calculated with the Pythagoras theorem (3.9):

$$a = (R^2 - (R - h)^2)^{0.5} \quad (3.9)$$

When the height "h" and "R" are chosen, the weight of the ball can be calculated accordingly Archimedes theorem (3.10):

$$W_{ball} = V_{sphere,cap} \cdot \rho_{water} \cdot 1000 \quad (3.10)$$

Where:

- $V_{sphere,cap}$ = Volume of the sphere cap in m^3
- ρ_{water} = Density of water at 30 °Celsius (995.67 kg/m^3)

The density of water is chosen at 30 °Celsius because it is found that in experiments the temperature of water in the vessel will stabilize at approximately 30 °Celsius. The software used for slicing the 3D-printed balls is called PrusaSlicer. Depending on the amount of infill chosen, a calculated filament in grams will be given. The material used for a 3D print consists generally of PLA (PolyLactic Acid) or PETG (Polyethyleentereftalaatglycol), both with their own mass density. Due to the fact that PLA deteriorates in water over time, PETG is chosen as the material to be used for printing. PrusaSlicer uses the density of 3D printing PETG (1.27 kg/m^3) and it is, therefore, possible to approximately know W_{ball} when the ball is printed with a certain infill percentage.

In the journey to find the restrictions of a light weight printed ball, an infill of 4% - 5% was found. Lowering the infill even more would cause the 3D-print to fail. A limit in weight is found. The results

from this study, explained later, found a quite high leakage for these light pigs. Undersized ball pigging with an even smaller weight is not recommended for future research. Heavier pigs are recommended such that less leakage will be present. The final print for the 42 mm, 45 mm, and 48 mm balls was found to be 9.89 grams, 11.85 grams, and 14.64 grams, respectively. PETG exhibits hygroscopic behaviour, which means that it will attract water from the surroundings through adsorption and or absorption. The pig was put into water days before pigging such that the hygroscopic behaviour has saturated the pig. Then the pigs were weighed with an accurate weighing scale. The weights of the balls for the 42 mm, 45 mm, and 48 mm pig were, respectively, 9.89 grams, 11.85 grams, and 14.64 grams. Using the formulas and reversing the calculation, it is found that the balls should float in the water with a height ratio ($\frac{h}{d}$) of 0.331, 0.326 and 0.329 for the 42 mm, 45 mm, and 48 mm respectively. This means that approximately one-third of the 42 mm, 45 mm, and 48 mm ball diameter should be underwater when floating. An extra visual check verifies the one-third approximation.

3.3.3. Final undersized ball pigs

The final undersized ball pigs have a given dimension and weight. Figure 3.11 shows the printed balls at two opposite sides. The right figure shows the bottom of the balls which are much rougher than the accuracy with which it was printed. This is because the support material needs to be printed under the ball. The support makes it possible to print the ball outwards on the sides of the support material and not in the air. The support material can be broken from the ball afterwards. This leaves an inevitably rougher structure compared to the rest of the ball.

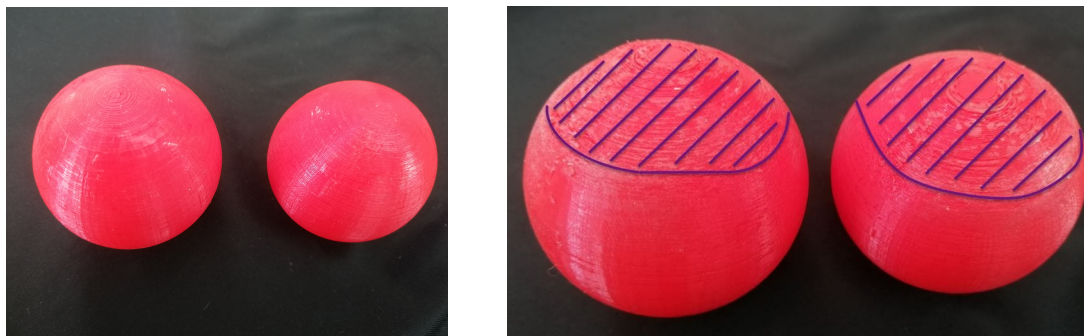


Figure 3.11: Left: Top printed surface of the balls with detailed accuracy. Right: Bottom printed surface of the balls with roughness from support material. The marked part is rough due to support material.

The printer settings were taken at 0.10 mm layer height, which leads to approximately 4 hours printing time per ball. The final specifications for the ball pigs are given in Table 3.1. The roughness created by the support material will not be taken into account even though it is present.

Table 3.1: Specifications of the undersized ball pigs

-	42 mm	45 mm	48 mm
Material [-]	PETG	PETG	PETG
Maximum Diameter [mm]	41.99	44.98	47.98
Minimum Diameter [mm]	41.10 ±0.15	44.29 ±0.15	47.43 ±0.15
Print settings	0.10 mm "detail"	0.10 mm "detail"	0.10 mm "detail"
Infill [%]	4	4	5
Weight [grams]	9.89	11.85	14.64
Ball fraction floating in water [-]	0.331	0.326	0.329

3.4. Operation

3.4.1. Operational explanation

The operational instructions for the pigging loop in the Process & Energy laboratory of TU Delft will be given here. Various actions need to be undertaken to obtain the right and synchronized data from the measurement devices under safe conditions. First of all, it should be checked whether the outlet of the flow loop is redirected into the outlet vessel. A submersible pump with a float present in the outlet vessel should be turned on with the intended remote control before starting the experiment. When the water level in the vessel reaches the top of the float, the pump will turn on and pump the water to the main vessel. The pump automatically stops when the level of the water becomes too low. By doing this, the outlet vessel can not flood.

The following step is to power all the measurement devices and to connect these to the monitor. The gas flow meter, liquid flow meter, pressure sensors, GoPros, and weighing scale should be powered. The National Instruments device, weighing scale and gas flow meter need to be connected to the monitor to gather all data in Labview.

The pump at the inlet can now be turned on with the bypass fully open and the analog liquid rotameters fully closed. The pump is allowed to reach steady state. Thereafter, the liquid valve is opened to obtain the desired amount of liters per minute, as registered by the digital liquid flow meter. After this, the setpoint of the gas flow meter can be changed and set to the desired flow. The air flow will change the liquid flow and therefore the liquid flow should be checked and set several times. The flow should reach a more or less stratified state over time in the loop. Whenever this is reached, the ball pig can be inserted in the pigging 'launcher'. The ball pig is now ready to be launched. The submersible pump in the outlet vessel should be turned off just before launching. The measurement is started redirecting the flow with the valves and the data are gathered. At the arrival of the ball pig in the outlet, two actions should be taken. The submersible pump is turned on while closing the analog liquid rotameters and turning off the inlet pump. After stopping this measurement in Labview, the data will be automatically saved to the chosen file destination.

3.5. Signal processing and data analysis

3.5.1. Signal processing

The data acquisition device samples the data at different rates depending on the measurement device. Raw data from the measurement devices need to be processed because of noise in the logged signal. Therefore, low pass filters will be used to reduce the noise in the signal. The different raw signals will be discussed here. The pressure sensors, hold-up sensor, and liquid flow meter are the three signals that will be filtered.

Signal processing pressure sensors

The outputs of the pressure sensors during the pigging run are registered and combined with the output of the pressure sensors when air and liquid flow are present without a pig. This is called a pre-pigging run. Therefore, the output of the pressure sensors shows the change of pressure caused by the pig. Raw data of a pigging run can be found in Figure 3.12. With the use of a Fast Fourier Transform in MATLAB, the amplitude spectrum of pressure versus time can be computed. The amplitude spectrum shows very small amplitudes just after a couple of Hz up to 480 Hz. Using a digital low-pass filter will reduce the amount of noise present in the raw data. The magnitude drops enormously after a couple of Hz. Therefore, a low-pass filter with passband frequency at 10 Hz is applied to the pressure data and the result is shown in Figure 3.13. The slugs created by the undersized ball pig can be found by the pressure sensors as peaks in the pressure sensor. Furthermore, the passing of the undersized ball pig can be found.

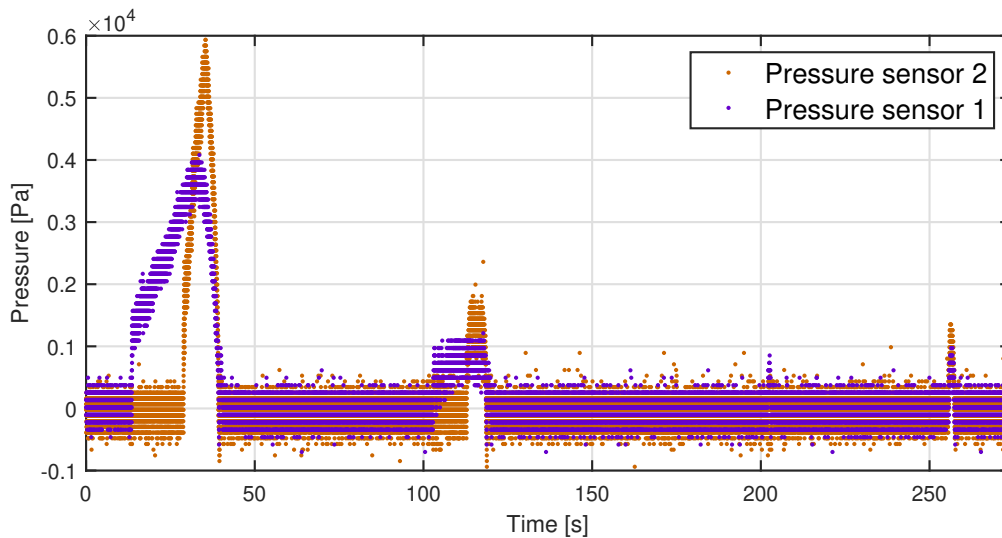


Figure 3.12: Raw output of the pressure sensors combined with a pre-pigging run. The pressure is plotted against time. A random run is chosen with an air flow of 180 L/min, 6 L/min water flow and 45 mm ball.

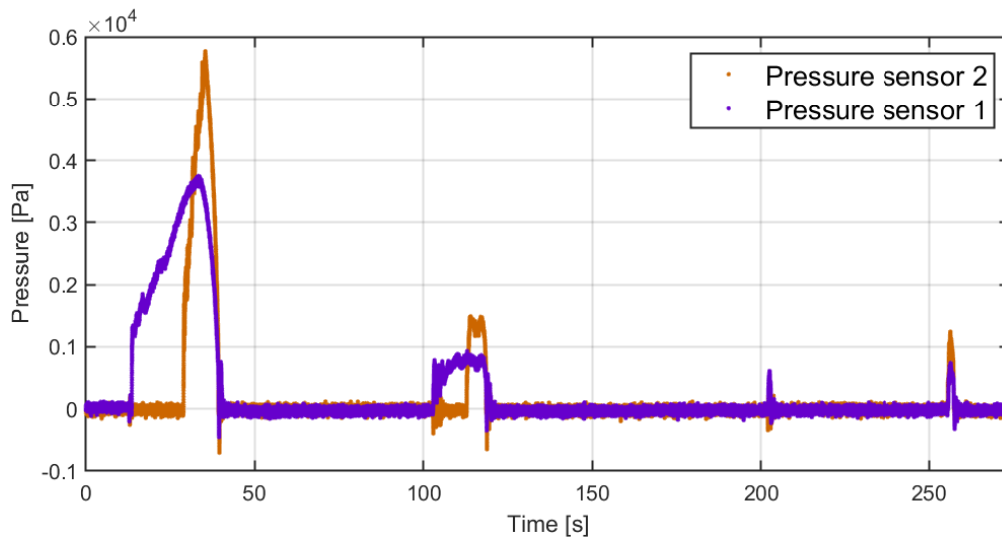


Figure 3.13: Raw pressure data of Figure 3.12 filtered with a low-pass filter and passband frequency of 10 Hz.

Signal processing liquid flow meter

The output of the liquid flow meter contains noise as well. One could take the same procedure by computing the FFT and using a low-pass filter. Here, the output of the liquid flow meter is used to set the flow in the pipe before pigging. Therefore, the average value of the liquid flow meter output is sufficient for data analysis. Using the "mean" function computes an average value. This average flow rate value in L/min will later be used to transfer the value to m/s. During the pigging run, it is found that the air and liquid flow change depending on the pressure in the pipe. The air mass flow controller adjusts itself until it converges again to the set value. The water pump follows and converges the water flow as well. Therefore, the water and air flow rate will be logged during a pigging run and averaged to a mean gas and liquid flow rate.

Signal processing gas flow meter

The gas flow meter is a mass flow controller and outputs a certain given output. This output is accurate and does not need any low-pass filter. Furthermore, the gas flow meter tries to converge to the given setpoint whenever the pressure after the controller changes. The creation of a slug or acceleration of the pig will increase or decrease the pressure in the loop after the flow meter. This pressure affects the given setpoint. For the calculation of the superficial gas velocity, a quantitative liquid flow rate is needed. The air flow rate output changes constantly during pigging. Therefore, the output of the flow meter is logged during the whole pigging run and the average is taken for the duration of pigging. This average is found to be higher than the given setpoint due to the fact of an increase in pressure. The valve is opened a little more to deliver the same normal liters per minute for a given setpoint. Thus, for the gas flow meter, an average flow rate is taken from the logged measurement during a pigging run and a change from normal liters per minute to actual liters per minute is computed as discussed in Chapter 3.2.1.

Signal processing hold-up sensor

The hold-up sensor registers useful data to analyze the slugs. Therefore, reducing the noise in the signal will help to improve the analysis. The improvement in the signal is done in the same manner as for pressure sensors. The FFT of the signal is computed and a low-pass filter with a passband frequency of 10 Hz is used. Figure 3.14 shows the results. Besides the filtered signal, also a physical restriction on the hold-up fraction is given. The unfiltered signal tends to overshoot the hold-up fraction above one whenever a big slug passes by. This is physically not possible. The final result represents the hold-up value before pigging, the passing of the slugs created by the undersized ball pig, and the reduced hold-up fraction after pigging. Detailed observations will be given in Chapter 3.5.2.

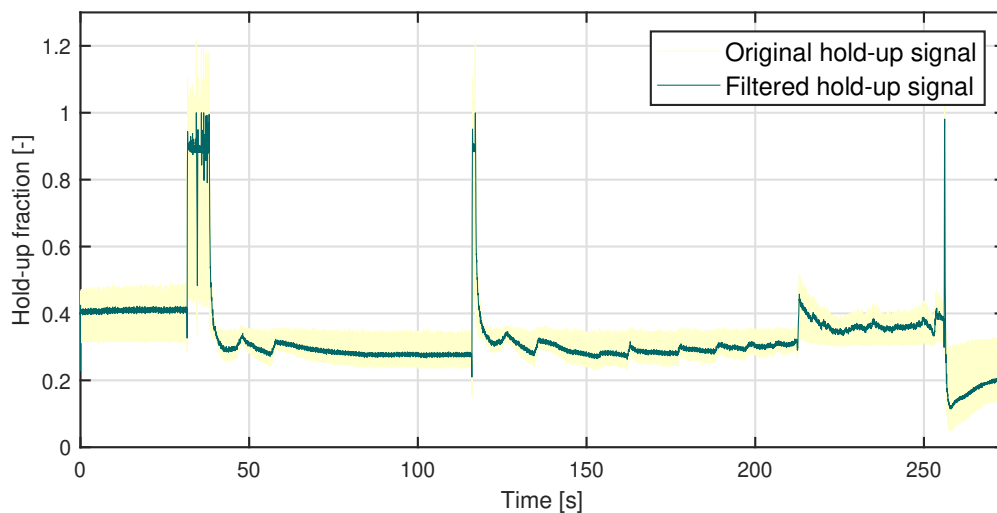


Figure 3.14: Output of the liquid hold-up sensor versus time. The unfiltered and low-pass filtered signal are shown. A restriction in hold-up fraction with a maximum of 1 is added for the filtered signal.

Signal processing weighing scale

The weighing scale in this specific configuration presents a slow sampling rate of 1.67 Hz. This is a difference in sampling rate compared to the other measurement devices. Within every 0.59 seconds, a measurement at that exact moment will be given. In between those measurements, the details can not be presented and will be unknown. The registered weight is sampled at 960 Hz even though the measured value will change only every 0.59 seconds. Therefore, only the measured weight at that specific time point is plotted and the resulting points are connected by lines. The weighing visualization can be presented as shown in Figure 3.15. The created ball pig slugs are found in the weight measurement as a sudden increase in weight. Figure 3.15 shows the creation of multiple slugs.

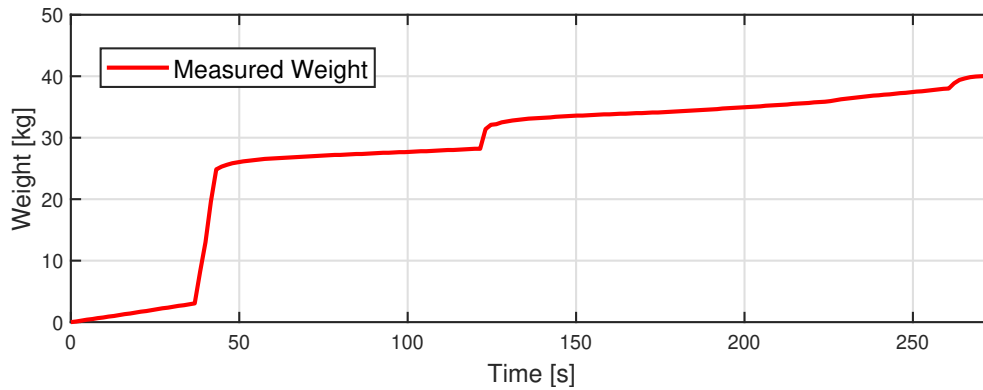


Figure 3.15: Output of the weighing scale during a pigging run.

3.5.2. Data analysis

The signal processing in the previous paragraph helps in the signal analysis. Here, the same data as used for the explanation of signal processing, which represents a typical measurement, will be shown and analyzed. Figure 3.16 shows the weight, hold-up fraction, and pressures during a pigging run. The pigging run is performed with a 45 mm diameter ball for a liquid flow of 6 L/min and air flow of 180 L/min. Multiple observations can be made from the pigging run. The observations will be discussed in Chapter 4. Here, the analysis of the data will be discussed. The data of Figure 3.16 are examined for every pigging run. Then for every pigging run, the following parameters will be defined:

- Superficial gas velocity (u_{SG}) and superficial liquid velocity (u_{SL})
- Mixture velocity (V_m)
- Average pig velocity (V_{pig})
- Liquid surge weight (W_{surge}), Liquid steady state weight (W_{SS}), Liquid slug weight (W_{slug}), total initial liquid weight (W_{t0}) and leakage.
- Number of slugs

Definitions of u_{SG} and u_{SL}

First of all, the superficial gas velocity and superficial liquid velocity will be defined. In Chapter 3.5.1 it is stated that the average flow rates of air and water will be taken from the registered data during the whole pigging run. This means that for air, the actual computed liters per minute will be taken. The velocities of air (u_{SG}) and water (u_{SL}) can be calculated with Equation (3.11) and (3.12), respectively, as discussed before in Chapter 2.2.

$$u_{SG} = \frac{\dot{V}_G}{A} \quad (3.11)$$

$$u_{SL} = \frac{\dot{V}_L}{A} \quad (3.12)$$

Where:

- \dot{V}_G is the air flow rate in m^3/s
- \dot{V}_L is the water flow rate in m^3/s
- A is the surface area of the pipe in m^2

Definition of V_m

The mixture velocity of air and water in the pipe V_m is defined as shown in Equation (3.13).

$$V_m = \frac{\dot{V}_G + \dot{V}_L}{A} \quad (3.13)$$

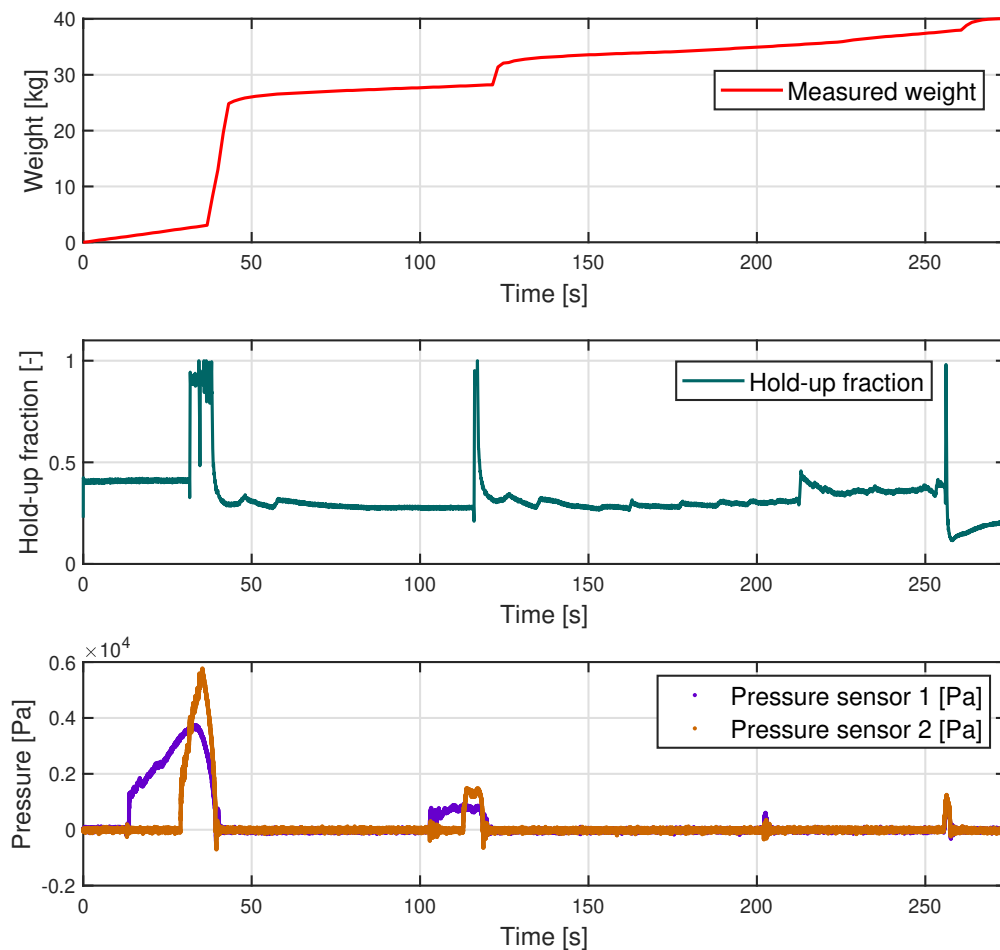


Figure 3.16: Full output of one registered pigging run. Measurement signals are filtered and plotted with a shared time axis. The weight, hold-up fraction, and pressures are shown. Liquid velocity: 6 L/min, Air velocity: 180 L/min, Ball diameter: 45 mm.

Definition of V_{pig}

The average pig velocity V_{pig} is determined with the data provided by the pressure sensors and hold-up sensor. Whenever the undersized ball pig or already created slug passes the first pressure sensor, a sudden increase in pressure is measured. The first pressure sensor is located 74 cm behind the pig launcher. At this distance, there is a chance of the first pressure increase due to an already created slug. The pig would then pass the pressure sensor at a later time point. Due to the fact that the distance is very small, it is assumed that the ball pig will pass the first pressure sensor whenever a first increase in pressure is registered. The ball pig will pass the hold-up sensor at the end of the flow loop. Behind the pig, a lower hold-up fraction is observed compared to the propelled fluid on the front of the pig. This means that whenever the pig passes the hold-up sensor, a sudden decrease should be seen. The lowest point of the registered hold-up after the passing of the slugs will be taken as the end position of the ball pig. The distance between the first pressure sensor and the end of the hold-up sensor will be divided over the time for the pig to pass these points. The division will compute the average pig velocity (V_{pig}). The pressure sensors should decrease back to zero shortly after the hold-up sensor is passed because the hold-up sensor is almost placed at the end of the loop. This means that atmospheric conditions can be reached again directly after the hold-up sensor. This is indeed observed for many runs and found to be correct.

Figure 3.17 shows a black and red marked line at the locations where the pig passes the first pressure sensor and the end of the hold-up sensor, respectively.

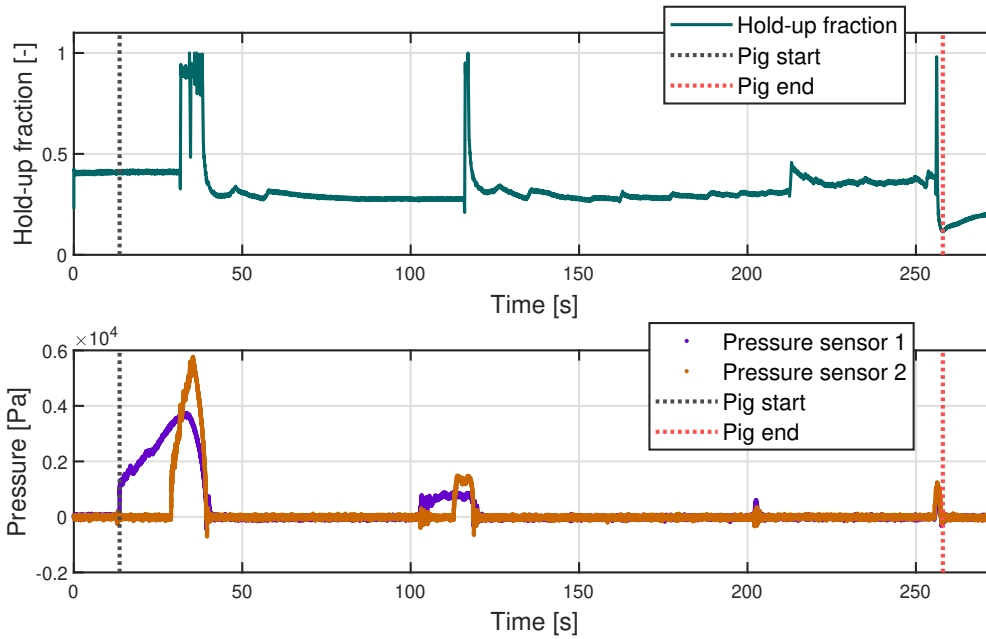


Figure 3.17: Same pigging run as 3.16. The two manually black and red marked lines represent a time difference. It is the difference in time of the pig passing the first pressure sensor and the pig passing the end of the hold-up sensor. The time difference is used to compute the average pig velocity (V_{pig}).

Definition of W_{surge} , W_{SS} , W_{slug} , W_{t0} and leakage

The liquid surge weight (W_{surge}), and herewith the liquid surge volume, can be determined with the weighing scale. The liquid surge weight during a pigging run can be determined when the liquid 'Steady state' Weight (W_{SS}) is taken into account.

During stratified flow, the liquid accumulates in the vessel and shows a linear relationship with time. Fitting a linear line to the initial logged weight for every pigging run will determine W_{SS} . A pigging run will collect extra liquid in front of the ball next to the steady state volume flowing into the vessel. The total liquid weight collected during the pigging run (W_{slug}) minus W_{SS} determines W_{surge} . W_{SS} is different for each air and water flow combination. Thus, for each pigging run, a linear fit for W_{SS} will be computed. At a certain time, the pig will have left the loop and is captured in the weighing vessel. This is the end time for weighing. The pig arrival is detected with a remote camera, which is located above the weighing vessel. This results in W_{slug} to be measured with a ± 1 second delay. In Equation (3.14) it concludes as follows:

$$W_{surge} = W_{slug} - (W_{SScoef} \cdot T_{pig}) \quad (3.14)$$

Where:

- W_{slug} is the logged weight during pigging
- W_{SScoef} is the linear directional coefficient of W_{SS}
- T_{pig} is the time the pig is in the loop

This can also be represented with an actual measurement which is represented in Figure 3.18. Here, the slug weight during a pigging run is shown in red and the steady state weight is indicated with a black marked linear line. The difference presents the surge weight, which is of interest during pigging. It represents the extra weight at the end of the loop due to the presence of the pig. The computed surge weight is different for each combination and each diameter pig. Another variable is defined as the total

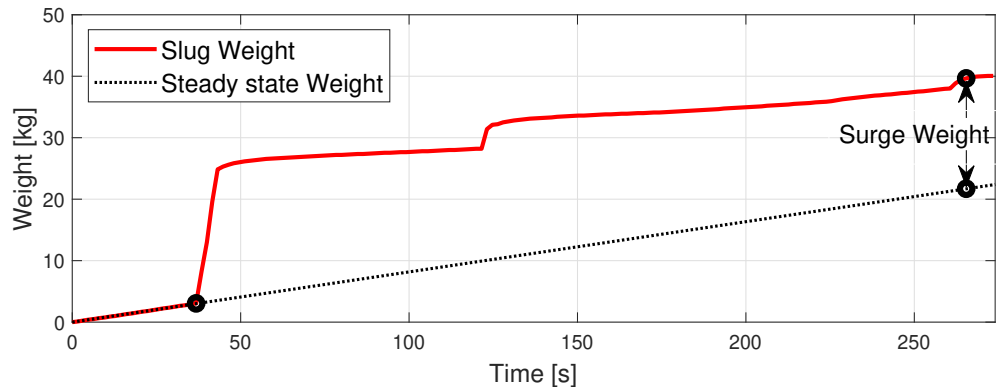


Figure 3.18: Same pigging run as 3.16. The computed surge weight for every pigging run is found by subtracting the steady state weight (black marked linear line) from the measured slug weight (red line). The end time of weighing is found with a remote camera in the vessel.

initial liquid weight (W_{t0}) during stratified flow. This weight is defined at $t = 0$, representing the time at which the pig is released. The total initial liquid weight is the liquid weight present in the flow loop during stratified flow. At steady state, during stratified flow, this gives:

$$W_{t0} = A \cdot L \cdot \alpha_L \cdot \rho_{water} \quad (3.15)$$

Where A , L , ρ_{water} and α_L are the surface area of the pipe, length of the flow loop, the density of water at 30 °C and hold-up fraction of the liquid, respectively, as defined before. α_L is taken from the hold-up sensor measurement and assumed to be equal over the whole length of the pipe as discussed in Section 3.2.5. W_{t0} can be used to evaluate W_{surge} . This is done with the following equation:

$$Leakage = 1 - \frac{W_{surge}}{W_{t0} - W_{SS}} \quad (3.16)$$

This results in the leakage, which represents the fraction of the weight initially present in the flow loop that is leaked by the presence of the pig. A leakage equal to 1 means that the pig has leaked all liquid that was present in the pipe, at the time that the pig was launched into the flow loop. A fraction equal to 1 would be representative for a really small pig, not interfering with the flow and leaking all the liquid. A fraction equal to 0 would be representative for a pig not being able to leak any liquid and push it all forward. This would also occur for an oversized pig. A leakage below 0 is representative for a pig having a pig velocity that is lower than the water velocity. In this case, the water flow will overtake the pig instead of leaking past the pig. The effectivity of undersized ball pigging is lost when the leakage drops below zero.

The definition of leakage will be used in the following sections to compare the pigging results for various pigs and various experimental combinations.

Definition of number of slugs

The number of slugs is defined as the number of created slugs in front of the pig during a whole pigging run. This is found with the data from the local hold-up sensor. Figure 3.16 displays hold-up data for a pigging run. In this figure, three distinct peaks of the hold-up fraction (having a value of 1) can be observed. This means that three so-called slugs have passed the hold-up sensor. The size of these slugs can be determined and recognized as the width of this peak. With the hold-up fraction peaking for a couple of seconds or just one second, one can distinguish the slug sizes. The exact size of the slugs cannot be determined because the speed of these slugs differ and are unknown. Depending on the superficial velocities in the pipe, pig diameter, and the amount of liquid present in the pipe, intermittent slugs are dominantly observed. Occasionally, a dispersed bubble as defined in Figure 2.3 can be observed.

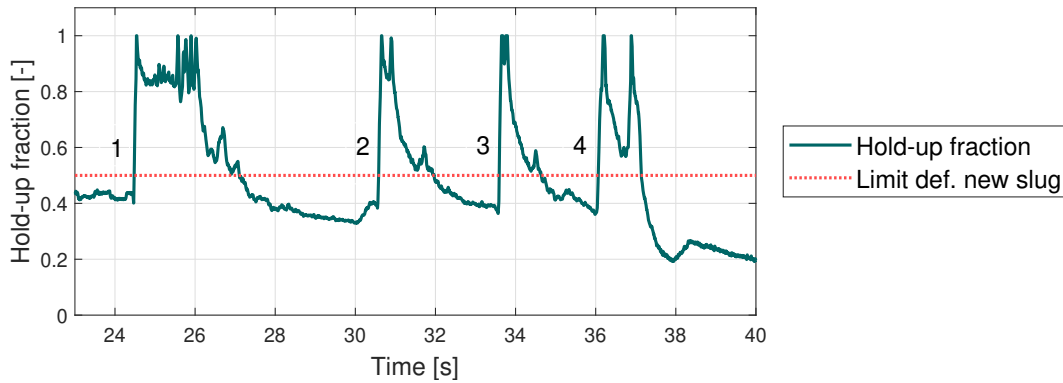


Figure 3.19: Registered hold-up fraction for a random pigging run. The defined limit for a new slug is set at a fraction of 0.5. For this particular run it results in 4 slugs being created during the whole run.

The determination of the number of created intermittent slugs is somewhat subjectively defined by a threshold criterion. This criterion is indicated in Figure 3.19. Every time a peak in hold-up fraction drops below a subjective limit of 0.5 hold-up fraction, a newly created slug is identified. For this particular pigging run, 4 slugs are created. The approach for this definition of the number of slugs is somewhat subjective and is only used to compare the number of created slugs for various pig diameters. It is observed that the initial hold-up for stratified flow will not exceed a fraction of 0.5 for a pigging run with multiple slugs. In other words, this means that in all pigging runs, before actually launching the pig in the flow loop, a fraction lower than 0.5 is found. The subjective limit definition for a new slug can thus be used and justified for every pigging run.

The number of created slugs is used in the next chapter when making some observations regarding pigging for various pig diameters.

4

Results

The main aim of this study is to understand the fluid flow structure of undersized ball pigs and create correlations. This chapter will show the observations and results of the pigging experiments for the different configurations. First of all, the general observations of the conducted pigging runs will be discussed. Next, the global observations, results of the computed pig velocity, the leakage, and created slug number will be shown. The global results will be used in the next chapter to create correlations and find an appropriate scaling for the pig velocity. At last, the local observations from the video recordings will be shown and compared with the global results.

4.1. General observations

The first part of this chapter starts with the general observations of the undersized ball during pigging experiments. Afterwards, the creation and propagation of a slug due to the undersized ball pig is shown with the use of the recordings. Next, the repeatability of the pigging runs will be discussed and confirmed with the use of graphs. At last, an initial discussion will be started on the recovery time for the flow loop to return to its initial conditions.

4.1.1. Undersized ball pig behaviour

The 3D-printed undersized balls are only a selection of balls that could have been printed and manufactured. Changing the ball diameter, weight, roughness, and elasticity all cause different behaviour inside the pipe.

PUR and Silicone balls

Before the 3D-printed balls were used, balls with the same material as used in the experiments of Shell [4] came to mind. Those are balls made of PUR (Polyurethane) with 75 Shore A hardness. More on Shore A hardness can be found in [6]. These balls have a density of 1260 kg/m^3 which is higher than water. Such balls are expected to sink to the bottom of the pipe. Still, these balls were used just as in the Shell experiments. By changing the liquid and air flow to different values and combinations, it is observed that these rather 'heavy' balls will roll over the bottom of the pipe and not flow through the pipe. Furthermore, these balls take a velocity that is much lower than the mixture velocity. Undersized ball pigs are generally not able to reach the mixture velocity, but in this case the 'heavy' balls are barely moving. The air flow will easily pass over the PUR ball, because the ball is at the bottom of the pipe. A larger cross-sectional area for the air gives effortless passing and results in a small pressure difference over the pig and inherently will show a lower pig velocity. These balls are rolling instead of 'flowing' due to the submersion in liquid and the presence of friction at the bottom of the pipe. Next, balls made of silicone with 40 Shore A hardness with a lower density were used. They showed the same result. Therefore, as discussed in 3.3.2, 3D-printed balls have been used.

3D-printed balls

The 3D-printed balls float with one-third of the diameter of the pig in the liquid ($\frac{h}{d} \approx 0.33$). A floating pig on the liquid is a dominant observed phenomenon for these pigs. In comparison with the rather 'heavy' pigs, these adapt better to the flow. Due to the floating, the leakage of the gas is lower which implies an increased pressure gradient and increased shear force over the pig. High pig velocities were observed in combination with frequent vertical movement due to slug accumulation. It would cause a vibrant movement, which could be heard at the beginning of the loop. The pig would also touch the top of the pipe at high slug accumulation, creating wall friction just before the propagation of the slug. More on this in Chapter 4.1.2. The 3D-printed pigs were very practical at low velocities because they floated on the liquid building enough viscous and pressure forces from the gas flow. The rather 'heavy' pigs would hardly 'feel' the air flow due to the pigs being submerged in the liquid. This means that at low velocities, floating pigs come into play.

4.1.2. Slug shooting

A dominant phenomenon and observation found during pigging is the creation of a slug. Figure 4.1 shows snapshots of a video recording during a pigging run with the same time interval between each snapshot. The snapshots start with a liquid accumulation in front of the pig. This accumulation has been developed upstream of the flow loop. It can be observed that the accumulation is separating from the ball pig when moving in time. At a certain point, part of the accumulation located at the pig will separate from the pig. That liquid will advance and accelerate forward, while overtaking the upstream part of the accumulation. The accumulation separated from the pig results in an accelerating slug. The slug distances from the pig, and little accumulation is left at the front of the pig. The last two snapshots show a new creation of accumulation in front of the pig some time after the release of the first accumulation. All these accumulations together will result in a total slug weight created by the pig. Furthermore, it can be observed that next to the acceleration of the slug, the pig itself is accelerating as well. The last two snapshots differ from the assumed linear trend when following the pig in each snapshot. Later, in Chapter 4.3.2, the explanation of a dynamic velocity for the pig will be explained. The behaviour discussed here is less visible at really high pig velocities.

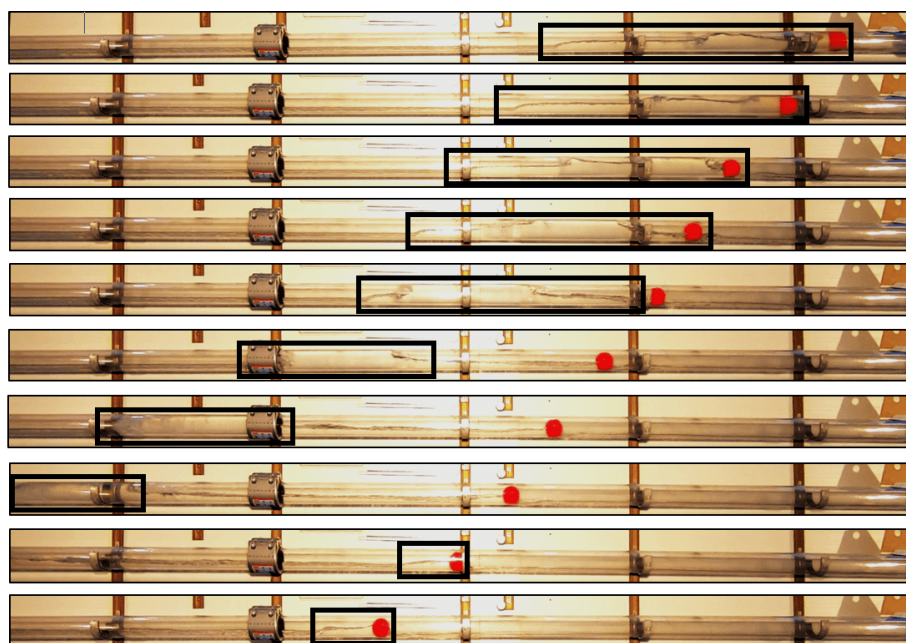


Figure 4.1: Snapshots of a video recording during a pigging run. The specific conditions were: 45 mm ball, 270 L/min air, 6 L/min water. It can be observed that the accumulation behind the ball grows in time and eventually creates a slug. The slug and pig both accelerate. The pig accelerates with a time delay after the acceleration of the slug. A new accumulation directly starts to grow. The liquid accumulation and slug are marked in black.

4.1.3. Repeatability

During this study, a total of approximately 100 runs are done. To draw reliable conclusions, one should know how repeatable the experiments in this specific flow loop are. Furthermore, it is of importance to know whether this pigging behaviour can be considered as completely random or well correlated. Therefore, a couple of random pigging runs have been done with the same experimental conditions. The results of two runs with the approximate specific experimental conditions: $Q_{liq} = 6$ L/min, $Q_{air} = 270$ L/min and $D_{pig} = 45$ mm are shown in Figures 4.2, 4.3, and 4.4, respectively. In Figure 4.2 the weight and hold-up fraction for each run can be found. The first slug created after the opening of the valve corresponds really well for each run. The weight and length of the hold-up fraction are well represented. The number of slugs and the size of each created slug is in the rest of the pigging run quite well correlated. The only difference is the difference in time when these created slugs pass the hold-up sensor. The time needed for the disturbances in front of the pig to grow and turn into a slug varies here. A time difference in the passing of the slugs past the hold-up sensor implies a time difference in the slugs measured by the weighing scale. In Figure 4.2 this can be easily seen. The hold-up fraction measured in run 1 shows the passing of slugs earlier than in run 2 when looking at the second peak. The weighing scale therefore also peaks earlier. The third peak shows the opposite behaviour with an earlier passage of the slug in run 2 than in run 1. The total measured weight during both pigging runs is almost the same. This means that the averaged quantities for the measured weight and the number of slugs are repeatable. However, local slugs differ in speed and time of passing.

Figures 4.3 and 4.4 display the data of the two pressure sensors for the two same runs as discussed in Figure 4.2. Figure 4.3 represents the data for pressure sensor 1. The location of pressure sensor 1 is shown in Figure 3.1. Figure 4.4 represents the data for pressure sensor 2. The location of this pressure sensor is also displayed in Figure 3.1. The runs show almost the same behaviour and the same pressure magnitude. Pressure sensor 1 increases rapidly for both runs just after the opening of the valve and the maximum value differs little. After the first peak, a deviation is visible for pressure sensor 1. This is due to the difference in slug arrival time as discussed for Figure 4.2. Pressure sensor 2 confirms this behaviour. At first, the pressure profile follows really well for both runs, but after the first peak a shift is visible due to slug time and speed. The pressure profiles are not the same, but the passing and maximum values can be observed quite well. The averaged quantities for the pressure and the maximum pressure values for the passing slugs are repeatable. However, local pressure values differ due to a shift in the passing time of the slugs. The local slugs differ in speed and time of passing. Overall, the results of these pigging runs are consistent and show similar behaviour in the pressure profile. The difference in results will be discussed in Chapter 5.

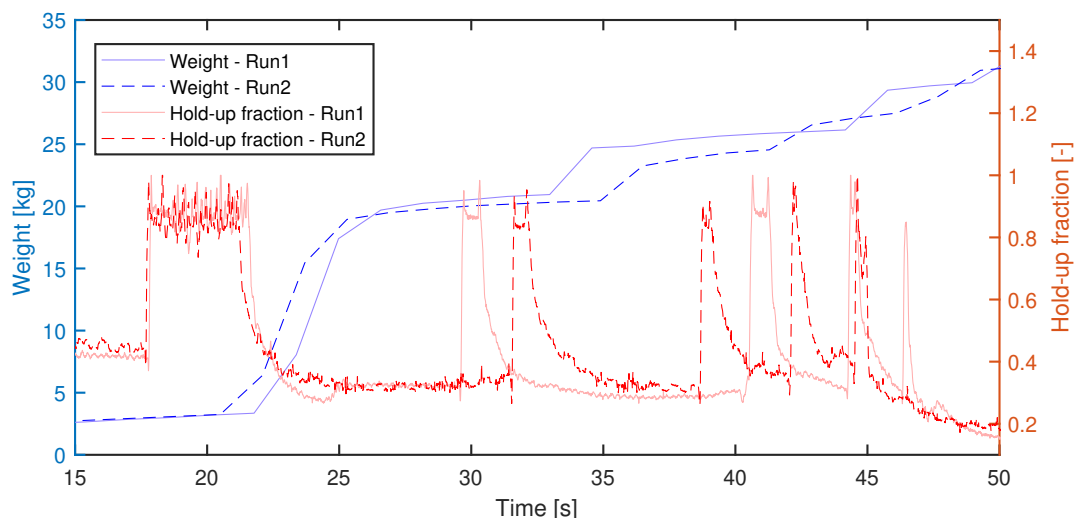


Figure 4.2: Measured weight and hold-up for two runs under almost the same experimental conditions. The two runs correspond well as is clear from the total weight and the number of slugs.

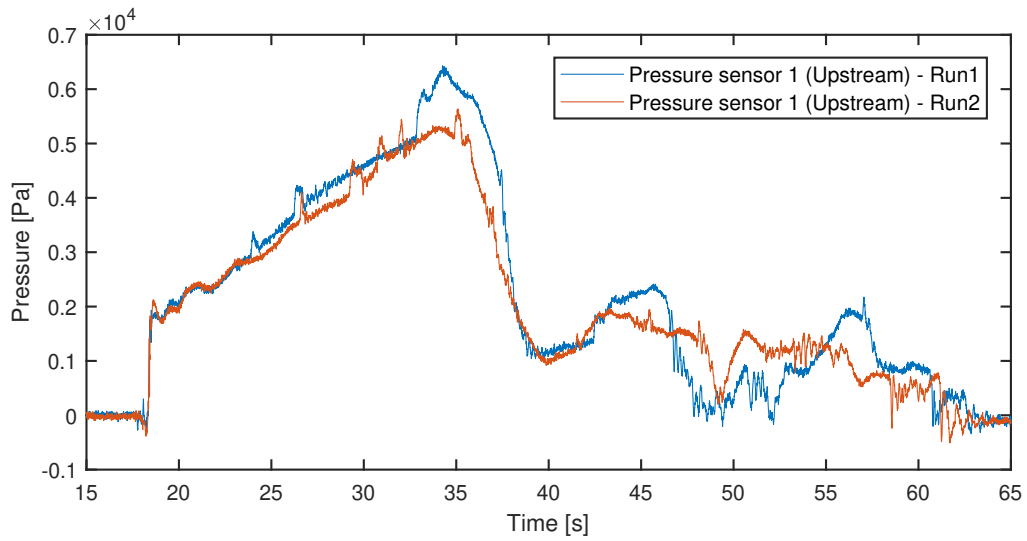


Figure 4.3: Measured pressure by pressure sensor 1 for two runs with approximately the same experimental conditions. The pressure for the two runs corresponds quantitatively well. On the right half, a shift in pressure logging is seen due to a time shift in slug passing.

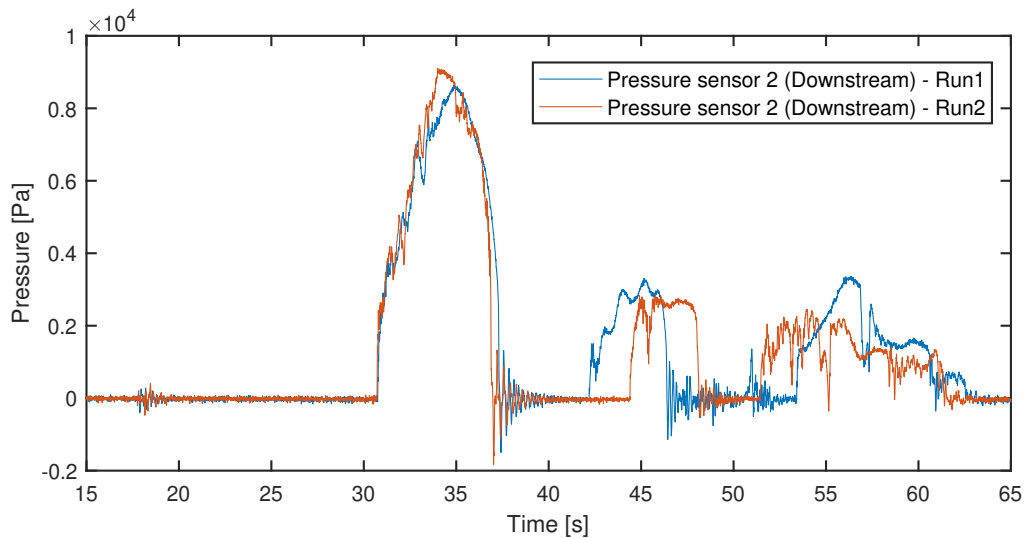


Figure 4.4: Measured pressure by pressure sensor 2 for two runs with approximately the same experimental conditions. The pressure for the two runs corresponds quantitatively well. On the right half, a shift in pressure is seen due to a shift in slug passing time.

4.1.4. Recovery time

During pigging, most of the liquid present in the pipe is discharged at the end. This depends not only on the flow, but also on the diameter of the pig. After every run, a recovery time was needed for the flow loop to return to the initial conditions. This is a normal practice for pigging specialists in industry. The liquid outflow rate will be much lower after pigging. Therefore, it can be of importance to look into the recovery time of the flow loop. This means that the initial hold-up fraction in the pipe before pigging is approximately equal to the hold-up fraction after pigging. A steady hold-up fraction implies a steady state multiphase flow. Such a run can be found in Figure 4.5. Here, a full pigging run is shown for the hold-up sensor. At t_1 the start of pigging is presented by a vertical red line. The starting point is computed using the pressure data. At t_2 the end of pigging is introduced with a green vertical line and found as discussed in Section 3.5.2. t_3 is a yellow vertical line representing the first time at which the initial hold-up is found after pigging. This value is estimated using the logged data. The blue line indicates the initial hold-up in the pig:

$$t_{f,recover} = \frac{t_3 - t_2}{t_2 - t_1} \quad (4.1)$$

For this pigging run with experimental conditions: $Q_{liq} = 6$ L/min, $Q_{air} = 270$ L/min and $D_{pig} = 45$ mm the recovery time fraction is $t_{f,recover} \approx 6.69$.

This recovery time fraction can be really useful in industry to determine the pigging interval for each set of conditions. Once the conditions in the pipe are known and the recovery time fraction is available, one knows the time to wait for another pig with the trivial equation:

$$t_w = t_{f,recover} \cdot t_p \quad (4.2)$$

Where t_w and t_p represent the waiting time and pigging time, respectively. The figure shows that the increase in the hold-up fraction during recovery is not fully linear. The hold-up fraction increases exponentially at the beginning, linearly in the middle, and exponentially at the end. Keep in mind that the hold-up sensor is placed almost at the end of the loop and the registered hold-up fraction is locally measured.

This study did not focus on the analysis of the recovery time in the pigging runs. Therefore, future research on this specific parameter could be of real interest.

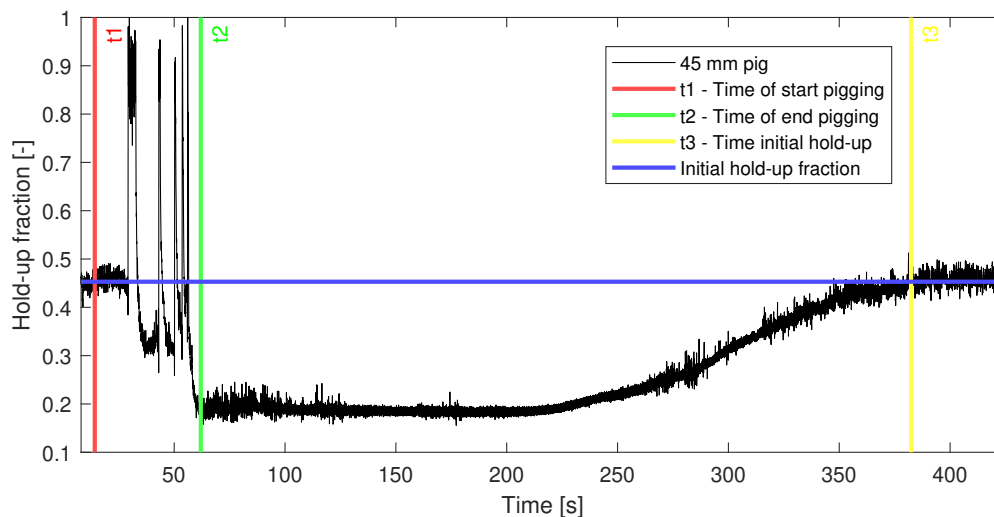


Figure 4.5: A full pigging run with logged hold-up fraction. Specific experimental conditions: $Q_{liq} = 6$ L/min, $Q_{air} = 270$ L/min and $D_{pig} = 45$ mm. Here t_1 , t_2 and t_3 represent the start of pigging, end of pigging, and the time to reach initial hold-up again, respectively. The blue line represents the initial hold-up fraction before pigging.

4.2. Experimental observations and results

This section presents the experimental results. First of all, the average pig velocity during a run is shown. The pig velocity for various experimental conditions is displayed. Next, the leakage (as discussed in Section 3.5.2) will be analyzed. At last, the number of created slugs during a pigging run is presented.

4.2.1. Pig velocity

The pig velocity is one of the main parameters on which this study is focused. The understanding and creation of a correlation will be helpful for industrial applications. Therefore, the results for the pig velocity will be shown first. Pigging runs have been done for various air and water flow rates. In Tables B.1-B.4 of Appendix B, a full representation of the performed pigging runs is given. From these tables, it can be observed that the water and air flow rates are limited to a maximum value in the pigging runs. This maximum was set for safety reasons, but also because a slug flow was created from the stratified base flow. This means that wavy stratified flow at high water and air flow rates turned occasionally into slug flow. At these flow rates, it could take 10 minutes before the disturbances grew to the point of initiating slugs. Therefore, it was not possible to create a steady state flow before pigging. A limit was set in the experimental conditions. According to Figure 2.4 stratified flow should still be present at these liquid flow rates, but this is not the case. The pig launcher and new pipe couplings create quite some disturbance of the flow in the pipe. Therefore, a limit for pigging in stratified flow is found in this experimental loop. The ratio of water flow rate to air flow rate is quite low as can be observed in the tables, namely $\frac{6L/min}{90L/min} = 0.0666$ and $\frac{4L/min}{630L/min} = 6.34 \cdot 10^{-3}$, respectively.

The computed pig velocity for every run is shown in Figure 4.6. Here the pig velocity is plotted versus the superficial gas velocity of the pigging run. The different ball pigs are each visualized with a different colour. Yellow represents the 42 mm pig, red represents the 45 mm pig, blue represents the 48 mm pig and green the 50 mm pig. The difference in superficial liquid velocity is not taken into account in this figure, but can be observed as point clusters in the figure. This means that the pig velocity is not really dependent on the liquid flow rate.

When looking at Figure 4.6, a linear behaviour can be observed for the pig velocity versus the superficial gas velocity. The increase in ball pig diameter shifts the lines to a higher pig velocity. An increase in diameter reduces the leakage, which increases the pressure difference over the pig and results in an increase in the pig velocity. At low superficial air velocities, the linear behaviour vanishes, which can be seen for the red and yellow points colliding at $u_{SG} = 1.5$ m/s. More on this in Chapter 5. The superficial gas velocity has a large effect on the pig velocity. This is because of the high air rate flow compared to the rather low water flow rate.

To show the dependency of the water flow rate regarding the pig velocity, a figure with the superficial liquid velocity on the x-axis is created. In this figure, only the 48 mm pig results are displayed. The pig velocity versus the superficial liquid velocity can be found in Figure 4.7. Four different air flow rates are displayed. The air flow rates are 180 L/min, 270 L/min, 360 L/min and 450 L/min in cyan, red, purple, and yellow, respectively. The computed pig velocity is really dependent on the air flow rate. If the air flow rate increases, the data points for the pig velocity increase as well.

The dashed lines in Figure 4.7 are the computed average pig velocity for each air flow rate. With the superficial liquid velocity on the x-axis, one can look at the dependency of the water flow rate. When the superficial liquid velocity increases for every air flow rate, no trend in the dashed lines can be found. The data points lay above and below the average line when the superficial liquid velocity is increased. The ratio of the water flow rate to the air flow rate is so small that an increase in the water flow rate does not necessarily mean an increase in the pig velocity in the experiments. Intuitively, an increase in the superficial liquid velocity shows an increase in pig velocity. This is not visible in these results. In this study, the variance in the results of the experiments is larger than the dependency of the water flow rate in the experiments when looking at the pig velocity. The same result is found for the other pig diameters, but the details are omitted.

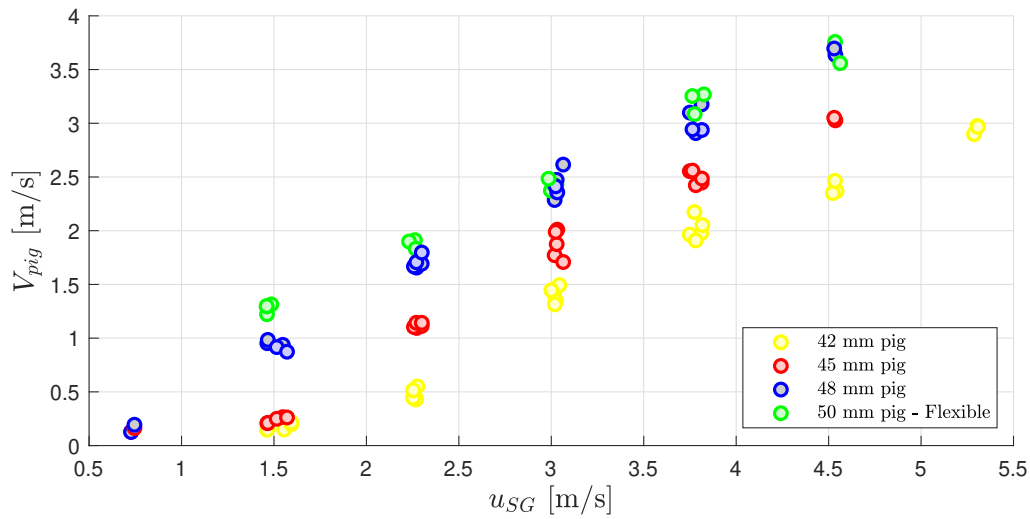


Figure 4.6: Pig velocity versus superficial air velocities for all the pigging runs. The difference in water flow rate with the same air flow rate can be observed as the cluster points at each superficial gas velocity. Yellow, red, blue and green represent the 42 mm, 45 mm, 48 mm and 50 mm ball pig diameter, respectively.

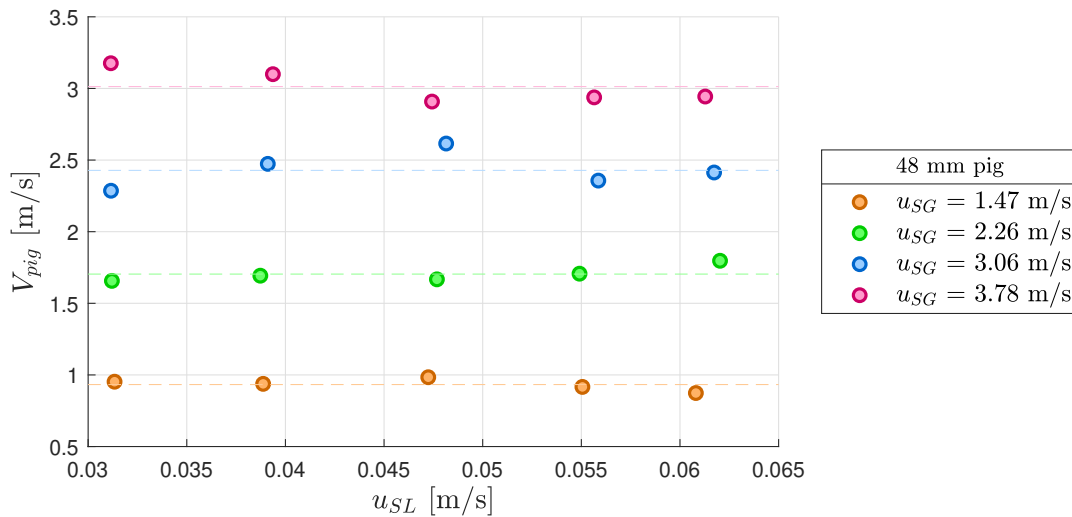


Figure 4.7: Pig velocity versus superficial liquid velocity for the 48 mm pig at four different air flow rates. The scattered points show no relation for when the superficial liquid velocity is changed, while keeping the air flow rate fixed. The dashed line shows the averaged pig velocity for each air flow rate.

4.2.2. Leakage

Besides the pig velocity, the leakage is also an important parameter. When knowing the behaviour at varying pigging conditions, one can design a slug catcher smaller than initially planned. As discussed before, this liquid slug weight can also be converted into surge weight. Next, a leakage can also be defined, as defined in Chapter 3.5.2.

Therefore, the leakage is determined for every pigging run at the experimental conditions as shown in Appendix B.1, Tables B.1 - B.4. Figures 4.8, 4.9, 4.10, and 4.11 show the leakage versus superficial gas velocity for a 42 mm, 45 mm, 48 mm, and 50 mm pig, respectively. The results are shown for the five different liquid flow rates. These are represented in green, yellow, orange, red, blue for $Q_{liq} = 4$ L/min, $Q_{liq} = 5$ L/min, $Q_{liq} = 6$ L/min, $Q_{liq} = 7$ L/min and $Q_{liq} = 8$ L/min, respectively. Furthermore, a limit is set at zero for the y-axis. A leakage value lower than zero implies a low pig velocity such that the liquid flow will overtake the pig instead of leaking past the pig. The bulk velocity of the water will be higher than the pig velocity. This means that pigging with leakage values below zero works ineffective and obstructs the flow. Similar conditions should not be used in industrial applications.

Figure 4.8 shows the results for a 42 mm pig. At low u_{SG} , leakage values of around 0.5 can be observed. A leakage of 0.5 is quite high for a pig. It means that half of the liquid is left behind. From $u_{SG} = 2.5$ m/s and higher, an approximate positive linear trend in the leakage versus u_{SG} is found. This means that the behaviour of higher u_{SG} results in less effectiveness because more leakage occurs. This behaviour can be explained by the phenomenon of leakage of liquid along the pig. Higher u_{SG} corresponds to a higher pig velocity as shown in Figure 4.6. A higher pig velocity results in a higher leakage along the pig. The higher pig velocity is not able to change all the dynamics of the liquid due to inertia in such a short time span. The pig will flow with the easiest trajectory (floating on the liquid) and thus is leaving (leaking) more liquid past the pig. Besides the linear behaviour at high u_{SG} , parallel shifting lines can be observed when increasing the liquid flow rate. The 42 mm pig has shown a minimum leakage value of 0.47 for these experimental conditions. This implies that the pig was able to capture a minimum of 53% of the liquid present during stratified flow and the leakage was at a minimum of 47%. The pointy increase of leakage at $u_{SG} \approx 1.5$ m/s compared to $u_{SG} \approx 2.25$ m/s for the 42 mm pig is not understood and not found for the other size pigs. The behaviour for the 42 mm pig at low velocities should be further researched through new pigging experiments ($u_{SG} < 1.5$ m/s).

The behaviour of the 45 mm pig can be seen in Figure 4.9. Here, the limit for the effectivity of the pig is at approximately $u_{SG} = 0.75$ m/s. The effectivity of the 42 mm pig at these low velocities is not known, because these velocities have not been performed for the 42 mm pig. At approximately $u_{SG} = 2$ m/s, again, an approximate positive linear trend can be observed for the leakage versus the u_{SG} . Furthermore, parallel shifting lines appear when increasing the liquid flow rate. For a 45 mm pig, a smaller minimum leakage is observed at low u_{SG} . Furthermore, the leakage drops to zero when approaching really low velocities. The minimum leakage is 0.1 for these experimental conditions. The behaviour suggests less leakage and more slug capturing during pigging. Next, it can also be observed that the maximum leakage at high velocities for the 45 mm pig is lower than for the 42 mm pig.

At last, the results for the 48 mm and 50 mm pigs are displayed in Figure 4.10 and Figure 4.11, respectively. The effectivity for the 48 mm pig is at approximately $u_{SG} = 0.75$ m/s, which is quite similar compared with the 45 mm pig. The leakage for the 45 mm and 48 mm pig drop below zero at that specific u_{SG} . The leakage for the whole velocity range is just a little lower than for the 45 mm pig. From approximately $u_{SG} = 2$ m/s and higher, an approximate positive linear trend is found with parallel shifting lines when increasing the liquid flow rate. The same behaviour is seen for the 50 mm pig. A maximum of approximately 0.65 (65%) and 0.5 (50%) for the leakage is displayed for the 48 mm and 50 mm pig, respectively. The whole loop is almost cleared at low velocities for the 50 mm pig and 50% at high velocities. This should always be 100% for an oversized ball pig as discussed in Chapter 3.5.2.

The results of these experiments generally show a decrease in leakage when increasing the liquid flow rate for the same size ball pig and when increasing the ball pig diameter. An increase in the superficial gas velocity results in an increase in the leakage. The pig velocity increases with increasing superficial gas velocity and decreases the ability of the pig to push liquid with a lower momentum downstream. The difference in momentum is too large. The pig takes the easiest trajectory, flowing on the liquid towards the top of the pipe. More leakage is present around the pig and this results in lower liquid capturing. This observation is confirmed in Figure 4.12.

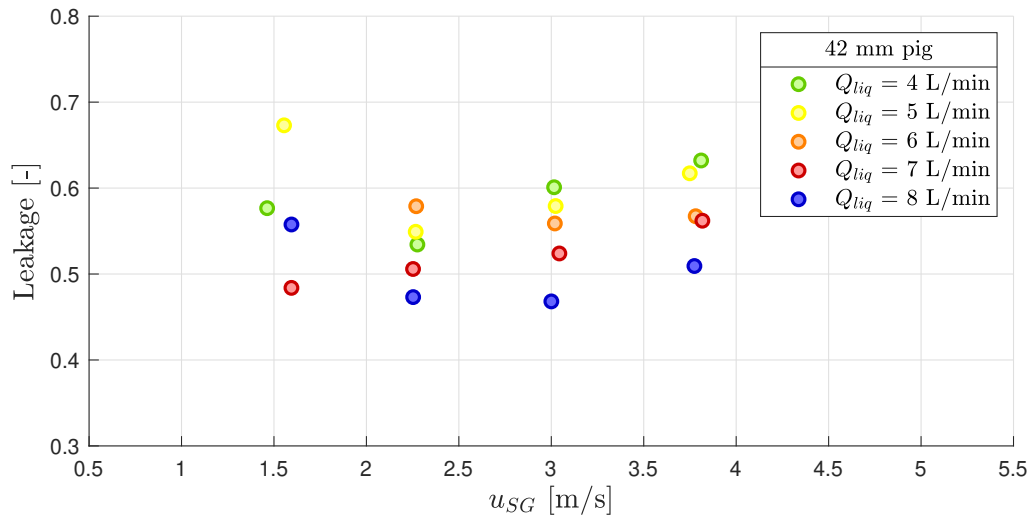


Figure 4.8: Leakage versus superficial gas velocity for 42 mm pig with varying liquid flow rate.

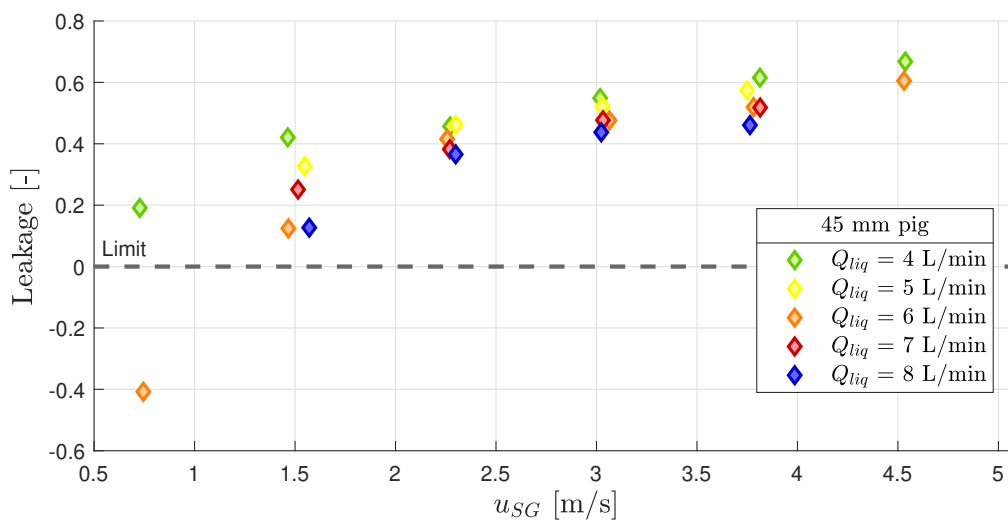


Figure 4.9: Leakage versus superficial gas velocity for 45 mm pig with varying liquid flow rate.

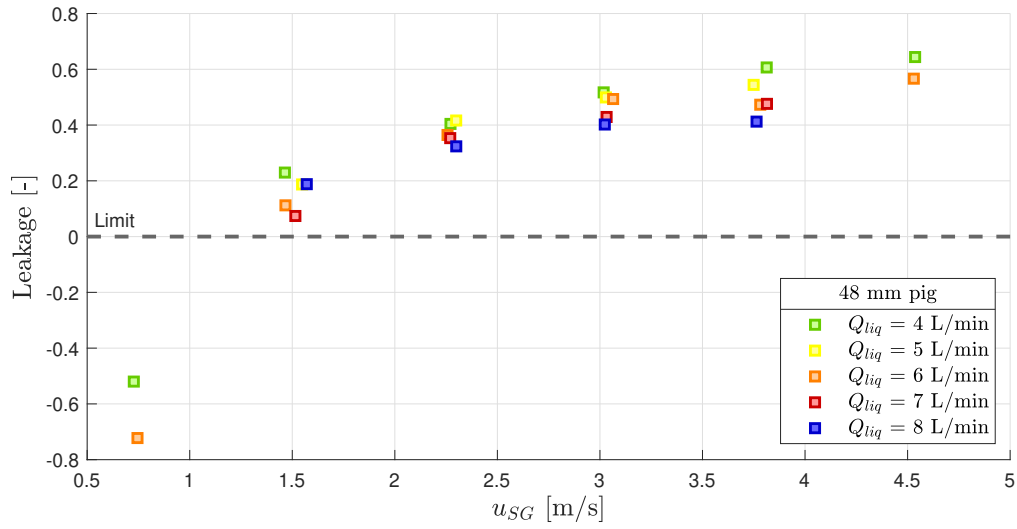


Figure 4.10: Leakage versus superficial gas velocity for 48 mm pig with varying liquid flow rate.

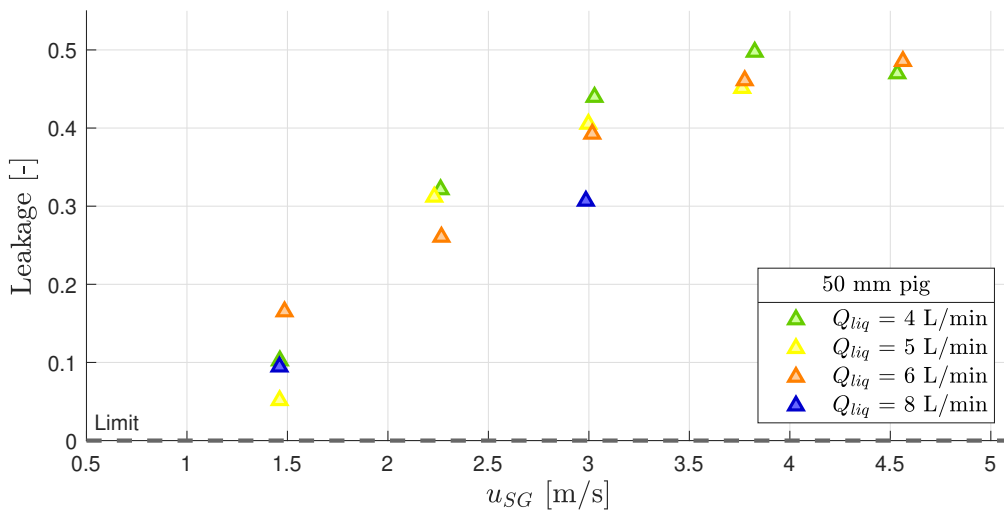


Figure 4.11: Leakage versus superficial gas velocity for 50 mm pig with varying liquid flow rate.

Figures 4.8, 4.9, 4.10, and 4.11 include much data for various experimental conditions. To look into the behaviour of the pig size and the leakage, one can zoom in at a specific superficial gas velocity. This is done in Figure 4.12 for the range between $u_{SG} = 3.74$ m/s and $u_{SG} = 3.82$ m/s. Here, the results for each pig size are shown, including the variation of the liquid flow rate. The difference in superficial gas velocity is so small ($u_{SG} = 3.75$ m/s versus $u_{SG} = 3.815$ m/s) that it seems to lead to only a small difference in the leakage. Looking at Figure 4.12 it can be concluded that increasing the liquid flow rate will decrease the leakage for each size pig. Next, it can be noted that a larger pig diameter will result in a lower leakage for each liquid flow rate. Here, the leakage does not only depend on the gas flow rate, but also on the liquid flow rate. A higher liquid flow rate corresponds to a lower leakage when the zero leakage limit is passed and the positive linear behaviour of the superficial gas velocity versus leakage appears.

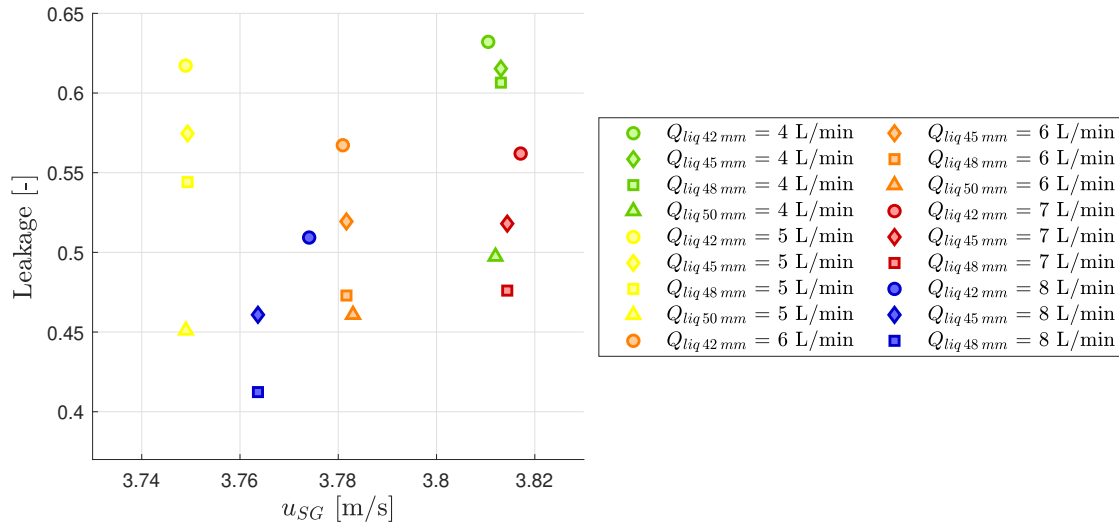


Figure 4.12: Leakage versus superficial gas velocity for 42 mm, 45 mm, 48 mm, and 50 mm ball pigs zoomed in between $u_{SG} = 3.74$ m/s and $u_{SG} = 3.82$ m/s with varying liquid flow rate.

4.2.3. Number of slugs

The creation of a slug as discussed in Chapter 4.1.2 was often observed during the pigging experiments with all the different experimental conditions. It is of interest to study these slugs and in particular the number of slugs during a pigging run. An extension of this research could look into the size of each slug and the time delay between these slugs at particular conditions.

For now, this study will only focus on the number of slugs created at various experimental conditions. In Chapter 3.5.2 a definition for the passing of a created slug is described. This definition is used in the analysis for the pigging runs with a superficial gas velocity higher than $u_{SG} = 2$ m/s. The result of the number of created slugs versus the superficial gas velocity is presented in Figure 4.13. The analysis for the number of created slugs is not done below $u_{SG} = 2$ m/s, because of the limit for the use of pigging discussed in 4.2.2. The results are shown for various pig sizes corresponding to a green diamond, grey point, purple square and orange triangle for the 42 mm, 45 mm, 48 mm, and 50 mm pig, respectively. Regarding the pig size, it can be observed that a larger pig results in less created slugs. The 48 mm and 50 mm pig creates only 1 slug at high superficial air velocities ($u_{SG} = 4$ m/s), compared to approximately 2/3 and 4/5 created slugs for the 45 mm and 42 mm pig, respectively. At lower superficial air velocities ($u_{SG} = 2.5$ m/s) more slugs are created for both the 45 mm and 48 mm pigs. The 42 mm pig produces approximately the same number of slugs over the whole u_{SG} range. Taking note of the observations of the number of created slugs, a link with industry can be made. In industry, solid buoyant pigs with high leakage (i.e., small pig diameter ratio) can be carefully used prior to by-pass pigging, to separate one large slug into multiple small slugs to reduce the size of slug catchers.

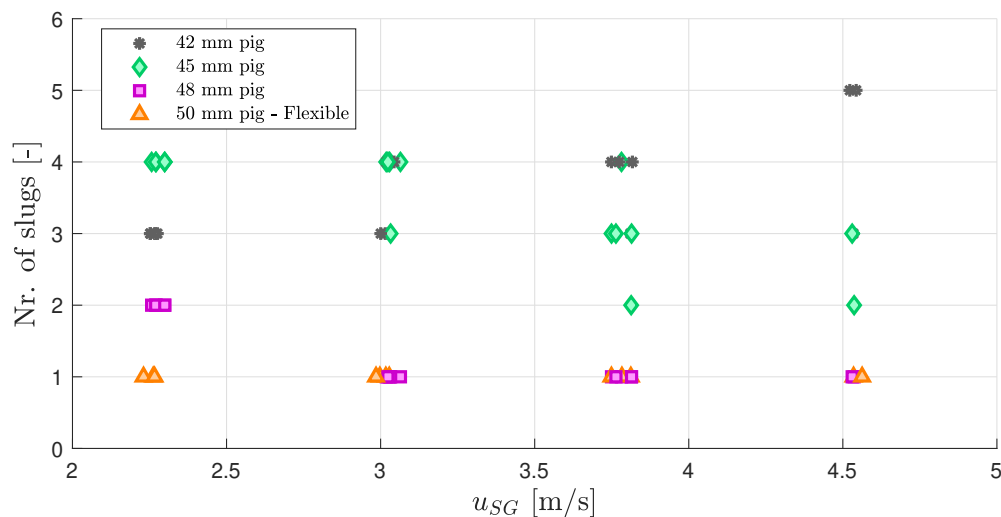


Figure 4.13: Number of created slugs during pigging runs versus superficial gas velocity for the 42 mm, 45 mm, 48 mm, and 50 mm pig.

4.3. Local observations

This section compares the global pigging results with local results which are found using the video recordings. The video recordings of a couple of pigging runs are analyzed and the pig is tracked with the video processing flowchart as discussed in Section 3.2.6. Next, the tracking process of one individual pigging run is analyzed. Further clarification on the behaviour of this pigging run is given.

4.3.1. Global and local velocities

First of all, a comparison will be made between the global averaged pig velocity over the whole flow loop and the local tracked pig velocity. For this comparison, runs for the 45 mm pig size are used. A total of 9 runs are analyzed. The analysis of the video recordings requires much attention, tweaking, and computing power to obtain justified pig tracking. Differences in light intensity, interruption, and slug creation at the interface of the pig change during the presence of the pig in the field of view. Subsequently, optimal settings need to be found by iterating the process. The settings are hard to determine for the whole video because of the presence of multiphase flow.

Figure 4.14 shows the global and local pig velocity in red and blue circles, respectively. The pig velocity is plotted together with the air velocity. In this data set, the liquid flow rate for every two points (global and local) is the same at a specific air velocity, but are not necessarily the same when changing the air velocities. The linear trend as observed in Figure 4.6 can also be observed here. When looking at the plotted values, an acceptable match between the global and local pig velocity can be observed. The local pig velocities acquired via video tracking are persistently a little higher than the global pig velocities. With this data set, a maximum error of 12% between local and global pig velocity is found. A trend in the mismatch between local and global pig velocity for higher air velocities is not found. A possible cause of the mismatch between the local and global pig velocity is the start of the pig with zero velocity. The computed global velocity includes the initial increase in pressure where the pig is still accelerating. The local velocity does not include this. This causes the average local pig velocity to be higher than the global pig velocity.

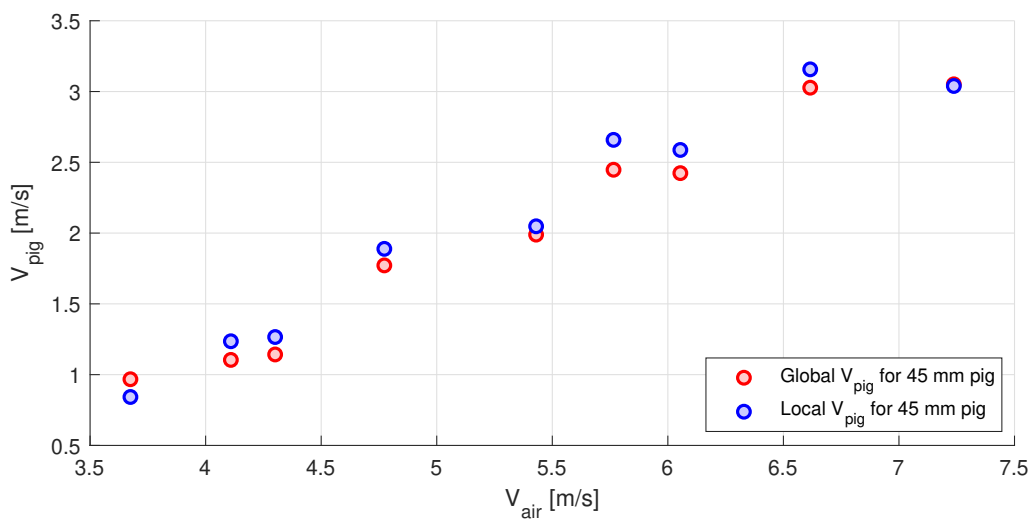


Figure 4.14: The global and local pig velocity versus air velocity. The global pig velocity is determined as discussed in Chapter 3.5.2. The maximum error for this specific data set is 12%.

4.3.2. Local velocity

One of the analyzed video recordings will be looked at with more detail. Figure 4.15 shows the observed local pig velocity during its time in the Field Of View in the video recordings. In the run shown in Figure 4.15 a pig passed the field of view in approximately 3 seconds. The pig tracking routine presents a wavy pig velocity with a value between approximately 0.5 m/s and 3 m/s. This variation is due to the slug growth and the slug propagation as discussed in Chapter 4.1.2. The pig propagates through the loop and at the front of this pig a liquid slug is developing. The initially low velocity and inertia of the growing liquid disturbance decrease the pig velocity. The pig velocity decreases until the moment that the liquid disturbance is too large. Now the air can no longer bypass the liquid and as a consequence the pressure behind this disturbance increases. The air pressure behind this disturbance eventually causes the disturbance to propagate a slug. The pig accelerates because of the increased air pressure behind the pig. After this acceleration, another disturbance will be created, which in turn decreases the pig velocity again. This sequence differs in time and magnitude for varying experimental conditions. Figure 4.15 shows this sequence for the wavy velocity. Here, only the acceleration and deceleration of the pig are observed. The computed local velocity passing the video recordings can be totally different from the computed global velocity due to a wavy dynamic pig velocity.

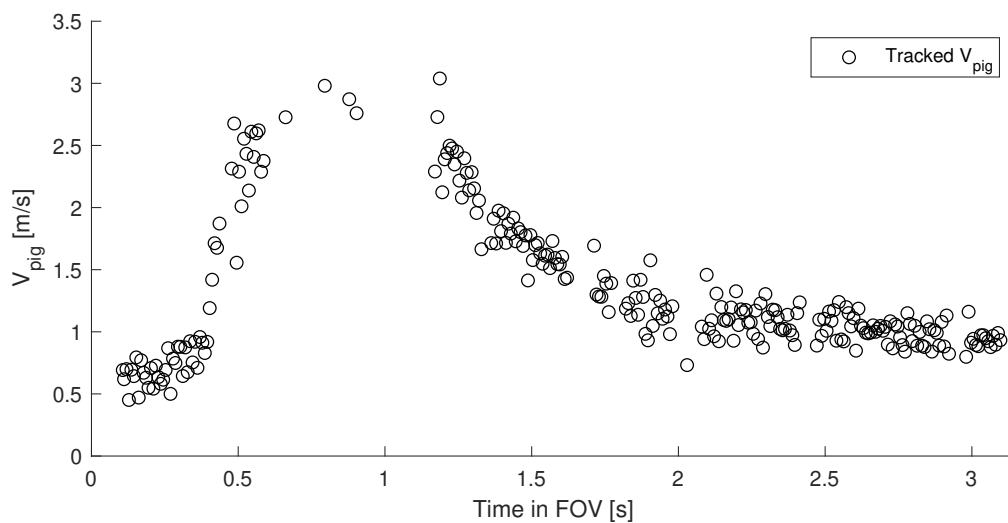


Figure 4.15: Local pig velocity found with the use of the video recordings. The tracked pig velocity is shown during the time that the pig is approximately present in the FOV of the cameras.

5

Analysis and Comparison

Chapter 4 has shown the results of the various pigging experiments done. This chapter will look at the results in more detail. The main parameters, pig velocity and leakage, will be investigated and a non-dimensional analysis is performed. Three regions for the pig velocity are found. These regions are also found in a previous numerical study on undersized ball pigging [19] and will be explained. Next, correlations for the pig velocity and leakage will be presented. Besides, an analytical leakage model will be used to compare the experimental leakage.

5.1. Pig velocity

5.1.1. Scaling

First of all, a larger understanding of the pig velocity will be discussed. Figure 4.6 presented the results of the pig velocity versus the superficial air velocity. A more comprehensive result can be shown with the use of a non-dimensional analysis. A non-dimensional analysis on undersized ball pigging is investigated in Chapter 2.4. Dividing the pig velocity by the mixture velocity ($\frac{V_{pig}}{V_m}$) will be called the normalized pig velocity. Whenever the normalized pig velocity approaches 1, a ball pig with a diameter ratio of 1 is used. The ball pig flows with the same velocity as the flow and no leakage will occur. An undersized ball pig is never able to approach 1, because leakage of the gas and liquid is present. The result of the various pig diameters for the normalized pig velocity is shown in the left graph in Figure 5.1. The clusters of points are the pigging experiments with various u_{SL} at a fixed u_{SG} .

For the creation of correlations and further scaling, the 42 mm, 45 mm and 48 mm data are used. The 50 mm data are not used, because a different weight, flexibility, and nearly oversize pig misrepresents correlation with the other equal property pigs. The next step for a more distinct data representation is the averaging of the clustered points. Averaging the clustered points creates individual data points for a given u_{SL} at fixed u_{SG} . This is done to better detect the factors associated with the pig velocity. Next, as found from the non-dimensional analysis, the area ratio can also be taken into account. Thus, the pig velocity will be divided by the mixture velocity and divided by the area ratio. The area ratio is defined as: $A_{ratio} = \frac{d^2}{D^2}$. Representing the data with averaged u_{SL} quantities and taking the area ratio into account will compute Figure 5.1 on the right. This figure will be used for a more in-depth investigation.

5.1.2. Correlations

As discussed in Figure 4.6, here in Figure 5.1 it can also be observed that an increase in u_{SG} will increase the pig velocity. Furthermore, an increased shift is apparent when increasing pig size. Next, the area ratio is taken into account to close the distance between the various pig diameter lines. The interesting part on the right of Figure 5.1 is that the normalized pig velocity divided by the area ratio versus u_{SG} takes the shape of three different regions. These three regions become visible for the experimented pig sizes. The three different regions are marked in Figure 5.2 for the 45 mm pig and are labelled as Region A, Region B, and Region C.

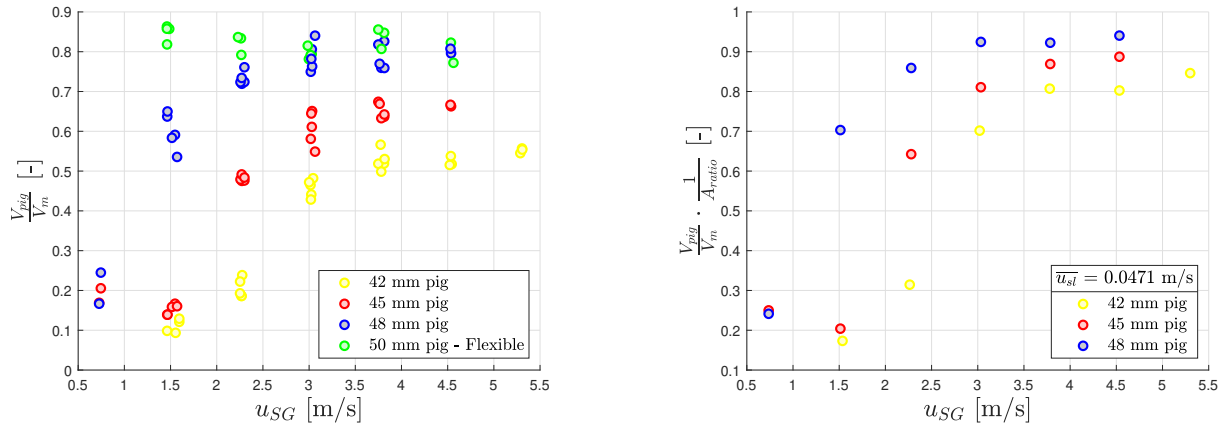


Figure 5.1: Left: Averaged pig velocity divided by the mixture velocity versus u_{SG} for the experimented data. Right: Averaged pig velocity divided by mixture velocity and divided by area ratio of the pig. Data points with difference in u_{SL} are averaged to $\overline{u_{SL}} = 0.0471$ m/s.

In Region A a slight to moderate decrease is seen in the normalized pig velocity with increased u_{SG} . This decrease is so small and should actually increase when increasing u_{SG} . Increasing the flow velocity is inevitably coupled to an increased pig velocity. This means that the pig is roughly insensible to a change in normalized pig velocity at increased u_{SG} in Region A. In region B, the normalized pig velocity increases significantly from 0.25 to 0.8 with increased u_{SG} and can be approached by a power law. Then in Region C, the normalized pig velocity does not increase significantly but experiences a rather stable level with increased u_{SG} . The approached power law can be used for region B and region C.

The appearance of three different regions is not limited to the 45 mm pig, but can also be observed for the 42 mm and 48 mm pigs. When looking at Figure 5.2 it can be observed for the 42 mm pig that the start of Region B shifts to the right. This means that Region A will be present for a larger u_{SG} range. On the other hand, it can be observed that for the 48 mm pig Region A is not present. At least, it is not visible for the experimental conditions tested. Region B shifts to the left for the 48 mm pig and Region C (stable platform) also shifts to the left. Region B and Region C can be approached with a power law for the three different pig diameters. Figure 5.3 shows the fitted power laws with the u_{SG} axis limit set to Region B and Region C. The coefficients for the power laws can be found in Table 5.1.

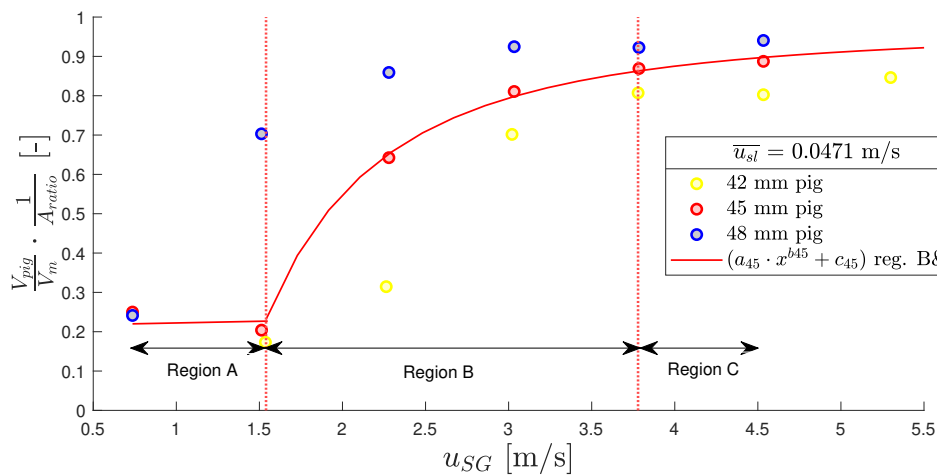


Figure 5.2: Averaged pig velocity divided by the mixture velocity and area ratio versus u_{SG} . There are three distinguished regions, called Region A, Region B and Region C for small to large u_{SG} , respectively.

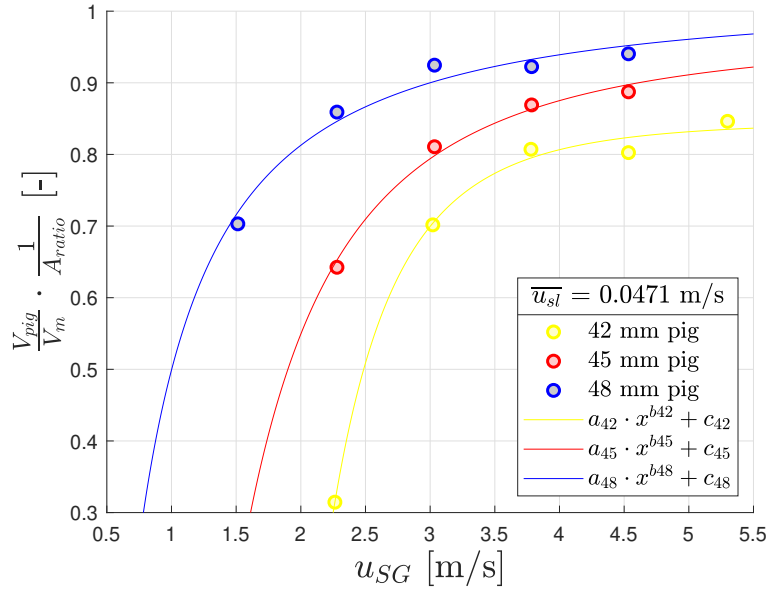


Figure 5.3: Fitted power law correlation for the normalized pig velocity versus u_{SG} . The power law formulas are made for the three various pig diameters and can be used for Region B and Region C. The coefficients for the power law formulas are presented in Table 5.1.

5.1.3. Interpretation

The three selected regions in Figure 5.2 have been presented before in a previous study on undersized ball pigging by M. Jiang [19]. As discussed before, in the previous study, numerical pigging simulations have been performed under single phase flow conditions. The study argues that under single-phase flow conditions, the normalized pig velocity from Region A to Region B is apparently by the change of the fluid velocity profile from laminar to turbulent. In this study, multiphase flow is present, which adds much complexity. Still, an attempt is made to relate the multiphase findings to the single phase correlations. A simplified calculation will be made on the local Reynolds number for air at the pig interface for various pig sizes. The local Reynolds number will be calculated for the velocities at the transition region. Here the velocity and influence of the water will be neglected.

Table 5.1: Correlation coefficients for Figure 5.3.

-	42 mm	45 mm	48 mm
a_{xx}	-22.370	-1.871	-0.525
b_{xx}	-4.579	-2.154	-1.312
c_{xx}	0.846	0.970	1.024

To calculate the local Reynolds number for air, a surface area past the pig is needed. In this way, u_{SG} can be converted into local air velocity. In Figure 5.4 the cross-sectional view of an undersized ball pig in a pipe is shown. This cross-sectional view is reproduced from [28]. The undersized area is needed to compute the local air velocity. First of all, the height (h_{α_L}) can be computed with the use of the following equation (5.1) from [28]:

$$A_L = \cos^{-1}\left(\frac{R - h_{\alpha_L}}{R}\right) \cdot R^2 - (R - h_{\alpha_L})^2 \cdot \tan\left(\cos^{-1}\left(\frac{R - h_{\alpha_L}}{R}\right)\right) \quad (5.1)$$

Where A_L is the surface area of the liquid present in the pipe. In the proceeding calculation, an averaged hold-up of $\alpha_L = 0.35$ is used to calculate the surface area of the liquid and gas present in the pipe. This is a frequently experienced value for stratified flow during the experiments. The leak area ($A_{Leak,L}$) will be used later.

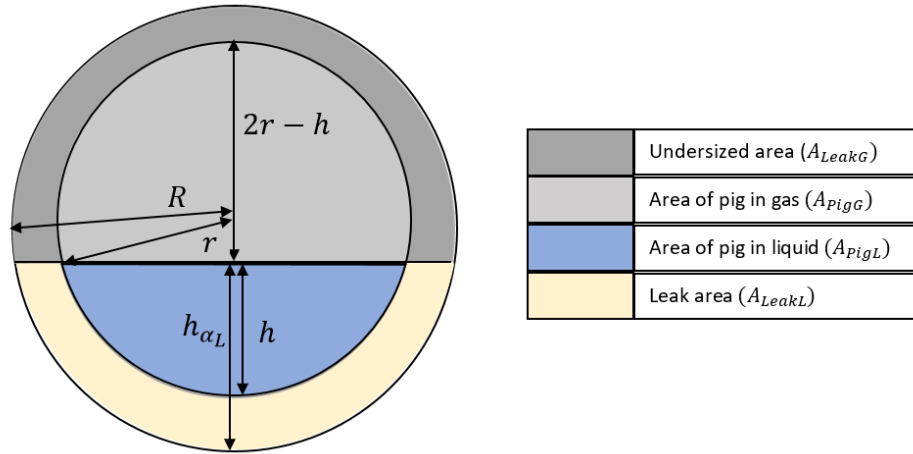


Figure 5.4: Cross-sectional view of an undersized ball pig in a pipe. Here, the cross-sectional view is divided in different cross-sectional areas. Reproduced and adapted from Richa [28].

The height h is used earlier in Table 3.1 for the 42 mm, 45 mm, and 48 mm pig to determine the 'ball height fraction floating in water'. The area of the pig in liquid ($A_{Pig,L}$) can then be determined with Equation (5.2).

$$A_{Pig,L} = \cos^{-1}\left(\frac{r-h}{r}\right) \cdot r^2 + (r-h)^2 \cdot \tan\left(\cos^{-1}\left(\frac{r-h}{r}\right)\right) \quad (5.2)$$

The undersized area ($A_{Leak,G}$) can then be determined using the area of pig in gas ($A_{Pig,G}$) and the following Equation (5.3):

$$A_{Leak,G} = (A - A_L) - (A_{Pig} - A_{Pig,L}) \quad (5.3)$$

Where A_{Pig} is the frontal surface area of the pig and A is the surface area of the pipe. The computed undersized area ($A_{Leak,G}$) can then be used to determine the local air velocity with the following equation (5.4):

$$u_{G,local} = \frac{\dot{V}_G}{A_{Leak,G}} = \frac{u_{SA} \cdot A}{A_{Leak,G}} \quad (5.4)$$

With this local air velocity, a local Reynolds number for air can be computed, as shown in Equation (5.5).

$$Re_{G,local} = \frac{u_{G,local} \cdot L_{local}}{\nu_G} \quad (5.5)$$

Where the local Reynolds length scale (L_{local}) will be assumed to be equal to $R - r$. The kinematic viscosity for air will be chosen at 20 °C and atmospheric pressure. This results in: $\nu_G = 1.6 \cdot 10^{-5} \text{ m}^2/\text{s}$. Performing these calculations for the three pigs, using u_{SG} at the transition from Region A to Region B, a result for the local Reynolds numbers for air is presented in Table 5.2.

Table 5.2: Computation results of the local Reynolds number for air at the transition from Region A to Region B.

-	42 mm	45 mm	48 mm
Transition u_{SG} from Reg. A to B.	2 m/s	1.5 m/s	0.75 m/s
$u_{G,local}$	11.02 m/s	13.27 m/s	17.80 m/s
$A_{Leak,G}/A \cdot 100$	18.1 %	11.3%	4.2%
L_{local}	5 mm	3.5 mm	2 mm
Local gas Reynolds number: $Re_{G,local}$	3444	2902	2225

With this crude approximation of the local Reynolds number for air, at the transition region, a remarkable result appears. The local Reynolds numbers are approximately 2000 to 3000 for the various undersized ball pigs. Reynolds numbers around 2000 - 3000 are generally accepted as the transition from laminar to turbulent flow, as discussed in Chapter 2.2. The presence of the pig and all its disturbances will decrease this transition value below the generally accepted value. Note that the local Reynolds numbers are too high, but they still approximate the transition behaviour from laminar to turbulent flow. Referring to the transition regime, it means that the transition from laminar to turbulent air flow at the pig changes the behaviour of the normalized pig velocity. Apparently, the turbulent flow will rapidly increase the normalized pig velocity as is observed in Region B, represented in Figure 5.2. This confirms the transition behaviour as suggested by Jiang [19] even though single-phase and multiphase flow are quite different.

The Reynolds number is the ratio of the inertial forces and the viscous forces, as discussed in Chapter 2.2. At low Reynolds numbers, a local laminar flow for air is present and viscous shear forces are dominant. At higher Reynolds numbers a turbulent flow is present and inertial forces become dominant. Figure 5.2 shows three distinguished regions with a transition from Region A to Region B when the local Reynolds number for air approaches the turbulent regime. This means that, when translating the Reynolds number into forces, Region A will be dominantly affected by the viscous shear forces. At the transition region and in Region B, inertial forces will start to play a role due to the development of a turbulent flow regime. From Region B to the beginning of Region C, viscous shear forces will start to play a minor role and the inertial forces become the dominant factor. The transition of Regions B and C, at approximately $u_{SG} = 3.75$ m/s, has a local Reynolds number for the air of 6457, 7256 and 11126 for the 42 mm, 45 mm, and 48 mm pig, respectively. Note that this is a crude approximation of the Reynolds number in stratified flow and should only be used in an attempt to distinguish the regions. The high Reynolds numbers are present in the turbulent flow regime. At the transition region and in Region C, inertial forces will play the dominant role and the viscous shear forces will start to be negligible when compared with the pressure forces. The result is a stable level for the normalized pig velocity versus the superficial air velocity.

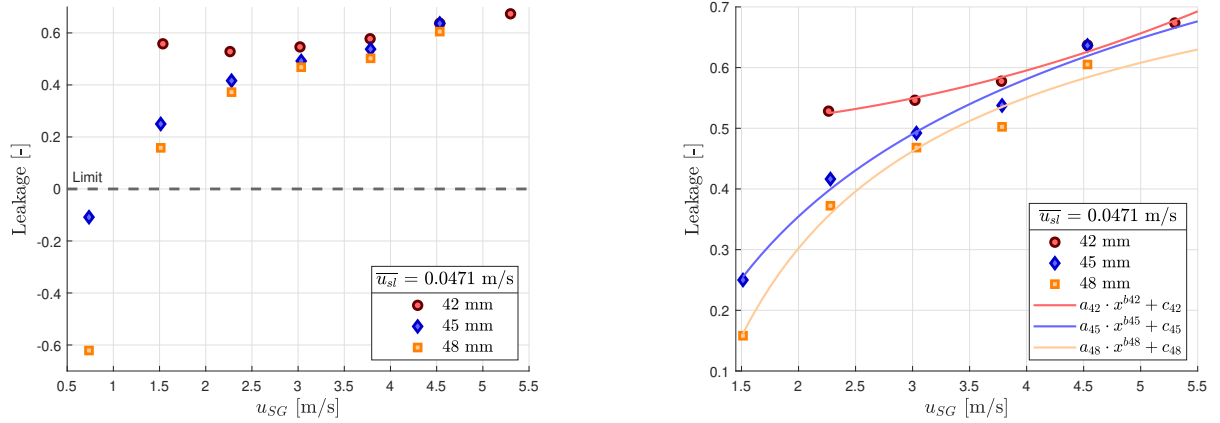


Figure 5.5: Left: Leakage of the pig versus u_{SG} . Right: Leakage of the pig versus u_{SG} with fitted power laws for the various pig diameters. The difference in u_{SL} , for the experimental conditions, is averaged to $\overline{u_{SL}} = 0.0471$ m/s for the left and right graphs.

-	42 mm	45 mm	48 mm
a_{xx}	0.005254	-2.214	-1.045
b_{xx}	2.128	-0.1774	-0.7122
c_{xx}	0.4949	2.312	0.94

Table 5.3: Correlation coefficients for Figure 5.5.

5.2. Leakage

Next, a better definition of the leakage will be presented. First, part of the data presented in Figure 4.8, 4.9 and 4.10 will be selected, plotted together, and correlations will be created. After the displayed correlations, an analytical leakage model will be used to compare with the experimental leakage.

5.2.1. Correlations

In Chapter 5.1.2, Figure 5.1, an average has been computed for the normalized pig velocity versus u_{SG} with varying u_{SL} . This resulted in an average of $\overline{u_{SL}} = 0.0471$ m/s. The same is done in the left graph of Figure 5.5 for the leakage versus u_{SG} . This means that Figure 4.8, 4.9, and 4.10 are each averaged to one u_{SL} and presented in one graph. The leakage, as discussed in 4.2.2, increases with u_{SG} . Besides, at low u_{SG} the effectivity of undersized ball pigging is lost because the leakage drops below zero. The difference in leakage of pigging with various pig diameters reduces at high u_{SG} . The result from the study by M. Jiang [19] showed that the single phase leakage will decrease when the pig diameter increases. This is in agreement with the results found in this multiphase experimental study.

A curve is fitted to the results shown in the left graph of Figure 5.5 for the turbulent flow regime (Region B & Region C). A power law fit is used, just as for the pig velocity, and can be seen in the right graph of Figure 5.5. The coefficients for this power law can be found in Table 5.3. The correlations can only be used in the approximated turbulent Region B and Region C as presented in Figure 5.2.

5.2.2. Comparison with a model

The correlations approximate the leakage due to the presence of the undersized ball pig. The results will now be compared with an analytical leakage model. This model is adopted from the OLGA manual for dynamic multiphase pipeline simulations¹. The model approximates the leakage flow rate past an undersized ball pig with the assumption of a fully liquid-filled pipe. It is called slip-induced leakage.

Regarding the model, assume a pipe that only contains and flows liquid. In this pipe, an undersized ball pig will be deployed which is propelled by air. Due to the slip between this undersized ball pig and the fluid surrounding it, some fluid ahead of the pig will start to leak between the pipe wall and the pig. A calculation of the local Reynolds number at this point will probably result in a small Reynolds number producing a laminar water flow. The pipe wall is at zero velocity and the pig flows with V_{pig} . A laminar flow then induces an average water film velocity given by Equation (5.6).

$$V_f = \frac{1}{2} \cdot V_{pig} \quad (5.6)$$

While doing this, the effects of pressure gradient and gravity are neglected. This can only be done when the gap between the pipe wall and the pig is very narrow. Assuming a centred pig in the pipe, the volumetric leakage flow rate is then given by Equation (5.7).

$$Q_{fl} = \frac{\pi(D^2 - d^2)}{4} \cdot V_f \quad (5.7)$$

Where D is the inner pipe diameter in meters and d is the outer pig diameter in meters.

For stratified flow, a liquid hold-up will be present. The OLGA model assumes that for stratified flow, the total leakage of gas and water is proportional to the hold-up of each respective phase at that position. This means that the computed volumetric leakage flow rate for water will be multiplied by the averaged hold-up values from the experiments. In this way, the model can be used to compare the experimental leakage with the leakage derived from the model. First of all, a verification of the assumption of a laminar water film will be made. The local Reynolds number will be calculated in the same manner as performed in Chapter 5.1.3 using Figure 5.4. Using the same averaged hold-up value of $\alpha_L = 0.35$ and the averaged u_{SL} from Figure 5.1 ($\overline{u_{SL}} = 0.0471$ m/s), an approximation of the local Reynolds number for liquid can be made. The only difference is the area chosen to compute the local liquid velocity at the pig. Here, the leak area is used ($A_{leak,L}$). Equation (5.4) and (5.5) change to the following two equations for the liquid:

$$u_{L,local} = \frac{\dot{V}_L}{A_{leak,L}} = \frac{u_{SL} \cdot A}{A_{leak,L}} \quad (5.8)$$

$$Re_{L,local} = \frac{u_{L,local} \cdot L_{local}}{\nu_L} \quad (5.9)$$

With ν_L equal to $8.005 \cdot 10^{-7}$ m²/s for water at 30 °Celsius. The resulting local Reynolds numbers for the liquid are 1770, 1239, and 708 for the 42 mm, 45 mm and 48 mm pig, respectively. Assuming a laminar water flow will be quite valid, even though the Reynolds numbers are not deeply in the laminar flow regime. In this model, we neglect the influence of the high Reynolds number of air in the turbulent regime on the velocity profile of the liquid.

The theoretical leakage is computed for one specific u_{SL} and will be compared with the experimental results for the various pig diameters. Figure 5.6 presents the leakage versus u_{SG} at $u_{SL} = 0.0314$ m/s for the various pig diameters in the turbulent regime for air (Region B & Region C). Furthermore, the analytical model is computed at these conditions for the various pig diameters and displayed. The model does not, by any means, approximate the experimental results. For example, the model gives a leakage factor for the 48 mm pig that is almost a factor 3 smaller than the experimental leakage factor. The model values for the 42 mm and 45 mm pigs approximate the experimental results much better, but still not very closely. Besides, for the 42 mm and 45 mm pigs, the gap becomes so large that the laminar flow assumption is not valid anymore.

¹<https://www.software.slb.com/products/olga>

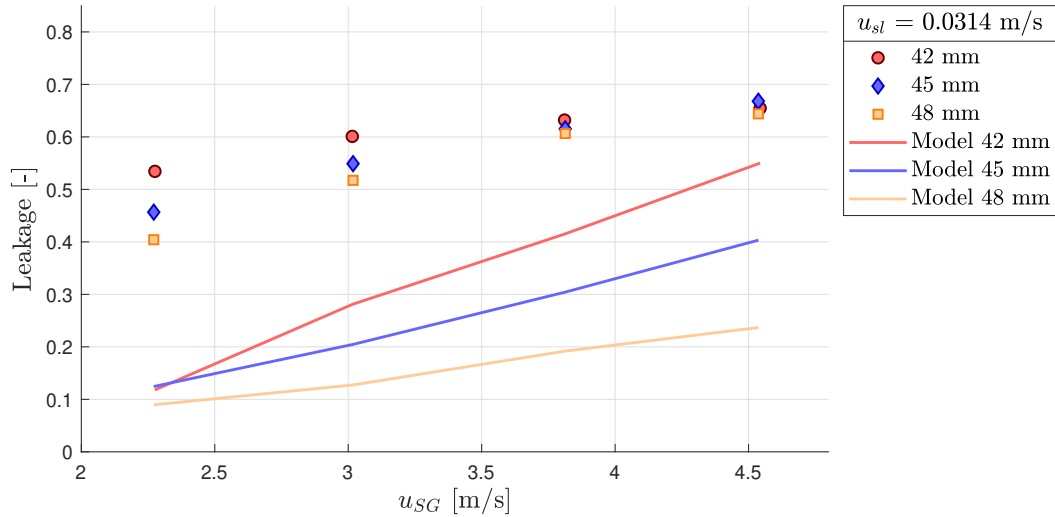


Figure 5.6: The leakage results from experiments, for $u_{sl} = 0.0314$ m/s, is plotted versus u_{SG} . The results are shown for the 42 mm, 45 mm, and 48 mm pig in red, blue and orange, respectively.

The model as used in the OLGA software is not able to approximate the leakage as obtained in the flow loop experiments. The previous study [19] also found that this model has shortcomings in single-phase numerical pigging. Both for the laminar and turbulent flow regime, another relationship for the average fluid film velocity (V_f) between the pipe wall and the pig was presented.

This newly defined relationship in the turbulent regime is used to compare the experimental results, again, with the model. The relationship for the average fluid film velocity in the turbulent regime is taken from the Master Thesis by M. Jiang in [19] as:

$$V_f = V_{pig} \cdot 1.625 \cdot Re^{-0.134} \quad (5.10)$$

This relationship gives a lower average fluid film velocity at high Reynolds numbers than given by the OLGA model ($V_f < 0.5 \cdot V_{pig}$). This means that the leakage computed by the model (5.10) is even lower than with the OLGA model, giving thus an even larger difference with the experiments. The present analytical model should be modified and extended with additional relevant parameters in future research. First of all, the pressure gradient cannot be neglected in the model at Region B & Region C. The pig velocity significantly increases in Region B, due to the transition of the air from laminar to turbulent flow, increasing the role of the pressure gradient. This means that, even though the local Reynolds number for the liquid is laminar, we cannot neglect the influence of the high Reynolds number for air in the turbulent regime. The effect of gravity (and buoyancy) should also be taken into account. The ball pigging experiments show a quite significant leakage. This is due to the fact that the pigs were buoyant in the flow, i.e., they are not centred in the pipe, but more located at the top of the pipe. Next, the disturbances can also alter the results due to the propagation of slugs. These aspects should be taken into account when proposing an improved model.

5.3. Discussion

The statements and correlations discussed are, for now, limited to the reported loop experiments and the created ball pigs. The average pig velocity, liquid leakage, and number of slugs are determined assuming that the pig is in steady state along the whole length of the flow loop. This is not fully valid, because many aspects in the flow loop are in reality unsteady.

Some unsteady aspects of the flow loop will be discussed. The major unsteady aspects having an impact on the results are the following:

- Predominantly at high velocities it was observed that the opening of the valve of the pig launcher, redirecting the flow, produced such a disturbance in the stratified flow that an intermittent slug was already rapidly created. The origin of the first intermittent slug is not limited to the interference of the pig. This will alter the results of the computed leakage when compared with the leakage created solely by the presence of the pig.
- The inlet section at the beginning of the flow loop is used to create a stable stratified flow. The pig launcher, which is placed directly after the inlet section, redirects the flow sideways before entering the straight segments of the flow loop. This causes a disturbance and undeveloped flow at the straight segments of the flow loop. The new pipe couplings also add some disturbance to the flow. As a result, a lower limit of stratified flow is found during the pigging experiments when compared to the flow map shown in Figure 2.4. The presence of stratified flow or wavy stratified flow will also play a role in the results found with pigging.
- An averaged pig velocity is computed using the first pressure sensor and the end of the hold-up sensor. This computation is not entirely correct, because the pig still undergoes a large acceleration after passing the first pressure sensor.

The accuracy and sampling rate of the measurement apparatus should also be taken into account. The weighing scale has a quite low sampling rate, which could differ from the computed leakage at high velocities. The gas and liquid flow meters are limited to a certain accuracy. The hold-up fraction is also assumed to be equal over the whole length of the flow loop. This is not necessarily fully true as it is based on a local measurement taken almost at the end of the flow loop. It is also assumed that the redirected flow at the end of the loop, to the weighing scale with a flexible hose, does not interfere with the logged weight.

The data analysis is performed with the use of graphs and clicking on the points for the first increase in pressure, the pig passing the end of the hold-up sensor, and weight estimation. Although the values were selected with good care, they maybe could be determined with a higher accuracy by using an automated script.

6

Conclusions

In this Master Thesis Project, multiphase pigging experiments were performed to obtain more insight on the flow around an undersized ball pig in a horizontal pipe. It builds on the single-phase numerical pigging simulations by M. Jiang [19]. In this study, the pig velocity and the liquid leakage were of particular interest. The influence of pigging in a 52 mm pipe with various undersized ball pig sizes (mainly 42 mm, 45 mm, and 48 mm) and experimental conditions were presented. General observations, global experimental results, and local experimental results of undersized ball pigging were shown. Next, a non-dimensional analysis was performed on the main parameters of the undersized ball pig, which are the pig velocity and the liquid leakage. At last, the experimental leakage results have been compared with approximations from the leakage model, as used in the commercial package OLGA for dynamic multiphase pipeline simulations. The main findings from this study are listed below. First, conclusions based on pigging observations will be presented. Next, conclusions based on the global - and local experimental results are shown, using the factors associated with undersized ball pigging. At last, conclusions based on the more in-depth analysis and the leakage model are given.

Conclusions based on the pigging observations:

- In this study, pigging experiments have been performed for (wavy) stratified flow. The flow becomes rapidly unstable at liquid flow rates of 10 L/min ($u_{SL} = 0.0785$ m/s, $u_{SG} \approx 1.5$ m/s). Without the presence of the pig, intermittent slugs will be created. Two-phase flow regime maps for gas - and liquid flow in horizontal pipes show that stratified flow should be present at these velocities. The pig launcher and new pipe couplings create quite some disturbance to the flow. This lowers the maximum flow velocities for stratified flow. Therefore, a safe upper limit is set for pigging in a (wavy) stratified flow ($u_{SG} \approx 4$ m/s, $u_{SL} \approx 0.0628$ m/s).
- Pigs with a higher density than the liquid phase will be submerged in the liquid layer. Such pigs with a diameter ratio (the ratio between the pig diameter and the inner pipe diameter) of approximately 0.9 will have a high gas leakage area. High gas leakage results in an increased risk of pig stall. This is more pronounced for low flow velocities. For the industry, it is recommended to create buoyant pigs (e.g., 3D-printed balls) when using a diameter ratio of approximately 0.9 to adapt to low flow velocities during pigging.
- It is observed that the pigs accumulate liquid at the front of the ball and create one or multiple liquid slugs during the time that the pig is present in the flow loop. The created liquid slug will propagate and separate from the pig at a certain point. The separated slug fills the cross-sectional area of the pipe and the liquid will be accelerated due to an increase in pressure behind the slug. During the time that there is a low amount of liquid in front of the pig, it will accelerate until it eventually decelerates when a new liquid accumulation is created in front of the pig. This typical behaviour is less pronounced for high pig velocities.

- The undersized ball pigs show frequent vertical movement due to liquid slug accumulation and propagation. During liquid slug accumulation, friction at the top of the pipe wall cannot be neglected for buoyant pigs as they will float on the liquid.

Conclusions based on the global and local results:

- The change in superficial liquid velocity did not lead to significant changes in the pig velocity. The influence of a small change in the superficial liquid velocity disappears under the large difference of the gas and liquid flow rate. The gas flow rate is on average 90 times larger than the liquid flow rate.
- The undersized ball pig velocity increases linearly with increasing superficial gas velocity (u_{SG}).
- The liquid leakage past the undersized ball pigs increases with increasing superficial gas velocity and decreases with increasing superficial liquid velocity. The liquid leakage increases linearly with increasing superficial gas velocity starting at approximately $u_{SG} \approx 2$ m/s. A larger diameter ratio pig results in a lower liquid leakage.
- The buoyant pigs show a liquid leakage of approximately 60% for the highest superficial gas velocities used in the experiments. The difference in liquid leakage between the various pig sizes decreases for large superficial gas velocities ($u_{SG} \approx 4$ m/s).
- The liquid leakage drops below zero for low superficial gas velocities ($u_{SG} \approx 0.5$ m/s). Undersized ball pigging becomes ineffective for these velocities, because the liquid flow will overtake the pig instead of leaking past the pig.
- The number of created liquid slugs decreases when the superficial gas velocity is increased. The number of slugs also decreases when increasing the diameter ratio of the pig. For large diameter ratio pigs (0.923 and 0.961) and high superficial gas velocities, it is observed that the pig velocity is higher than the velocity of the created slugs. This causes the different slugs to be merged into one liquid slug before the end of the loop. Smaller diameter ratio pigs (0.807 and 0.865) create multiple liquid slugs over the whole range of measured superficial gas velocities. This typical behaviour could be of interest in the industry; the split of one large liquid slug into multiple smaller liquid slugs can reduce the size of the slugcatcher.
- The analysis of the video recordings showed that the average local - and global pig velocities differ approximately 12% for the 45 mm pig. The local pig velocity is wavy over the length of the field of view of the recordings. The pig velocity is found to be dynamic over the whole length of the flow loop due to liquid slug accumulation and propagation.

Conclusions based on the comparison with the leakage model:

- The normalized pig velocity (being the pig velocity divided by the mixture velocity) increases with increasing superficial gas velocity within three different regions. In the first region, at low and increasing superficial gas velocity, almost no increase in the normalized pig velocity can be observed. In the second region, the normalized pig velocity increases significantly. In the third region, the normalized pig velocity reaches a stable level. The normalized pig velocity in the second and third region can be described with a fitted power law.
- The transition from the first to the second region can be described by using a crude approximation for the local Reynolds number of the gas. The local Reynolds number for the gas is between 2000 and 3000 in the transition region.
- The local Reynolds number for the gas is in the laminar regime for the first region, in the turbulent regime for the second region, and in the high turbulent regime for the third region. In the first region, the viscous shear force of the gas plays the major role. In the second region, the inertial forces of the gas start to become more important. In the third region, the inertial forces of the gas are dominant for movement of the pig.

- An analytical leakage model, provided by the OLGA commercial package for dynamic multiphase pipeline simulations, does significantly underpredict the experimental liquid leakage.

Overall conclusion:

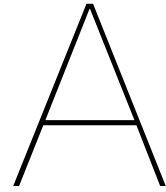
- The results in this study show that undersized ball pigging is associated with some distinct observed phenomena. The observations contribute to the understanding of the fundamental fluid flow structures around an undersized ball pig.
- The influence of the diameter ratio and the fluid flow velocities on the pig velocity and on the liquid leakage have been determined. The measured influence of these parameters will help in the estimation of the pig velocity and the estimation of the leaked volume when industrial pipeline conditions are known. The measured influence of these parameters can also help in shaping improved models and creating engineering correlations which determine the pig velocity and the liquid leakage.



Recommendations

This Master Thesis Project has given several insights on the multiphase flow around an undersized ball pig in a horizontal pipe. It could be of great interest to extend this study to get an even more comprehensive understanding of the different parameters involved. The following recommendations are proposed for future research on undersized ball pigging:

- Perform undersized ball pig experiments with higher pig densities. The 3D-printed buoyant undersized ball pigs in this study were limited to one certain buoyancy. The pigs showed a high liquid leakage even at large diameter ratios. Changing the density of the pig will give more insights on the factors and parameters associated with the multiphase flow around an undersized ball pig. In this way, a comprehensive map can be created such that a desired leakage can be chosen.
- Perform ball pig experiments with the size of the pig equal to the size of the inner pipe diameter. To do this, sufficient safety precautions need to be taken. Compare the results of these pigs with the undersized ball pig results presented in this study, such that the influence of undersized ball pigging can be better understood.
- Perform pigging experiments at higher pressures. In this study, the maximum pressure during pigging was at approximately of 0.4 barg. In industrial pipelines, much higher pressures are present.
- Benchmark the presented results with upscaled results from the industry. The created results and correlations should also be adjusted such that they can be implemented and verified in the one-dimensional pipe flow models which are used in the industry.
- Extend and improve the use of the video recordings in the current experimental set-up to investigate the fundamental fluid flow structures around an undersized ball pig. In this context, it is also recommended to look at single-phase pigging experiments.
- Adjustments can be made to the liquid leakage model presented by the OLGA commercial package to increase the accuracy of the model. An improved model is desirable for multiphase pipe simulations in the industry.
- Perform CFD simulations for the undersized ball pig under multiphase flow conditions. The performed simulations should be compared with the presented experimental results. Detailed recommendations for such simulations can be found in a numerical undersized ball pigging study by M. Jiang [19].



Experimental setup

A.1. Flowloop characteristics

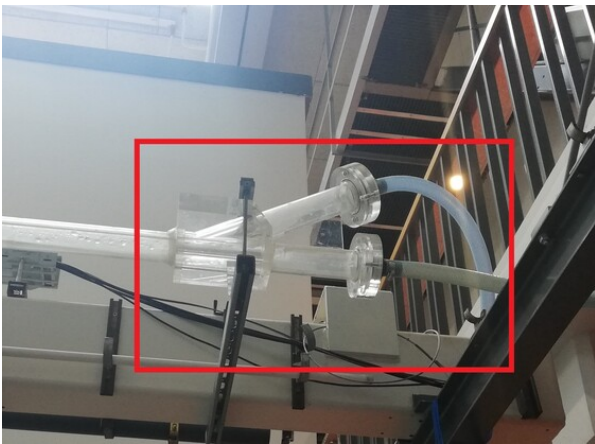


Figure A.1: Inlet section of air and water



Figure A.2: Pig launcher

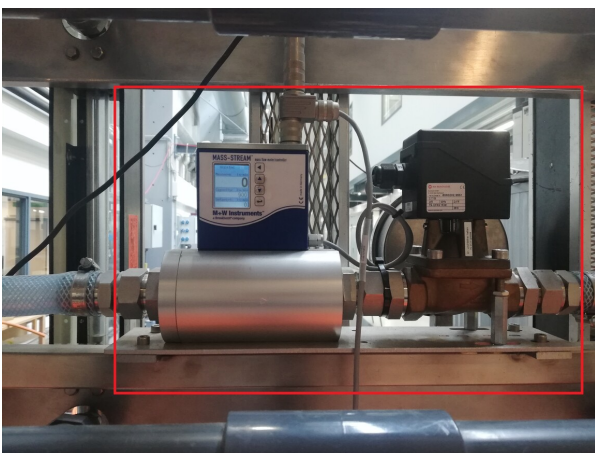


Figure A.3: Air flowmeter and controller



Figure A.4: Liquid flowmeter



Figure A.5: Picture taken at the end of the flowloop showing the upstream loop



Figure A.6: End of the flowloop

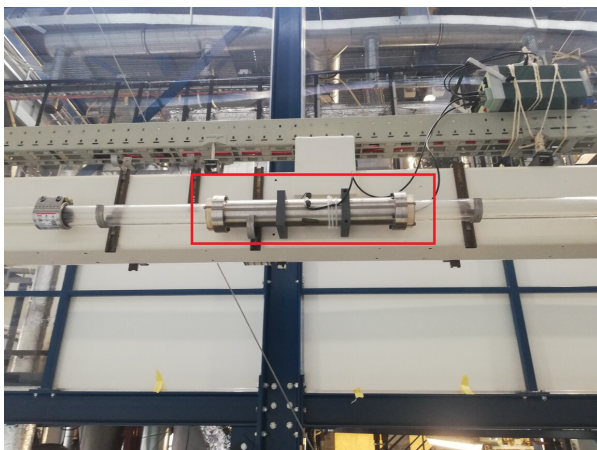


Figure A.7: Hold-up sensor

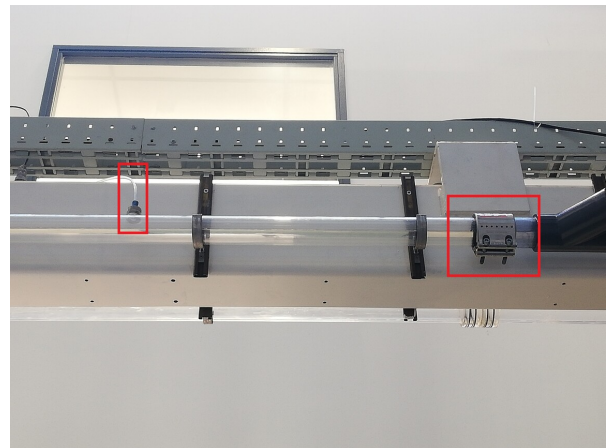


Figure A.8: Pressure sensor (left) and the new pipe coupling (right)



Figure A.9: GoPro camera

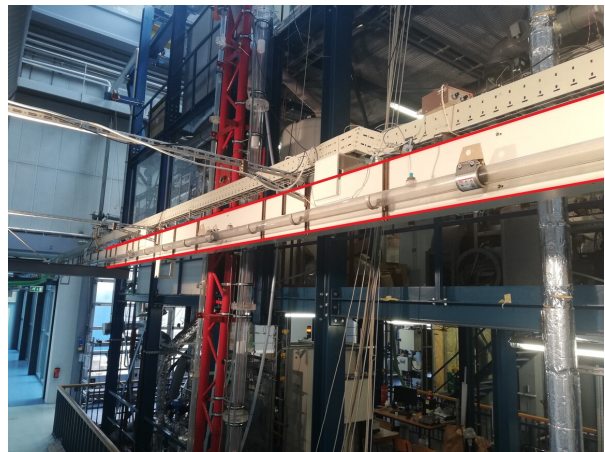


Figure A.10: Lighted flowloop for the video recordings

A.2. Calibration certificate liquid flow meter



Werksprüfschein Works Calibration Certificate			
Gerät <i>Instrument</i>		Magnetisch-Induktiver-Durchflusssensor <i>Magnetic Inductive Flow Sensor</i>	
Typ <i>Model</i>	MVM-200-QA	Messbereich <i>Flow range</i>	5,00...200,00 l/min
Serien-Nr. <i>Serial-No.</i>	65769	Datum <i>Date</i>	10.03.2021 11:09:41
Kalibrierverfahren <i>Calibration method</i>		Vergleichsmessung über Analogausgang <i>Comparative measurement via analogue output</i>	
	Messwert Prüfling <i>Reading device under test</i> mA	Durchfluss <i>Flow rate</i> l/min	Messabweichung <i>Measuring deviation</i> %
Kalibrierergebnisse <i>Calibration results</i>	4,3921	4,9389	-0,76
	7,1865	39,8564	-0,06
	10,3814	79,7945	-0,03
	13,5771	119,6989	0,01
	16,8427	160,5790	-0,03
	19,9317	199,0257	0,06
Skalierung <i>Scaling</i>		4,00...20,00 mA = 0,00...200,00 l/min	
Kalibriert durch <i>Calibrated by</i>		Unterschrift <i>Signature</i>	
L. Tarche			
Mass Flow ONLINE B.V. De Tol 83 NL-7321 KJ Apeldoorn		Phone Fax	sales@massflow-online.com http://www.massflow-online.com

Figure A.11: Calibration certificate of the liquid flowmeter

The derivation for the minimum and maximum superficial liquid velocity at a certain setpoint will be shown here. The superficial liquid velocity for a setpoint is given by the following equation (A.1).

$$\overline{u_{SL}} = Q_{liquid}[L/min] \cdot \frac{1}{60 \cdot 1000} \frac{1}{0.25 \cdot \pi \frac{1}{10^6} \cdot 52^2} \quad (A.1)$$

$$\overline{u_{SL}} = Q_{liquid} \cdot 7.84 \cdot 10^{-3} \quad (A.2)$$

Due to the inaccuracy of the flowmeter, resistor and tolerance of the inner pipe diameter, the actual velocity differs. An inaccuracy of 1% Reading Difference is given by the manufacturer. The maximum liquid flow rate used in this study is 8 L/min. 1% Reading difference from 8 L/min will be taken. 0.05 % Reading Difference is present from the inaccuracy of the resistor. This results in 1.05% Reading Difference for a certain setpoint.

$$u_{SL} = \overline{u_{SL}} \cdot \left(\frac{52}{52 \pm tol}\right)^2 \pm 1.05 \cdot \frac{8}{100} \frac{1}{60 \cdot 1000} \frac{1}{0.25 \cdot \pi \frac{1}{10^6} \cdot (52 \pm tol)^2} \quad (A.3)$$

$$u_{SL} = \overline{u_{SL}} \cdot \left(\frac{52}{52 \pm tol}\right)^2 \pm 1.05 \cdot \frac{8}{100} \frac{1}{60 \cdot 1000} \frac{1}{0.25 \cdot \pi \frac{1}{10^6} \cdot 52^2} \left(\frac{52}{52 \pm tol}\right)^2 \quad (A.4)$$

$$u_{SL} = \overline{u_{SL}} \cdot \left(\frac{52}{52 \pm tol}\right)^2 \pm 6.59 \cdot 10^{-4} \cdot \left(\frac{52}{52 \pm tol}\right)^2 \quad (A.5)$$

Using a tolerance of 0.7 mm gives a minimum and maximum range when choosing a certain setting velocity ($\overline{u_{SL}}$):

$$u_{SLmin} = 0.9736 \cdot \overline{u_{SL}} - 6.42 \cdot 10^{-4} \quad (A.6)$$

$$u_{SLmax} = 1.0275 \cdot \overline{u_{SL}} + 6.77 \cdot 10^{-4} \quad (A.7)$$

B

Pigging results

B.1. Performed combinations for the experimental conditions

Table B.1: Experimental conditions for 42 mm pig. Here the performed combinations of water and air flow are shown. Total of 26 pigging runs.

Water flow [L/min]	Air flow [L/min]						
4	-	180	270	360	450	540	630
5	-	180	270	360	450	540	630
6	-	180	270	360	450	540	630
7	-	180	270	360	450	-	-
8	-	180	270	360	450	-	-

Table B.2: Experimental conditions for 45 mm pig. Here the performed combinations of water and air flow are shown. Total of 24 pigging runs.

Water flow [L/min]	Air flow [L/min]						
4	90	180	270	360	450	540	-
5	-	180	270	360	450	-	-
6	90	180	270	360	450	540	-
7	-	180	270	360	450	-	-
8	-	180	270	360	450	-	-

Table B.3: Experimental conditions for 48 mm pig. Here the performed combinations of water and air flow are shown. Total of 24 pigging runs.

Water flow [L/min]	Air flow [L/min]						
	4	90	180	270	360	450	540
5	-	180	270	360	450	-	-
6	90	180	270	360	450	540	-
7	-	180	270	360	450	-	-
8	-	180	270	360	450	-	-

Table B.4: Experimental conditions for 50 mm pig. Here the performed combinations of water and air flow are shown. Total of 16 pigging runs.

Water flow [L/min]	Air flow [L/min]						
	4	-	180	270	360	450	540
5	-	180	270	360	450	-	-
6	-	180	270	360	450	540	-
7	-	-	-	-	-	-	-
8	-	180		360	-	-	-

Bibliography

- [1] Mamoun Abdel-Hafez and Sheruzzaman Chowdhury. "Pipeline inspection gauge (PIG) position estimation using IMU, odometer and set of reference stations". In: *ASCE-ASME J. Risk and Uncert. in Engrg. Sys., Part B: Mech. Engrg.* 2 (June 2015).
- [2] S. Barua. *An experimental verification and modification of the McDonald-Baker pigging model for horizontal flow*. University of Tulsa dissertation. 1982.
- [3] Ibtissem Belgacem and Reda Mekhlouf. "Slug Frequency in Horizontal Pipeline Subject to a Sudden Contraction: State of the Art and Laboratory Testing Data". In: *Journal of Engineering Physics* (Dec. 2018).
- [4] P. Bhattacharjee. *Undersized ball pigs using dynamic*. Shell Global Solutions (Internal Report). 2017.
- [5] Barry G. Bubar. *Chapter 15 - Pipeline Pigging and Inspection*. Boston: Gulf Professional Publishing, 2011, pp. 319–339. ISBN: 978-0-12-383867-4.
- [6] V.C. Chandrasekaran. "7 - Typical Rubber Testing Methods". In: *Plastics Design Library* (2007), pp. 16–22.
- [7] Jianheng Chen et al. "Bypass pigging technology on amelioration of pigging-induced liquid flow: An experimental and modelling study". In: *Ocean Engineering* 198 (2020), p. 106974.
- [8] J. Cordell and H. Vanzant, eds. *The pipeline pigging handbook 3rd*. Clarion Technical Publishers Scientific Surveys Ltd, 2003. ISBN: 0-9717945-3-7.
- [9] R. Davidson, ed. *An introduction to pipeline pigging*. Golf Professional Publishing, 1995. ISBN: 978-0901360397.
- [10] Mariana J.C. Diaz. *Two-phase slug flow experiments with viscous liquids*. NTNU Doctoral Thesis. 2016.
- [11] A. Entaban et al. "By-Pass Pigging - A 'Simple' Technology with Significant Business Impact". In: *IPTC - International Petroleum Technology Conference*, number 16905, Beijing, China (Mar. 2013).
- [12] T. Fethke et al. *Development and performance of a speed controlled pig in a single phase pipeline*. TU Delft bachelor thesis. 2016.
- [13] H. Goedecke. "Ultrasonic or MFL Inspection: Which Technology Is Better for You?" In: *Pipeline and Gas Journal* 230 (Oct. 2003), pp. 34–41.
- [14] Matthew Harrison. *Introducing gyroid infill*. 2018. URL: <https://mattshub.com/blogs/blog/gyroid-infill>.
- [15] Kyle Hegeman et al. "Approximate Ambient Occlusion For Trees". In: *Proceedings of the 2006 Symposium on Interactive 3D Graphics* (Mar. 2006), pp. 87–92.
- [16] M.H.W. Hendrix et al. "Experiments and modeling of by-pass pigging under low-pressure conditions". In: *Journal of Process Control* 71 (Nov. 2018), pp. 1–13.
- [17] Maurice H. W. Hendrix. *Experiments and modelling for by-pass pigging of pipelines*. TU Delft PhD. 2020.
- [18] R.A.W.M. Henkes. "Lecture 5 and 6 on Modelling of gas-liquid flow in pipelines". TU Delft University Lecture. 2021.
- [19] M. Jiang. *Numerical Study of the Flow Around an Undersized Ball Pig in a Horizontal Pipe*. TU Delft master's thesis. 2018.
- [20] D.A. Jones and D.B. Clarke. *Simulation of the Flow Past a Sphere using the Fluent Code*. Dec. 2008.

- [21] K. Kohda, Y. Suzukawa, and H. Furukawa. "Analysis of Transient Gas-Liquid Two-Phase Flow in Pipelines". In: *Journal of Energy Resources Technology* 110.2 (June 1988), pp. 93–101.
- [22] A. Kousalya Selvaraj. *Lagrangian Autonomous Sensors, A smart ball approach to pipeline inspection*. Pipeline Discipline Newsletter, Shell Global Solutions (internal report). 2016.
- [23] M. Makarova. *Design of experimental loop to demonstrate pigging activity*. UiT master's thesis. 2017.
- [24] J.M. Mandhane, G.A. Gregory, and K. Aziz. "A flow pattern map for gas—liquid flow in horizontal pipes". In: *International Journal of Multiphase Flow* 1.4 (1974), pp. 537–553.
- [25] Alvis E. McDonald and Ovin Baker. "A Method of Calculating Multiphase Flow in Pipe Lines Using Rubber Spheres to Control Liquid Holdup". In: *Drilling and Production Practice All Days* (Jan. 1964).
- [26] Kazuioshi Minami and Ovadia Shoham. "Pigging Dynamics in Two-Phase Flow Pipelines: Experiment and Modeling". In: *SPE Production Facilities* 10.04 (Nov. 1995), pp. 225–232.
- [27] Katarina Monkova et al. "Three Approaches to the Gyroid Structure Modelling as a Base of Lightweight Component Produced by Additive Technology". In: *DEStech Transactions on Computer Science and Engineering* (Dec. 2017).
- [28] B. Richa. *Undersized ball pig modelling*. Shell Global Solutions (Internal Report). 2016.
- [29] Andrés Salazar et al. "PIG's Speed Estimated with Pressure Transducers and Hall Effect Sensor: An Industrial Application of Sensors to Validate a Testing Laboratory". In: *Sensors* 17 (Sept. 2017), p. 2119.
- [30] Simon Schneiderbauer and Michael Krieger. "What do the Navier-Stokes equations mean ?" In: *European Journal of Physics* 35 (Jan. 2014), p. 015020.
- [31] A. Singh and R.A.W.M. Henkes. "CFD modeling of the flow around a by-pass pig". In: *BHR Group - 8th North American Conference on Multiphase Technology* (Jan. 2012), pp. 229–243.
- [32] Jackie Starks et al. *Miniaturized Inexpensive Hands-On Fluid Mechanics Laboratory Kits for Remote Online Learning*. June 2017.
- [33] L.C. Thronson. "Design & Construction of Harp Type Slug Catchers". In: (Oct. 2017).
- [34] Christophe Vallée et al. "Experimental investigation and CFD simulation of horizontal stratified two-phase flow phenomena". In: *Nuclear Engineering and Design* 238.3 (2008), pp. 637–646.
- [35] J. Weisman et al. "Effects of fluid properties and pipe diameter on two-phase flow patterns in horizontal lines". In: *International Journal of Multiphase Flow* 5.6 (1979), pp. 437–462.
- [36] H. Yuen et al. "Comparative study of Hough Transform methods for circle finding". In: *Image Vis. Comput.* 8 (1990), pp. 71–77.
- [37] Hang Zhang et al. "Chatter vibration phenomenon of pipeline inspection gauges (PIGs) in natural gas pipeline". In: *Journal of Natural Gas Science and Engineering* 27 (2015), pp. 1129–1140.
- [38] Jun Zhou et al. "Experiment and Dynamic Simulation of PIG Motion during Pigging Operation in a Slope Pipeline". In: *International Journal of Chemical Reactor Engineering* 16.9 (2018).
- [39] M.L. Zoetewij. *Long liquid slugs in horizontal tubes: Development study and characterisation with electrical conductance techniques*. TU Delft PhD. Dec. 2007.